# Structure and Dynamics of Binary Colloids in an External Potential : Role of Depletion Interaction

By

**Mahammad Mustakim**

**PHYS11201404005**

**National Institute of Science Education and Research, Bhubaneswar**

*A thesis submitted to the*

*Board of Studies in Physical Sciences*

*In partial fulfillment of requirements*

*for the Degree of*

**DOCTOR OF PHILOSOPHY**

*of*

**HOMI BHABHA NATIONAL INSTITUTE**



April, 2022

# Homi Bhaba National Institute

## Recommendations of the Viva Voce Committee

As members of the Viva Voce Committee, we certify that we have read the dissertation prepared by Mahammad Mustakim entitled "Structure and Dynamics of Binary Colloids in an External Potential : Role of Depletion Interaction" and recommend that it may be accepted as fulfilling the thesis requirement for the award of Degree of Doctor of Philosophy.
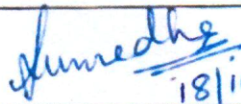
Chairman - Prof. Bedangadas Mohanty          *Bondhanty* 18/10/2022

Guide / Convener - Dr. A. V. Anil Kumar          18/10/22

Examiner - Prof. Padma Kumar Padmanabhan          18/10/22

Member 1 - Dr. Sumedha          *Sumedha* 18/10/22

Member 2 - Dr. Joydeep Bhattacharjee          18/10/22

Member 3 - Dr. Debasish Chaudhuri          *Debasish Chaudhuri* 18/10/22

Final approval and acceptance of this thesis is contingent upon the candidate's submission of the final copies of the thesis to HBNI.

I/We hereby certify that I/we have read this thesis prepared under my/our direction and recommend that it may be accepted as fulfilling the thesis requirement.

Date : 18/10/22

Place : NISER, JATNI          **Signature**          **Signature**

                                **Co-guide (if any)**          **Guide**

i

## STATEMENT BY AUTHOR

This dissertation has been submitted in partial fulfillment of requirements for an advanced degree at Homi Bhabha National Institute (HBNI) and is deposited in the Library to be made available to borrowers under rules of the HBNI.

Brief quotations from this dissertation are allowable without special permission, provided that accurate acknowledgement of source is made. Requests for permission for extended quotation from or reproduction of this manuscript in whole or in part may be granted by the Competent Authority of HBNI when in his or her judgment the proposed use of the material is in the interests of scholarship. In all other instances, however, permission must be obtained from the author.

Mahammad Mustakim

## DECLARATION

I hereby declare that I am the sole author of this thesis in partial fulfillment of the requirements for a postgraduate degree from National Institute of Science Education and Research (NISER). I authorize NISER to lend this thesis to other institutions or individuals for the purpose of scholarly research.

Mahammad Mustakim

## List of Publications arising from the thesis

**Journal**

1. "Sub-Arrhenius diffusion in a classical system: Binary colloidal mixture in an external potential", Mahammad mustakim and A.V. Anil Kumar, Physica A, **2021**, 563, 125462

2. "Super-Arrhenius diffusion in a binary colloidal mixture at low volume fraction: an effect of depletion interaction due to an asymmetric barrier", Jalim Singh, Mahammad Mustakim and A.V. Anil Kumar, Journal of Physics: Condensed Matter, **2021**, 33, 125101

3. "Depletion induced demixing and crystallization in a binary colloids subjected to external potential barrier", Mahammad Mustakim and A.V. Anil Kumar, J. Phys. Chem. B, **2022**, 126, 1, 327–335

4. "Dynamics of the binary colloidal mixture over a potential barrier: system size scaling", Mahammad mustakim and A.V. Anil Kumar (under preparation)

Mahammad Mustakim

*To*
**My Parents**
*and other family members*

# ACKNOWLEDGEMENTS

First, I would like to thank my supervisor, Dr. A.V. Anil Kumar, whose expertise was invaluable in formulating the research questions which led to completing this Ph.D. thesis work. I would like to express my gratitude to him for giving me the opportunity to work under his guidance. I sincerely thank him for providing me the necessary freedom in my scientific research, always keeping patience with me and allowing me to learn at my own pace; always making himself available for discussions, and reviewing papers and thesis chapters with promptness. It has been an honor working with him.

I would also like to express my gratitude to all my doctoral committee members; Prof. Bedangadas Mohanty, Dr. Sumedha, Dr. Joydeep Bhattacharjee, and Dr. Debasish Chaudhuri for all their feedback and suggestions throughout my Ph.D. course, which immensely helped me in improving my research work. I wish to show my appreciation to Dr. Jalim Singh for collaborating with me on one of the projects.

This work would not have been possible without the environment and facilities provided by the School of Physical Sciences, NISER. The computation work of this thesis was done at the KALINGA cluster of NISER. I thank HBNI and NISER for providing me with a suitable scientific environment and opportunity to complete this thesis work.

I am lucky enough to have friends along with me on this journey, which makes life easier and enjoyable. I want to especially thank Saili Dutta, Manoar Hossain, and Soheli Mukherjee for all those moments of fun we shared together. Thanks a lot for being there for me.

Lastly and most importantly, I want to thank my parents; their love, support, and patience encouraged me to complete this Ph.D. journey. I am grateful to all of my family members and friends for their loving support.

# **ABSTRACT**

We have investigated the phase behavior and dynamics of a binary colloidal mixture of soft spheres subjected to an external repulsive potential of both symmetric and asymmetric form using canonical ensemble molecular dynamics simulations. At low volume fractions, in the presence of a Gaussian potential we studied the temperature dependence of the diffusivities of both the particles at low temperature regimes and found out that the larger components of the mixture deviate from the general Arrhenius behavior in the diffusion process. The depletion interaction between the external potential barrier and larger component increases with decreasing temperature which makes the effective activation energy for barrier crossing temperature-dependent, leading to sub-Arrhenius diffusion in larger particles. The smaller particles follow the Arrhenius law in their diffusivities as their activation energy is temperature independent. In a classical system like ours, exhibiting a sub-Arrhenius diffusion is seldom reported in the literature before. We further studied the effect of depletion interaction at a higher volume fraction of the system and found that above a certain volume fraction, which is much less than the freezing volume fraction of individual components, the large particle rich phase forms a crystalline domain in the region of the external barrier. Because of the crystallization process, the diffusion of larger particles reduces sharply at low temperature and high volume fractions leading to a cross-over from sub-Arrhenius dynamics to super-Arrhenius dynamics as we increase the volume fraction. The dependence of these properties on the system size has been also investigated and found to be independent of the system size for larger system sizes, but the scaling of the dynamical properties of the larger components break down at smaller system sizes. We further expand our investigations to asymmetric Gaussian function as the external potential and studied the effect of depletion interactions on the structure and dynamics of the colloidal mixture. The diffusivity of the larger particles exhibits a cross-over from sub-Arrhenius to super-Arrhenius behavior as the asymmetry in the external potential increases, while the smaller particles show normal Arrhenius behavior for all asymmetry parameters and temperatures.

# Contents

# Summary

The primary aim of this thesis is to extensively study the role of depletion interactions in a binary colloidal mixtures of soft spheres under the influence of external potential barrier. The structural and dynamical changes are governed by the depletion interactions between the larger components of the mixture with the external potential barrier, which originates completely because of the entropy of the smaller particles in the mixture. This influences the overall diffusion process of the particles and its temperature dependence.

We have investigated the phase behavior and dynamics of this binary mixture of soft colloidal particles by using classical molecular dynamics simulations in a canonical ensemble. In the presence of symmetric potential, the depletion interactions between the external potential barrier and the larger components in the binary mixture significantly alter the structural and dynamical properties of the binary mixture. The effective attraction of larger particles towards the barrier leads to phase separation of the mixture into a large particle(l) rich phase and a small particle(s) rich phase. The dynamics of smaller particles significantly slow down at low temperatures at intermediate times similar to the supercooled liquids, even at quite low volume fractions. At lower temperatures, the larger components diffuse faster than the smaller ones due to this depletion interaction. The temperature dependence of diffusion of each component also shows interesting behavior. The larger particles undergo sub-Arrhenius diffusion while smaller particles obey normal Arrhenius diffusion. The depletion interaction between the external potential barrier and larger component increases with decreasing temperature which makes the effective activation energy for barrier crossing temperature-dependent leading to sub-Arrhenius diffusion. In general sub-Arrhenius diffusion is observed in systems where quantum effects play a predominant role in determining the rate of barrier crossing. Contrary to this, a classical system like ours, a binary colloidal mixture, exhibits a sub-Arrhenius diffusion which is hardly reported in any classical system. On further investigation of these effects with increasing the volume fraction of the system, we found that the extent of demixing increases as volume fraction increases.

And above a certain volume fraction, which is much less than the freezing volume fraction of individual components, the l-rich phase forms a crystalline domain. This crystalline domain is found to be diffusing perpendicular to the external potential barrier. Such moving crystals are earlier reported for non-equilibrium systems where the crystals are subjected to heating or exposed to light. Because of the crystallization process, the diffusion of larger particles reduces sharply at low temperature and high volume fractions leading to a cross-over from sub-Arrhenius dynamics to super-Arrhenius dynamics as we increase the volume fraction. The dependence of these properties on the system size has been also investigated and we found that there is no system size effects on both the components of the mixture. However, below a certain system size, and at low temperatures the larger particles do show little deviations in their dynamics although the qualitative nature remains same. The displacement distribution in these cases shows marked deviations from Gaussian distributions and the scaling of dynamical properties fails in these configurations.

We have further used an asymmetric Gaussian function as the external potential and studied the effect of depletion interactions on the structure and dynamics of the colloidal mixture. The diffusivity of the larger particles exhibits a cross-over from sub-Arrhenius to super-Arrhenius behavior as the asymmetry in the external potential increases. Near the asymmetric side of the barrier, larger particles show higher local density forming a transient caging. The activation energy for the diffusion of larger particles is temperature-dependent: it decreases with decreasing temperature for low asymmetry and increases with decreasing temperature for high asymmetry. The non-Gaussian parameter, the potential of mean force, and the self intermediate scattering function indicate crowding of larger particles near the barrier leading to a slowing down of dynamics and super-Arrhenius behavior. Here again, the smaller particles show normal Arrhenius behavior for all asymmetry and temperature. Even though the results we obtained are for a binary mixture of colloids, we believe our findings are applicable to many other systems which involve barrier crossing.

# List of Figures

# List of Tables

# Chapter 1

# Introduction

The work outlined in this thesis is done in the context of soft condensed matter, which has steadfastly achieved the status of one of the most important areas of multidisciplinary research covering physical, chemical, and biological sciences. Soft matter systems are states of matter that can not be categorized completely into either simple liquid or crystalline solids, conveniently known as soft condensed matter or soft matter. As its name suggests, a soft matter system can easily be deformed. Some of the soft matter systems are polymers, gels, colloids, emulsions, surfactant assemblies, liquid crystals, many biological systems, etc. The characteristics and properties of these systems are strikingly different from that of simple liquid or crystals. At mesoscopic length scales, they are organized with structural features that are much larger than an atom, but much smaller than the overall size of the system. For instance, the long, chain like molecules in a polymer solutions never cross each other which leads to entanglement among them and produces viscoelastic effects in the solutions; liquid crystals, as the name suggests, show properties intermediate between a simple liquid (they can flow) and a crystalline solid (ordering in molecules). Colloids form an important class of soft matter systems both from a fundamental as well as applications point of view. The primary emphasis of this thesis is to study the structure and dynamics of a binary colloidal system in the presence of an external potential.

## 1.1 Colloids

Colloidal dispersion or colloids are a mixture of mesoscopic particles of size varying from 1 $nm$ to 1000 $nm$ dispersed in a fluid medium. The dispersed particles are called the dispersed phase and the medium is called the continuous phase. Colloid means glue like substance, and the term originated from the Greek word "kolla". We can find colloids everywhere. Depending on the nature of the materials the colloids are classified into many physical states. For example, both the dispersed phase and medium can be gas, liquid, or solid. Some of the examples of colloids are listed in Table-1.1. The scientific study of colloids started way back in the early 19th century when the Scottish botanist Robert Brown accidentally discovered the peculiar motion of pollen grain suspended in water by using a simple microscope. In 1827, while investigating how pollen grains impregnate the female ovule, he observed that minute particles suspended in liquid are in continuous random motion, later designated as "Brownian motion" [1, 2]. He also examined various products of organic bodies, window glass, many metals and minerals, in powder form and observed the same random motion as the pollen grains. Francesco Selmi, an Italian chemist, published the first systematic study of inorganic colloids. Selmi demonstrated that salts would coagulate such colloidal materials as silver chloride and Prussian blue and that they differed in their precipitating power. Later in 1860s, the Scottish chemist Thomas Graham [3], published his many works describing the properties of colloidal solution like low diffusivity, the absence of crystallinity, the lack of ordinary chemical relations, etc. The working theory was not known until Einstein proposed the "theory of Brownian motion" in 1905 [4]. The Brownian motion of colloids is caused by the random collision of colloidal particles by the molecules of the surrounding fluid, agitated by the thermal energy. Thus, colloidal particles are characterized by observable Brownian motion, originating from thermal energy of the order of $k_B T$ for each colloidal particle. Just as the pressure of an atomic gas is affected by the

| Continuous phase | Dispersed phase | Term | Examples |
|---|---|---|---|
| Solid | Solid<br>Liquid<br>Gas | Solid Sol<br>Solid Emulsion<br>Solid Foam | Concrete, Metal alloys<br>Butter, Cheese<br>Bread, Pressed powder, Sty-rofoam |
| Liquid | Solid<br>Liquid<br>Gas | Sol, Gel<br>Emulsion<br>Foam | Ink, Paint, Jelly<br>Mayonnaise, Milk<br>Whipped cream, Foam on bear |
| Gas | Solid<br>Liquid | Solid Aerosol<br>Liquid Aerosol | Smoke, Dust<br>Cloud, Fog, Smog |

Table 1.1: Examples of different types of colloids

interaction between the atoms, the physical properties of a colloidal dispersion depend on the potential of the mean force between colloidal particles. In contrast to pair interactions between atoms, interactions between colloidal particles can be tuned by choosing particle type, temperature, solvent, by supplementing additives such as electrolytes, polymers or colloidal particles, or by modifying the particle surface. The physical state of a colloidal dispersion is a function of the interaction between the colloidal particles.

The early years of the 20th century witnessed various key developments in physics and chemistry, which help in understanding the colloids better. These includes advances in the knowledge of the electronic structure of atoms, in the concepts of molecular size and shape, and in insights into the nature of solutions. Moreover, efficient methods for studying the size and configuration of colloidal particles were soon developed, for example, ultracentrifugal analysis, electrophoresis, diffusion, and the scattering of visible light and X-rays. More recently, biological and industrial research on colloidal systems has yielded much information on dyes, detergents, polymers, proteins, and other substances important to everyday life. All colloidal systems can be either generated or eliminated by nature as well as by industrial and technological processes. The colloids prepared in living organisms by biological processes are vital to the existence of the organism. Those produced with

inorganic compounds in earth and its waters and atmosphere are also of crucial importance to the well-being of life forms.

## 1.2    Colloidal Interactions

As mentioned earlier, the physical properties of colloids are determined by the potential of mean force between the colloidal particles. In close separation, the attraction between the colloidal particles increases and they tend to aggregate into large clusters causing precipitation and the desired dispersed state is lost. Most of colloid science is concerned with maintaining the dispersed state. Stabilization in colloidal system refers to processes where the particles remain evenly distributed throughout the volume of the fluid. Colloidal particles have large surface area compared to atoms or molecules. Thus understanding and control of interfacial forces is central to colloid science. These interfacial interactions can be tuned by changing temperature, medium, particle type, by adding electrolytes, salt, polymers, colloidal particles,etc or by modifying the surface of colloidal particles. One can achieve the desired dispersed state by balancing the attractive interaction with required repulsion by tweaking the interfacial forces.

### 1.2.1    Van der Waals attraction

The Van der Waals interaction is the dominant attractive interaction in a colloidal suspension. This force of attraction between any two atoms or molecules arises because of the interaction of fluctuating dipole moments among them which is a quantum mechanical effect. This interaction is independent of whether the particles are charged or uncharged. The dielectric properties of the colloidal particles and the background medium determine the strength of the interaction. For two identical colloidal spheres with radius $R$ and separated

4

by an interfacial distance $h$, the Van der Waals attraction is given by [5, 6]

$$
\begin{aligned}
W_{VDW}(h) &= -\frac{A}{6}\left[\frac{2R^2}{h^2+4Rh}+\frac{2R^2}{h^2+4Rh+R^2}+ln\left(\frac{h^2+4Rh}{h^2+4Rh+R^2}\right)\right] \quad (1.1)\\
A &= C\pi^2 n^2 \quad (1.2)
\end{aligned}
$$

where $A$ is the Hamaker constant which depends on the nature of both the dispersed phase and the medium; $h$ is the closest distance between the surfaces of two spheres, $n$ is the number density and $C$ is the dispersion coefficient. $C$ depends upon the electronic polarizability and frequency of the colloidal particle. At short interparticle separations (small $h$), the Van der Waals attraction is very strong and varies as, $W_{VDW}(h) \sim -AR/h$. In order to stabilize a colloidal dispersion a significant repulsion is needed preventing the particles getting too close and flocculate irreversibly. Another way to minimize the effect of Van der Waals attraction is by refractive index matching. The biggest contribution to the Van der Waals interaction is from the optical frequencies. If one can match the refractive index of the medium with the dispersed particles, the value of $A$ can be minimized. This will in turn reduces the strength of Van der Waals attraction and hence can increase the stability of the colloidal dispersion.

### 1.2.2   Electrostatic double layer repulsion

Usually the colloidal particles have electric charges on their surfaces when they are dispersed in a medium and the interaction arising from it must be accounted for while studying the colloidal interactions. This interaction is different from the bare Coulomb interaction, as there are dissolved ions in the solution. In particular, the electrostatic interactions are screened by dissolved ions; which modifies the interaction between two charged bodies to a screened Coulomb interaction which exponentially decays in strength with distance.

In Figure 1.1, we have two charged colloidal particles in solution of charged ions[5, 6]. The counterions will surround the particles around the surface and the coions will be de-
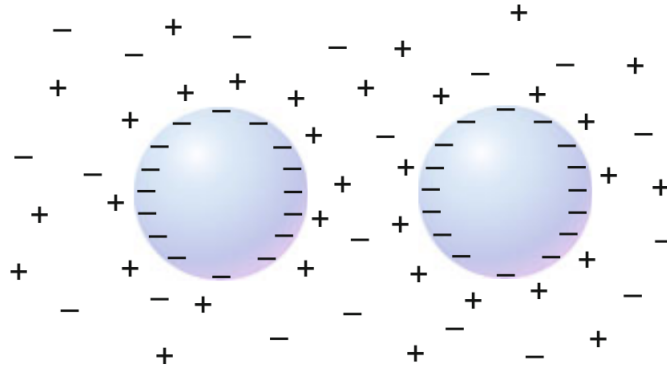
Figure 1.1: Two charged colloids in an electrolytic solution[5]

pleted from the surface. The inhomogeneous layer is termed "double layer" and its width depends on the ion concentration in the bulk solution. The colloidal surface charges are screened if more number of ions are present. When the two colloidal particles approaches towards each other and their double layers overlap, a repulsive pair potential develops which leads to a repulsive pressure. Dispersed like-charged colloids hence repel each other upon approach due to screened-Coulomb or double layer repulsion.

The interparticle separation dependence of double layer repulsion is approximately exponential,

$$W_{DR} = U_0 \, exp(-h/\lambda_D) \tag{1.3}$$

$$\lambda_D = \left( \frac{\epsilon\epsilon_0 k_B T}{2e^2 n_0 z^2} \right)^{\frac{1}{2}} \tag{1.4}$$

Here $h$ is interfacial distance; $\lambda_D$ is called the Debye screening length upto which this force is operational; $n_0$ is the ionic concentration in bulk solution, $e$ is the electronic charge, $z$ is the number of charges, and $\epsilon$ is the dielectric constant of the medium. Note that the Debye screening length is inversely proportional to the square root of ionic concentration. At distances larger than $\lambda_D$ , the strength of the direct electrostatic interaction between charged colloidal particles rapidly falls to zero, as schematically depicted in figure 1.2.
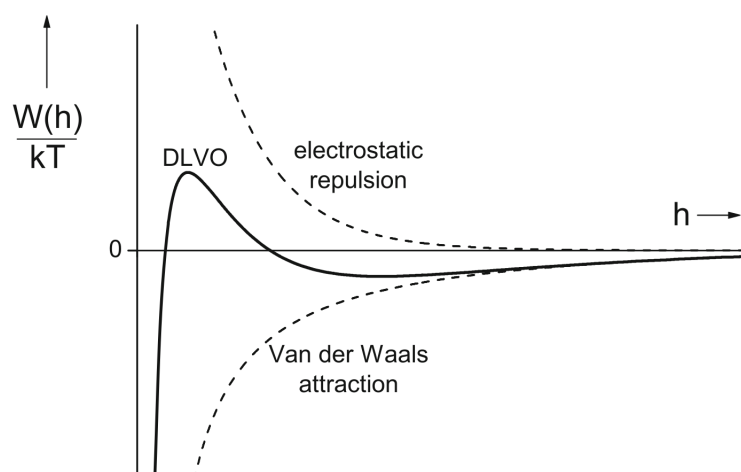
Figure 1.2: Schematic plot of a Van der Waals attraction and double layer repulsion between charged colloidal spheres and their sum, the DLVO interaction potential[5].

### 1.2.3 DLVO theory and stability of colloids

The basic understanding of colloidal interactions commenced in the 1940s when Derjaguin, Landau, Verwey and Overbeek (DLVO) pointed out that the stability of a colloidal dispersion is determined by the balance between the electrostatic interaction and the van der Waals interaction between particles [7, 8, 9]. The DLVO theory provides the foundation for the description of the interaction between colloidal particles. The stability of colloidal systems consisting of charged particles can be understood from the DLVO theory. In a dispersion of charged colloids in an electrolyte solution, the Van der Waals attraction between two colloidal particles are opposed by the repulsion originating from electrical double layers, hence retains the desired dispersed state. This foundation for the stability of colloids is known as the DLVO theory and has been remarkably successful in explaining the results of a vast number and broad range of experiments.

The DLVO potential describes the long range interaction between colloidal particles as the combination of a van der Waals attraction and an electrostatic double layer repulsion. The total DLVO potential is the addition of van der Waals(VDW) attraction and double

layer repulsion(DR) :

$$W_{DLVO} = W_{VDW} + W_{DR} \tag{1.5}$$

In Figure 1.2, the DLVO interaction potential $W_{DLVO}$ is schematically sketched together with its two contributions. At large $h$, there is no interaction between the colloidal particles, as it is short-ranged interaction potential. However, at very small separation $h$, the van der Waals attraction is strong, as the particles get very close into the so called primary minimum, which is deep enough for irreversible coagulation. Given a large enough period of time all particles will move toward their global minimum energy state, leading to the flocculation of the suspension. However, if the repulsive force is high and the maximum of $W_{DLVO}$ is sufficiently high (larger than a few $k_BT$), coagulation is prevented, and the dispersion remains stable. Flocculation does occur when particles are at the secondary minimum, but this flocculation is not strong enough and can be reversed to dispersed state by shaking the solution.

For practical purposes in the industries, the stability of colloids are desired. This can be achieved by tuning the interaction between the colloidal particles. One such example is by adding salt in the solution or increasing the ionic concentration in the solution. As the van der Waals interaction depend upon the ionic concentration, the DLVO will depend upon the ionic strength. At low salt concentration the electric double layer repulsion dominates and surpasses few $k_BT$ of energy barrier hence permanent dispersed phase or stable colloidal solution is achieved. Adding a little more salt still gives a repulsive interaction with a shallow minimum which gives rise to weak flocculation which can be reversed as mentioned earlier.

There are many ways where the stability can be achieved by increasing the repulsive force. One of the most important practical methods for stabilizing colloids is by coating the particle with a polymer layer which gives extra repulsive force at short interparticle

distances[10]. The chains are attached by one end at the surface of colloidal particles and the other end stick out into the solution. If two such modified colloids come close to each other, the osmotic pressure in between them increases dramatically due to steric hindrance of the polymer chains on both particles. This competition between the chains for the same volume leads to a repulsive force between them and provide an extra repulsion needed for stabilization.

## 1.3 Depletion Interaction

Apart from the direct interaction like Van der Waals interactions or electrostatic double layer repulsion, there is one indirect interaction known as "depletion" interaction which plays a very important role in the structure and dynamics of colloidal systems. This interaction is extremely useful in the understanding of colloids. Generally, depletion interaction arises when size asymmetric particles are present in a colloidal solution. The presence of smaller particles induce an entropic effect which results an effective attraction among the larger particles. In 1954, Asakura and Oosawa published a paper describing the depletion interaction for the first time in colloid polymer solution[11, 12]. They observed that by the addition of non-adsorbing polymers to colloidal suspensions the mixture phase separates into a colloid-rich and a polymer-rich phase. Flocculation or phase separation can occur, which depend on some parameters, such as the polymer concentration, the chain length, the solvent quality, and the size of particles. Depletion interaction is a crucial interaction that describe the underlying phenomena of many observations in the structure and dynamics of colloids successfully. An in depth knowledge of the depletion potential is necessary to understand the phase behavior of the colloid dispersion.

Lets try to understand this very important interaction as follows. Suppose we have only one type of colloidal particles in the container. They will move randomly in the container.

Now adding small particles will change the dynamics of the system. Because there are more number of smaller particles, the free energy of the system is dominated by the entropy of the smaller particles. So the partition function of smaller particles is given by,

$$Z = \frac{1}{N!} \left( \frac{V}{\lambda^3} \right)^N \tag{1.6}$$

The Helmholtz free energy of the system will be,

$$F = -k_B T \ln Z \tag{1.7}$$

When the volume of the system changes, the free energy of the system also changes to

$$dF = -N k_B T \frac{dV}{V} \tag{1.8}$$

From the above equation it is clear that the free energy of the system goes down as the change in volume increases. The volume available to the the small particles is not what it might seem first. As the smaller particles come closer to the larger particles, they can not get any closer than their radius. Each larger particles has some area surrounding it where the smaller particles can not get in, this region is known as "excluded volume region" or "exclusion zone" or "depletion zone". So the actual volume available for smaller particles is little less than what is anticipated. However, there are configurations where these exclusion zones overlap with each other. When two larger particles come closer and their exclusion zones overlap, it actually increases the effective volume available for the smaller particles to move around. As the change in volume increases the free energy of the system decreases, which is a favorable condition for the system. So there is an effective attraction between the larger particles just because the system wanting to lower its entropy in the presence of smaller particles. Another way to understand the depletion interaction is the osmotic pressure in the overlapped region, which is given by,

$$PV_{ov} = N k_B T \tag{1.9}$$

The overlapped region acts as a semipermeable membrane where the smaller particles can not pass through. As the number of the smaller particles in the overlapped region is less, the osmotic pressure will be less compared to other regions, hence the larger particles tend to stick with each other. So there is a net attractive force between larger particles arising from the unbalanced osmotic pressure.

For an example (see figure 1.3), the polymer molecules, can be treated as spheres of radius $R$, are excluded from a region of thickness $\delta$ away from the surface of the bigger particles (depletion zone). As the particles approach, the depletion zones overlap, with the result that there is a volume of solution between the particles in which the concentration of polymer molecules is less than that in the bulk solution. This means that the difference in osmotic pressure between the bulk solution and the depletion zone leads to a force pushing the particles together. It follows that the free energy of the polymers is minimized by states in which the colloidal spheres are close together. The effect of this is just as if there were an attractive force between the spheres even while the direct colloid–colloid and colloid–polymer interactions are both repulsive. For small depletant concentrations the attraction equals the product of the osmotic pressure and the overlap volume.
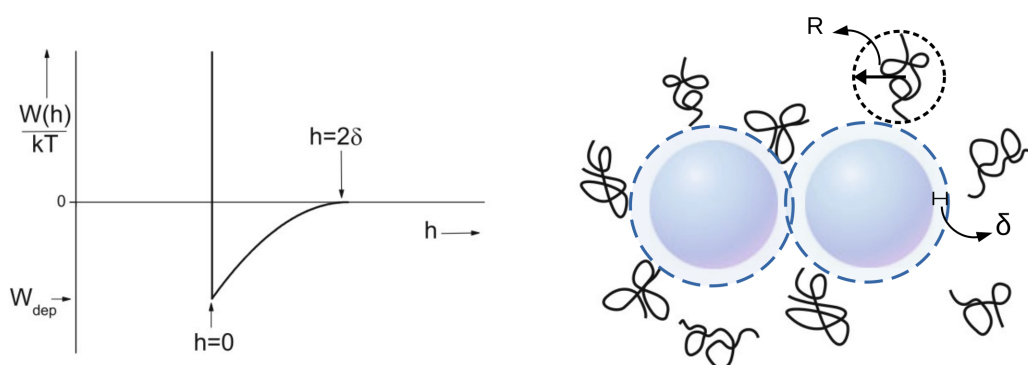


Figure 1.3: Sketch of the depletion interaction between two hard spheres[5]

The Asakura–Oosawa–Vrij (AOV) depletion potential equals[12, 13]:

$$W_{dep}(h) \;=\; \infty \qquad\qquad h < 0 \tag{1.10}$$

$$\;=\; -PV_{ov}(h) \qquad 0 \leq h \leq 2\delta \tag{1.11}$$

$$\;=\; 0 \qquad\qquad h \geq 2\delta \tag{1.12}$$

where $P = n_b K_B T$, is the osmotic pressure of depletants with bulk number density $n_b$. The overlap volume is given by

$$V_{ov}(h) = \frac{\pi}{6}(2\delta - h)^2(3R + 2\delta + h/2) \tag{1.13}$$

In figure 1.3, the AOV interaction potential $W_{dep}(h)$ between two hard spheres in a solution containing free polymers is plotted. The value of the potential $W_{dep}(h)$ is minimum when the particles touch each other ($h = 0$). The range of the depletion attraction is determined by the size $2\delta$ of the depletant, whereas the strength of attraction between them depends upon the depletant concentration. More number of depletants cause more osmotic pressure, hence the strength of attraction also increases. Because of the dependence of interaction potential on the size and concentration of the depletants, it gives a scope to independently modify the range and the strength of attraction between colloids. This opens up the ways to study the fundamental properties of the fluid systems, such as crystallization and gelation phenomena, using colloidal systems instead of low molar mass substances. Another advantage of studying the colloid-polymer mixtures is that it can be probed using microscopy, which gives opportunities for experimental studies.

## 1.4   Effect of depletion interaction

As described in the previous sections, the first explanation of depletion interaction came from Asakura and Oosawa[11] in 1954 and later by Vrij[13] in their model of colloid-polymer mixture. They showed that in the presence of non-adsorbing polymer chains, the

colloidal particles with hard core potential attract each other. This effective attraction between particles is a purely entropic effect; attraction originates from purely repulsive interactions. For some reasons this phenomena remained unnoticed for some years until 1980's. Many phenomena in physical, chemical and biological systems are explained in terms of depletion attraction among particles. One of the most common effect of this interaction is the phase separation of colloidal dispersions like it happened in Asakura-Oosawa model where the mixture phase separates into colloid-rich and polymer-rich phases. The depletion effect has garnered the attention of the scientific community over the last few decades because it plays an important role in many industrial and biological applications, especially in colloid science. This interaction is attributed to explain many phenomena such as phase separation of colloidal dispersions, protein crystallization, red blood cells clustering, etc.[14, 15, 16]. The colloid-polymer mixture is more interesting since it can be conceived as the simplest system consisting of hard spheres and non adsorbing polymers where the later is dissolved in the solution with very minimal interaction among themselves.

Depletion effects were observed even before Asakura and Oosawa gave the analytical description that the depletants can cause interaction among the larger components in the mixture. One such example is the clustering of the red blood cells(RBC) which was known to scientists in the 18th century that they form stacks of RBCs (known as "Rouleaux") in certain cases of illness[17, 18]. Later Asakura and Oosawa pointed out that it might occur due to the depletion interactions generated by the presence of serum protein in the blood, which acts as depletant[12]. In the beginning of 20th century, the production and transportation of rubber for latex and paint formation increased. To reduce the weight of the rubber and to separate the concentrated rubber, people used to mix plant and seaweed polysaccharides which phase separate it into liquid and concentrated phases. Since the rubber particles are light they come to the top (known as "creaming") leaving the dilute solution in bottom of the container[19, 20, 21]. This can be clearly interpreted as the result of depletion

effects because of the presence of polysaccharides. In 1942, Cohen observed that adding heparin can cause the aggregation of Tobaco Mosaic Virus(TMV) in the solution, which can further help to separate and isolate the virus[22]. There are many such examples of chemical and biological phenomena occurred before the Asakura and Oosawa model and back then nobody knew about this important interaction which can now be attributed to the effect depletion interactions. Until 1970 there were not many accounts of depletion effect studies, however, in the early 1970's Vincent and co-workers started to investigate the origin of flocculation of pigment particles in paint dispersions[23]. To know more about the stability of colloid-polymer mixture and the demixing of these particles, they performed experiments by taking latex particles (colloids) and polyethylene oxide (polymer)[24, 25, 26]. These experiments helped them to understand the phase behavior of colloid-polymer mixture. In another experiment, during the same time period, Hachisu[27] observed a fluid to solid phase transition when sodium polyacrylate is added to polystyrene latex particles[28]. The process of crystallization became fast when the polymer concentration increased. The theoretical study of depletion interaction among hard spheres due to the presence of non adsorbing polymers commenced with Vrij[13] and later was carried out by many other scientists. De Hek and Vrij also showed a direct link between experimental and theoretical study of phase separation in a mixed sterically stabilized silica dispersions with polystyrene in cyclohexane solution[29, 30]. Many mean field methods were also used to consider the excluded volume interactions and it provided insights in details of the configurations of polymers[31, 32, 33, 34]. Joanny et al.[31] calculated density profile of the polymer between two plates in the semi dilute regime by applying mean field treatment to the depletion interaction. Feigin and Napper[32] calculated the free energy of interaction between two flat plates mediated by non adsorbing polymers and observed that there is repulsive barrier for polymer concentration.

Depletion effects are well known to lead to phase separation in the bulk of colloids,

14

which consists of both large and small particles and is dominated by short-range repulsive interactions[35, 36, 37, 38]. Gast et al.[39] used thermodynamic perturbation theory to derive the free energy of a mixture of colloidal particles and polymers (known as penetrable hard spheres), based on pairwise additivity of the interactions between the colloids. It informs that the coexisting phases depends on the colloid-polymer size ratio $q = R_g/R$ and the volume fraction $\phi$ of the colloids. At low $q$, fluid-solid phases coexist, at high $q$, the gas-liquid coexist. The depletion thickness was assumed to be equal to the radius of gyration as used and popularized by Eisenriegler[40]. Experimental investigations work was done by Allain et al.[41] to determine the thickness of the depletion layer and found that it is nearly equal to the radius of gyration of polymers [42]. De Gennes derived an expression for the density profile of a semi-dilute polymer solution near a (non-attractive) wall and demonstrated that the depletion thickness equals the correlation length, the length scale over which the polymer segments are correlated. In dilute polymer solutions (below coil overlap) it is the radius of gyration. However, in semi-dilute solutions (above overlap) the correlation length becomes independent of the chain length and is a (decreasing) function of the polymer concentration. Hence, the depletion thickness decreases with polymer concentration in the semi dilute regime. De Gennes considered the depletion contact potential between two colloidal hard spheres in a semi-dilute polymer solution in a good solvent. For this case, where the only relevant length scales are the sphere radius $R$ and the correlation length $\xi$. Many other fundamental studies also commenced during this time by taking the size ratio of colloid and polymers differently. They consider the polymer to be larger than the colloids ($q > 1$, known as protein limit), generally relevant for polymer and protein mixtures. The opposite (small $q$) is know as colloid limit where the colloids are of larger size than the polymer chain. Lekkerkerker[43] proposed a "Free Volume Theory" (FVT) to study the phase behavior of colloid-polymer mixture which revealed that for $q < 0.3$, fluid-solid phases coexist for this limit, whereas at low colloid volume fractions, a gas-liquid phase

coexistence is found for $q > 0.3$. A three phase colloidal gas-liquid-solid coexist for the case of $q > 0.3$ as predicted by FVT, which was later confirmed by the experiments[38, 44].

At the end of the 20th century, many Monte Carlo computer simulation studies on the effect of depletion interaction published by taking different approach. Despite the success of FVT, it can only give the qualitative information for large $q$. For example, high concentration of polymer chain larger than the colloidal particles cause instability in the solution[45, 46]. In such a situations the classical Asakura-Oosawa-Vrij description is not enough to understand the underlying phenomena. Apart from spherical colloids, there has been also systematic studies of different shape of colloids such as colloidal rods[47], platelets[48], rocks[49], etc. There are many biological system where the depletion effect has been directly observed in a vesicle[50]. The polystyrene particles get attracted to the wall of vesicle due to presence of other small particles. Depletion interactions also modulate the binding between disordered proteins in crowded environments[51]. Hence, in general, depletion interaction is very robust in explaining lot of underlying phenomena occurring in chemical, physical, and biological systems with lots of applications in industry and also in day to day life.

## 1.5    Binary Colloidal system

The physics of colloids has been a growing filed of research in the soft condensed matter system since few decades owing to its ubiquitous applications in the chemical, biological, pharmaceutical, and food industries such as the production of pastes, paints, various drugs, etc. The colloidal dispersion constitutes of mesoscopic sized particles of range few nanometer to a micron dissolved in a solvent medium or fluid. Such systems are very useful model systems for basic research, since the colloidal particles can be tuned to a desired state by changing its interfacial interactions, adding different solutes or modifying its sur-

faces. The colloids have the properties of self organization when they are in large numbers. Because of this self organization colloids have large industrial applications[52, 53]. For example, suspensions of monodisperse polymethylmetacrylate (PMMA) particles can be stopped from coagulation and stabilized by adding small surfactant molecules grafted at their surfaces[54]. The self assembly of colloidal particles is an effective way to form 2D or 3D colloidal crystals which are used in fabrication of functional materials such as photonic bandgap crystals, plasmonic materials, and nanowire arrays [55, 56, 57, 58]. Many dense colloidal dispersions undergo dynamical arrest which are understood to lead to long-lived but non-equilibrium states of the system give rise to the demands of experimental and theoretical studies[59, 60] to understand their practical importance in the food, medical and numerous other industries. With the advancement of these studies, many models for hard spheres or charged colloids are investigated which allows to give quantitative description of phenomena like glass transition[61]. One of the simplest model of viscoelastic system which undergoes glass transition is polydisperse colloidal dispersion. The study of colloids provide a vast range of fundamental understanding of condensed matter system, ranging from crystallization to glassy states[62, 63, 64, 65]. A key feature that makes such studies feasible is the fact that due to the large size of colloids (as compared to atoms or small molecules) the characteristic time of their motions is many orders of magnitude larger than the corresponding times for atoms or molecules in ordinary solids and liquids.

Recently the binary colloidal system (two component system of different colloidal species) attract more attention to the researchers, as it provides rich phase behavior and structures in which particles with different characteristics offer the system more versatility than a single component system. For example, a binary system with different sized particles would have higher fluidity than a single component system[66]. Demixing and phase separation are the most common phenomena occuring in a binary colloidal hard spheres system[53, 67, 68]. As mentioned earlier, depletion interaction play an important role in this kind of dynamics

and structures as it causes an effective attraction among the larger colloids due to the entropic effect. One of the most intriguing problems of soft matter system is confinement of fluids in nanoscopic capillaries; an interesting interplay occurs between surface effects at the confining walls, such as wetting or drying[69], and finite size effects due to the finite capillary width. The larger colloidal particles face depletion interactions at the wall along with themselves. Thus understanding confined fluid and their phase behavior is important. A binary colloidal mixture, confined between hard walls shows the density of larger components increases near the wall. This is due to the depletion effect between the wall and larger particles when their excluded volume region overlaps and cause an effective attraction towards the wall. Consequently the smaller particles stay away from the wall, depleted from the wall region[70, 71, 72, 73]. Roth et. al.[71] showed that near a hard wall the larger particles get attracted towards it and the density increases due to depletion interaction. In contrast to hard particle models, soft repulsive pair potentials in binary systems have received much less consideration. This attraction between the wall and the larger component of the binary mixture is also true for softer wall with infinite confining potential[74]. This leads to the question that the depletion interactions can arise if a finite repulsive potential present in the system. The binary colloidal mixture is confined along one dimension in a slit pore. An external finite potential acts on the fluid mixture around the center of pore along the confinement, which can lead to the formation of microstructural domains in the binary mixture. It is observed that in the presence of an external repulsive potential, the larger particles overlap with exclusion volume region of the potential and leads to an effective attraction for larger particles towards the potential due to depletion interactions. It is shown that a microstructural rearrangement of larger particles in the binary mixture leads to demixing where a larger particle rich domain will be formed in the range of external repulsive potential. This conjecture has been verified by dynamical density functional theory calculations (DDFT)[75] as well as Monte Carlo simulations[74]. It must be noted that this

18

type of external repulsive potential can be realized experimentally[76].

Now the molecular dynamics(MD) study of same model system of binary colloids of soft spheres, without the confining wall, reveals that depletion interaction between the larger components and the barrier modifies the dynamics of both the components of the mixture significantly[77]. At higher temperatures, the mean squared displacements of both species in the mixture shows linear behavior and the smaller particles diffuses faster than the larger particles as expected. However, as temperature decreases, the mean squared displacement of smaller particles deviates from the linear behavior and a plateau appears at intermediate times. This is quite similar to the dynamics of supercooled liquids even though the density at which this behavior is observed is much lower compared to the supercooled liquids. This is further validated through the non-zero non-Gaussian parameter at intermediate times as well as non-exponential decay of self intermediate scattering function. However, even at lower temperatures, the larger particles undergoes normal diffusion as shown by linear behavior of the mean squared displacement. Also at lower temperatures, the long-time self-diffusion coefficient of larger particles decreases very slowly compared to that of smaller particles, thereby exhibiting a crossover of diffusivity of the two components in the mixture at lower temperatures. These contrasting behaviors of dynamics of the components are explained by the attractive depletion interaction between the potential barrier and larger particles. This depletion interaction decreases the effective barrier for larger particles, while it increases the effective barrier of the diffusion of smaller particles. Thus smaller particles get localized between the external potential barriers, slowing down their dynamics. Meanwhile, the larger particles continues to exhibit normal diffusion because of the decrease in the effective barrier height.

We further studied this model system and extended the investigation to include the barrier crossing problems in this thesis. The temperature dependence of diffusivity show interesting behavior at low volume fraction. The larger components follow sub-Arrhenius

19

behavior which is seldom reported before for a classical system. At higher density we observe crystallization in the region of external potential barrier. We also investigated this system for asymmetric external potential which reveals a sub to super Arrhenius transition in the diffusivity of larger particles as the asymmetry in the potential increases. All these investigations are carried out using the molecular dynamics simulations.

## 1.6 Simulation Method

In this section, we will briefly describe the molecular dynamics simulations, which was used in all the studies detailed in this thesis. Using computer simulations to study the equilibrium as well as the dynamic properties of condensed matter systems began in 1950s. Two most important methods of the molecular simulations were introduced then, namely the Monte Carlo simulations[78] and the molecular dynamics(MD) simulations[79, 80]. While Monte Carlo simulations estimate the average value of a system property by averaging over a collection of system configurations generated randomly from the probability distribution belonging to a particular statistical mechanical ensemble, the idea behind molecular simulations is to solve the Newton's equations of motion for the classical particles in the system. Thus, MD simulations provide the time averages of the physical properties of the system. Besides this, MD allows one to monitor the time evolution of the system, thus providing access to the dynamical properties of the system.

### 1.6.1 Principle

Molecular dynamics simulation is a numerical technique to generate a dynamical trajectory for a system composed of $N$ particles by integrating Newton's equations of motion. To carry out these simulations, we need a set of initial conditions and a good model to represent the interaction between the particles. Then the Newton's equation of motion for each particles are solved :

$$m_i \frac{d^2 \mathbf{r}_i}{dt^2} = \mathbf{f}_i = -\frac{\partial}{\partial \mathbf{r}_i} U(\mathbf{r}_1, \mathbf{r}_2....\mathbf{r}_N) \qquad (1.14)$$

where $U(\mathbf{r}_1, \mathbf{r}_2....\mathbf{r}_N)$ is the potential energy which depends on the particle coordinates only. These are $N$ coupled, second order nonlinear differential equations which can not be solved analytically. So we need to resort to a numerical integration scheme.

## 1.6.2   Initial conditions

Since we are solving second order differential equations, we need to know the initial positions and velocities of each particle in the system. Typically, we create an ordered structure for initial positions and melt it. This is to overcome the possibility of particles overlapping, if we create a randomly distributed initial positions. The velocities of the particles are selected randomly from a Maxwell-Boltzmann distribution centered on the desired temperature. Then these are scaled in such a way that the linear momentum of the center of mass is zero.

## 1.6.3   Evaluation of forces

The potential energy of the system can be divided into interactions between pairs, triplets, quadruplets, etc. of particles,

$$U(\mathbf{r}_1, \mathbf{r}_2....\mathbf{r}_N) = \sum_{ij} U_{ij}(\mathbf{r}_i, \mathbf{r}_j) + \sum_{ijk} U_{ijk}(\mathbf{r}_i, \mathbf{r}_j, \mathbf{r}_k) + \sum_{ijkl} U_{ijkl}(\mathbf{r}_i, \mathbf{r}_j, \mathbf{r}_k, \mathbf{r}_l) \quad (1.15)$$

The interaction energy is largely dominated by the pair term and we truncate this series at the first term. In simulations, many a times, the true pair potential is replaced by the effective pair potential which incorporates the average many-body effects into the first term. These inter particle pair potential is usually parameterised to reproduce the known experimental data. Then the force on each particle can be calculated by differentiating the pair potential and summing over all the pairs.

## 1.6.4 Boundary conditions

In most of the simulation studies, we are interested in the bulk properties of the system, which requires the number of particles $N$ to be very large, of the order of Avogadro's number. However the computational resources available today do not allow us to simulate such large systems. So we need to implement some boundary conditions. We could use hard walls, but then surface effects will assume significance and real bulk physics will be blurred. This is beacuse the fraction of particles near the walls goes as $N^{-1/3}$, which will be very substantial when we simulate a system of the order of $10^3$ particles. So we need to use periodic boundary conditions(PBC); i.e., the simulation box is surrounded by an infinite number of replicas of itself. Only $N$ particles inside the original simulation box are considered explicitly, but as soon as one particle leave from box, an image particle enters from the opposite side to replace it. Because of the PBC, we need to follow the minimum image convention while calculating the pair distances; i.e. for every pair of particles, we need to calculate the distance between the closest images of the particles.

## 1.6.5 Integration algorithms

In the previous subsections, we have already mentioned that we need to solve the Newton's equations of motion numerically. This means we need to discretize the trajectory and use an integration algorithm to advance the trajectory through small time steps. The apparent solution would be to use a Taylor expansion of the position at time $t+\Delta t$ around the position at time $t$.

$$\mathbf{r}_i(t + \Delta t) = \mathbf{r}_i(t) + \frac{d\mathbf{r}_i(t)}{dt}\Delta t + \frac{1}{2}\frac{d^2\mathbf{r}_i(t)}{dt^2}\Delta t^2 + O(\Delta t^3) \tag{1.16}$$

But this algorithm is proved to be inaccurate as well as unstable. Verlet[81] proposed a better algorithm by summing Taylor expansion of $\mathbf{r}_i(t + \Delta t)$ and $\mathbf{r}_i(t - \Delta t)$, thereby cancelling

all the odd terms. So we obtain,

$$\mathbf{r}_i(t + \Delta t) = 2\mathbf{r}_i(t) - \mathbf{r}_i(t - \Delta t) + \frac{d^2\mathbf{r}_i(t)}{dt^2}\Delta t^2 + O(\Delta t^4) \tag{1.17}$$

Since the first order terms in the expansions cancenl out, velocities are not used in this algorithm. But they can be obtained as:

$$\mathbf{v}_i(t) = \frac{1}{2\Delta t}\Big[\mathbf{r}_i(t + \Delta t) - \mathbf{r}_i(t - \Delta t)\Big] \tag{1.18}$$

Two equivalent algorithms producing the same trajectory are the velocity Verlet algorithm[82],

$$\mathbf{r}_i(t + \Delta t) = \mathbf{r}_i(t) + \mathbf{v}_i(t)\Delta t + \frac{1}{2}\mathbf{a}_i(t)\Delta t^2 \tag{1.19}$$

$$\mathbf{v}_i(t + \Delta t) = \mathbf{v}_i(t) + \frac{1}{2}\Big[\mathbf{a}_i(t) + \mathbf{a}_i(t + \Delta t)\Big] \tag{1.20}$$

and the leap-frog algorithm[83],

$$\mathbf{r}_i(t + \Delta t) = \mathbf{r}_i(t) + \mathbf{v}_i(t + \Delta t/2)\Delta t \tag{1.21}$$

$$\mathbf{v}_i(t + \Delta t/2) = \mathbf{v}_i(t - \Delta t/2) + \mathbf{a}_i(t)\Delta t \tag{1.22}$$

One disadvantage of the leap frog algorithm is that the velocities are not known at the same time as the positions, thereby making it difficult to calculate the total energy at any one point of time.

Higher order integration algorithms are possible and known to be more accurate than the above algorithms. The Gear Predictor- corrector algorithm[84] is one such method which uses more terms in the Taylor expansions of positions and velocities. It also uses the new forces after a time step to back correct for the extrapolation in time. In this thesis, we use a fourth order corrector-predictor algorithm for the molecular dynamics simulations. Here the predicted step is the Taylor expansion of positions and their derivatives,

$$\mathbf{r}_i^p(t + \Delta t) = \mathbf{r}_i(t) + \mathbf{v}_i\Delta t + \frac{1}{2}\mathbf{a}_i(t)\Delta t^2 + \frac{1}{6}\frac{d^3\mathbf{r}_i}{dt^3}\Delta t^3 \tag{1.23}$$

$$\mathbf{v}_i^p(t + \Delta t) = \mathbf{v}_i(t) + \mathbf{a}_i(t)\Delta t + \frac{1}{2}\frac{d^3\mathbf{r}_i}{dt^3}\Delta t^2 \tag{1.24}$$

$$\mathbf{a}_i^p(t + \Delta t) = \mathbf{a}_i(t) + \frac{d^3\mathbf{r}_i}{dt^3}\Delta t \tag{1.25}$$

$$\frac{d^3\mathbf{r}_i}{dt^3}^p = \frac{d^3\mathbf{r}_i}{dt^3} \tag{1.26}$$

After the prediction step, the forces and therefore the accelerations are calculated for the new positions. Then the correction in the predicted accelerations will be,

$$\Delta\mathbf{a}_i(t + \Delta t) = \mathbf{a}_i^c(t + \Delta t) - \mathbf{a}_i^p(t + \Delta t) \tag{1.27}$$

This error in acceleration is used to correct the predicted values during the correction step.

$$\mathbf{r}_i^c(t + \Delta t) = \mathbf{r}_i^p(t) + c_0\Delta\mathbf{a}_i(t + \Delta t) \tag{1.28}$$

$$\mathbf{v}_i^c(t + \Delta t) = \mathbf{v}_i^p(t) + c_1\Delta\mathbf{a}_i(t + \Delta t) \tag{1.29}$$

$$\mathbf{a}_i^c(t + \Delta t) = \mathbf{a}_i^p(t) + c_2\Delta\mathbf{a}_i(t + \Delta t) \tag{1.30}$$

$$\frac{d^3\mathbf{r}_i}{dt^3}^c = \frac{d^3\mathbf{r}_i}{dt^3}^p + c_3\Delta\mathbf{a}_i(t + \Delta t) \tag{1.31}$$

Here, $c_0, c_1, c_2$ and $c_3$ are known as Gear coefficients chosen for the stability and accuracy of the trajectories.

## 1.6.6 Thermostats

The integration of Newton's equations of motion(1.14) keeps the number of particles $N$, volume $V$ and, total energy $E$ constant, which implies that we generate the trajectory of the system in microcanonical ensemble. However, we may prefer to work with constant temperature, i.e., in canonical ensemble in order to compare the simulation results with experimental results. This can be done through using one of the thermostats.

24

The temperature of the system is directly related to the kinetic energy of the system through fluctuation-dissipation theorem. So we can change the temperature of the system by modifying the velocities of the particles. Thus the simplest method to control the temperature is through velocity rescaling; i.e. rescale the velocities of all the particles by a factor $\sqrt{T_d/T_i}$, where $T_d$ is the desired temperature and, $T_i$ is the instantaneous temperature of the system just before scaling. However, this scheme does not allow one to sample the true canonical ensemble and the scaling can affect the dynamics in an unpredictable way. A more physical way to use a thermostat is to couple the system to a thermal bath at desired temperature. Several such thermostats are in practise. For example, Berendsen thermostat[85] uses a weak coupling of the system to the heat bath. This is done by modifying the acceleration to

$$\mathbf{a}_i = \frac{\mathbf{f}_i}{m_i} + \frac{1}{2\tau}\Big(\frac{T_d}{T(t)} - 1\Big)\mathbf{v}_i \tag{1.32}$$

The additional term acts as a frictional force and $\tau$ is the coupling coefficient which determines the strength of the coupling. In the limit of infinite coupling, the scheme recovers microcanonical ensemble and in the limit of very small coupling, i.e. $\tau \to \Delta t$, it is equivalent to velocity scaling. So it can affect the system dynamics, if very small values of the coupling parameters are used.

Another thermostat which is used frequently in molecular dynamics simulations is Andersen thermostat[86], which again uses a coupling to a heat bath; but in this case coupling is done by stochastic forces on randomly selected particles. The coupling strength is determined by the frequency of collisions of particles with particles in the heat bath. At each collision, the particles gets a new velocity selected from a Maxwell-Boltzmann distribution at the desired temperature. This thermostat sample the canonical ensemble, but the dynamics of the system is observed to be depending on the collision frequency.

One of the most used thermostat in molecular dynamics simulations is the Nose-Hoover thermostat[87, 88, 89]. In this method, thermostat is considered to be a part of the system by adding a variable and associated effective mass to the system. Thus we define an extended Lagrangian and derive the equations of motion for particles as well as the new variable. This method sample the correct canonical ensemble and does not affect the system dynamics severely. The main drawback of this method is the temperature goes to the desired value in an oscillatory way and in some cases takes too long to achieve the canonical distribution.

Another thermostat which is also commonly used in MD simulations is the Gaussian thermostat[90]. This thermostat makes use of Lagrange's multiplier technique to constraint the temperature to the desired value. Hence the equations of motion become,

$$\dot{\mathbf{x}}_i = \mathbf{p}_i/m \tag{1.33}$$

$$\dot{\mathbf{p}}_i = \mathbf{F}_i - \lambda\mathbf{p}_i \tag{1.34}$$

Here $\mathbf{x}_i$ and $\mathbf{p}_i$ are the position and momentum vectors of $i^{th}$ particle and $\mathbf{F}_i$ is the net force acting on the particle. And $\lambda$ is the Lagrange's multiplier, determined by the Gaussian principle of least constraint as,

$$\lambda = \frac{\sum_i m\mathbf{F}_i \cdot \mathbf{p}_i}{\sum_i \mathbf{p}_i \cdot \mathbf{p}_i} \tag{1.35}$$

This thermostat samples isothermal-isokinetic ensemble and does not have any undue effect on the system dynamics. And it is found to be very accurate unless the number of particles are very less. It is also very easy to implement numerically and therefore used in the simulations for the work described in this thesis.

In this thesis work we have carried out the molecular dynamics simulations on a model system of colloidal mixture in canonical-isokinetic ensemble. These simulations solve the system of first order differential equations (equations 1.33, 1.34) numerically by the fifth order Gear predictor-corrector algorithm and Gaussian thermostat is used to constraint the

temperature. This model system comprises of small and large spherical colloids with diameters $\sigma_{ss}$ and $\sigma_{ll}$ respectively. These colloidal particles interact via a soft sphere repulsion which is given by

$$V_{ab}(r_{ij}) = \epsilon_{ab}\left(\frac{\sigma_{ab}}{r_{ij}}\right)^{12} \qquad (1.36)$$

where $r_{ij}$ is the inter-particle distance and $(a, b) \in (l(large), s(small))$. The cross interaction parameters are obtained using Lorentz-Berthelot mixing rule; i.e., $\epsilon_{sl} = \sqrt{\epsilon_{ss} * \epsilon_{ll}}$ and $\sigma_{sl} = (\sigma_{ss} + \sigma_{ll})/2.0$. The masses of two species are kept same since we do not want the effect of mass difference to be coupled with the effect of depletion interaction in the dynamics of the binary mixture. In addition to the interaction among the constituent particles, they are also subjected to an external repulsive barrier of Gaussian form at the center of the simulation box along $z-$ direction only[77],

$$V_{ext}(z) = \epsilon_{ext}\ e^{-\left(\frac{z-(L/2)}{w}\right)^2} \qquad (1.37)$$

Where $w$ is the width and $\epsilon_{ext}$ is the height of the external barrier. $L$ is the simulation box length and the periodicity of the applied external potential. The periodic boundary conditions are applied in all the three spatial directions. The simulations were done for different total volume fractions and different boxlengths to observe the changes in the structure and dynamics of the system when the volume fraction increases. It is repeated for three times for each state point and the average value of dynamical properties are calculated after the equilibration of the system. These model system has been extensively studied in both low and high volume fractions and we found that the depletion interactions between the large particles and the potential barrier causes interesting phenomena which are discussed in following chapters. In addition to this we have also taken an asymmetric external potential at the center of the simulation box and carried out the simulation with same parameters. These details will be described in the thesis at appropriate chapters.

27

## 1.7 Outline of the Thesis

In this chapter we introduced about colloids and their interactions. We explained how depletion interaction is such an important phenomena in colloid science and its impact on understanding the physical behavior of the colloidal system and its applications. We discussed some of the effects of depletion interaction in monodisperse colloids and then the binary colloidal system. A brief idea about the molecular dynamics simulations is described and the model system we have implemented in this thesis work has been explained. We further want to understand the effect of an external potential on the structure and dynamics of binary colloidal system and the results we obtained by the MD simulations will constitute this thesis. The remaining thesis will be structured as follows:

**Chapter 2** contains the results obtained from the MD simulations of binary colloidal mixture in a Gaussian potential. We found that a classical system like ours can also exhibit a sub Arrhenius diffusion in one of their components in the mixture.

**Chapter 3** gives the results obtained at different volume fractions. We discuss the structural and dynamical properties of the binary mixture with respect to the volume fraction. We show that crystallization happen near the barrier for larger particles at higher volume fractions, even though they are much below the freezing volume fraction.

**Chapter 4** describes the simulations at different box lengths and the study of the scaling of the dynamical properties with system size.

**Chapter 5** gives the results of the simulation of binary colloids in an asymmetric potential. A transition happens from sub Arrhenius to super Arrhenius diffusion as the asymmetry increases in the external potential.

**Chapter 6** will summarize the thesis and give some future directions of our work.

# References

[1] R. Brown, *Phil. Mag.* **4**, 161 (1828).

[2] R. Brown, *Phil. Mag.* **6**, 161 (1829).

[3] T. Graham, *Philosophical Transactions of the Royal Society (London)*, **151**, 183–224 (1861).

[4] A. Einstein, *Ann. Phys.* **17**, 549-560 (1905).

[5] H. N. W. Lekkerkerker, R. Tuinier, Colloids and the depletion interaction (Springer, New York, 2011).

[6] Richard A. L. Jones, Soft condensed matter (Oxford Univ. Press Inc., New York, 2002).

[7] B. V. Derjaguin, L. D. Landau, *Acta Physicochim.* **14**, 633 (1941).

[8] E. J. W. Verwey, J. T. G. Overbeek, Theory of the Stability of Lyophobic Colloids (Elsevier/Academic Press, Amsterdam, 1948).

[9] B. V. Derjaguin, Theory of Stability of Colloids and Thin Films (Consultants Bureau, New York, London, 1989).

[10] J. N. Israelachvili, Intermolecular and Surface Forces (Academic Press, 3rd edition, 2011).

[11] S. Asakura, F. Oosawa, *J. Chem. Phys.* **22**, 1255 (1954).

[12] S. Asakura, F. Oosawa, *J. Polymer Sci.* **33**, 183 (1958).

[13] A. Vrij, *Pure Appl. Chem.* **48**, 471 (1976).

[14]  R. Tuinier, J. Rieger, C. G. de Kruif, *Adv. Colloid Interface Sci.* **103**, 1 (2003).

[15]  W. C. K. Poon, *J. Phys.: Condens. Matter* **14**, R859 (2002).

[16]  Y. Snir, R. D. Kamien, *Science* **307**, 1067 (2005).

[17]  R. Fahraeus, *Physiol. Rev.* **9**, 241 (1929).

[18]  J. E. Thysegen, *Acta Med. Scand. Suppl.* **134**, 1 (1942).

[19]  J. Traube, *Gummi Zeitung.* **39**, 434 (1925).

[20]  H. C. Baker, *Inst. Rubber Ind.* **13**, 70 (1937).

[21]  C. F. Vester, *Kolloid Z.* **84**, 63 (1938).

[22]  S. S. Cohen, *J. Biol. Chem.* **144**, 353 (1942).

[23]  R. Li-In-On, B. Vincent, F. A. Waite, *ACS Symp. Ser.* **9**, 165 (1975).

[24]  B. Vincent, P. F. Luckham, F. A. Waite, *J. Colloid Interface Sci.* **73**, 508 (1980).

[25]  B. Vincent, J. Edwards, S. Emmett, A. Jones, *Colloids and Surfaces.* **17**, 261 (1986).

[26]  B. Vincent, J. Edwards, S. Emmett, R. Croot, *Colloids and Surfaces.* **31**, 267 (1988).

[27]  S. Hachisu, A. Kose, Y. Kobayashi, *J Colloid Interface Sci.* **55**, 499 (1976).

[28]  A. Kose, S. Hachisu, *J. Colloid Interface Sci.* **55**, 487 (1976).

[29]  H. De Hek, A. Vrij, *J. Colloid Interface Sci.* **70**, 592 (1979).

[30]  H. De Hek, A. Vrij, *J. Colloid Interface Sci.* **84**, 409 (1981).

[31]  J. F. Joanny, L. Leibler, P. G. De Gennes, *J. Polymer Sci. Polym. Phys.* **17**, 1073 (1979).

[32]  R. I. Feigin, D. H. Napper, *J. Colloid Interface Sci.* **75**, 525 (1981).

[33] J. M. H. M. Scheutjens, G. J. Fleer, *J. Phys. Chem.* **83**, 1619 (1979).

[34] J. M. H. M. Scheutjens, G. J. Fleer, *Adv. Colloid Interface Sci.* **16**, 361 (1982).

[35] A. D. Dinsmore, A. G. Yodh, D. J. Pine, *Phys. Rev. E.* **52**, 4045–4057 (1995).

[36] A. Imhof, J. K. G. Dhont, *Phys. Rev. Lett.* **75**, 1662–1665 (1995).

[37] U. Steiner, A. Meller, J. Stavans, *Phys. Rev. Lett.* **74**, 4750–4753 (1995).

[38] S. M. Ilett, A. Orrock, W. C. K. Poon, P. N. Pusey, *Phys. Rev. E.* **51**, 1344–1352 (1995).

[39] P. Gast, C. K. Hall, W. B. Russel, *J. Colloid Interface Sci.* **96**, 251 (1983).

[40] E. Eisenriegler, *J. Chem. Phys.* **79**, 1052 (1983).

[41] C. Allain, D. Ausserré, F. Rondelez, *Phys. Rev. Lett.* **49**, 1694 (1982).

[42] P. G. De Gennes, Scaling Concepts in Polymer Physics (Cornell Univ. Press, Ithaca, 1979).

[43] H. N. W. Lekkerkerker, *Colloids and Surfaces* **51**, 419 (1990).

[44] F. Leal-Calderon, J. Bibette, J. Biais, *Europhys. Lett.* **23**, 653 (1993).

[45] J. S. Van Duijneveldt, K. Mutch, J. Eastoe, *Soft Matter* **3**, 155 (2007).

[46] R. Tuinier, J. K. G. Dhont, C. G. de Kruif, *Langmuir* **16**, 1497 (2000).

[47] J. Buitenhuis, L. N. Donselaar, P. A. Buining, A. Stroobants, H. N. W. Lekkerkerker, *J. Colloid Interface Sci.* **175**, 46 (1995).

[48] Z. Dogic, K. R. Purdy, E. Grelet, M. Adams, S. Fraden, *Phys. Rev. E.* **69**, 051702 (2004).

[49] F. M. Van der Kooij, M. Vogel, H. N. W. Lekkerkerker, *Phys. Rev. E.* **62**, 5397 (2000).

[50] A. D. Dinsmore, D. T. Wong, *et al. Phys. Rev. Lett.* **80**, 409 (1998).

[51] F. Zosel F, A. Soranno, K. Buholzer, D. Nettels, B. Schuler, *PNAS* **117**, 24, 13480-13489 (2020).

[52] Z. Yi, T. Ngai, *Colloids Interfaces* **4**, 36 (2020).

[53] P. N. Pusey, Liquid, freezing and the glass transition (North Holland: The Amsterdam, Netherland, 1991).

[54] W. C. K. Poon, E. R. Weeks, C. P. Royall, *Soft Matter* **8**, 21 (2012).

[55] Arnout Imhof, *Nanoscale Materials*, 423-454 (2003).

[56] J. S. Foresi, *et. al. Nature* **390**, 143-145 (1997).

[57] L. Jian, H. Yanchun, *Langmuir*, **22** 4, 1885–1890 (2006).

[58] G. A. Ozin, S. M. Yang, *Adv. Funct.Mater.* **11**, 95–104 (2001).

[59] V. Trappe, P. Sandkuhler, *Curr. Opin. Colloid Interface Sci.* **18**, 494−500 (2005).

[60] K.A. Dawson, *Curr. Opin. Colloid Interface Sci.* **7**, 218−227 (2002).

[61] J. K. G. Dhont, An Introduction to Dynamics of Colloids (Elsevier Science: Amsterdam, 1996).

[62] S. Auer, D. Frenkel, *Nature*, **409**, 1020 (2004).

[63] E. Weeks *et al. Science* **287**, 637 (2000).

[64] K. N. Pham, *et. al Science* **296**(5565), 104-6 (2002).

[65] W. C. K. Poon, *MRS Bulletin* **29** (2), 96–99 (2004).

[66] K. Qin, A. A. Zaman, *Journal of Colloid and Interface Science* **266**, 461-467 (2003).

[67] S. E. Paulin, B. J. Ackerson, *Phys. Rev. Lett.* **64**, 2663 (1990).

[68] M. Dijkstra, R. van Roji, R. Evans, *Phys. Rev. Lett.* **81**, 2268 (1998).

[69] K. Binder, D. P. Landau, M. Müller, *J. Stat. Phys.* **110**,1411 (2003).

[70] R. L. C. Vink, A. De Virgiliis, J. Horbach, K. Binder, *Phys. Rev. E* **74**, 031601 (2006).

[71] R. Roth, S. Dietrich, *Phys. Rev. E* **62**, 6926 (2000).

[72] H. N. W. Lekkerkerker, A. Stroobands, *Physica A* **195**, 387 (1993).

[73] A. Ayadim, S. Amorkane, *Phys. Rev. E* **74**, 021106 (2006).

[74] A. V. Anil Kumar, *J. Chem. Phys.* **138**, 154903 (2013).

[75] R. Roth, M. Rauscher, A. J. Archer, *Phys. Rev. E* **80**, 021409 (2009).

[76] J. J. Thorn, E. A. Schoene, T. Li, D. A. Steck, *Phys. Rev. Lett.* **100**, 240407 (2008).

[77] A.V. Anil Kumar, *J. Chem. Phys.* **141**, 034904 (2014).

[78] N. Metropolis, S. Ulam, *J Am Stat Assoc.* **44** (247), 335–341 (1949).

[79] B.J. Alder, T.E. Wainwright, Molecular Dynamics by Electronic Computers (Inter-science Pub., London, pp. 97–131, 1958).

[80] B.J. Alder, T.E. Wainwright, *J. Chem. Phys.* **31**, 459 (1959).

[81] L. Verlet, *Phys. Rev.* **159**, 98-103 (1967)

[82] William C. Swope, Hans C. Andersen, *J. Chem. Phys.* **76**, 637 (1982).

[83] A. Askar, A. S. Cakmak, *J. Chem. Phys.* **68**, 2794 (1978).

[84] C. W. Gear, Numerical Initial Value Problems in Ordinary Differential Equations, (Prentice-Hall, Upper Saddle River, 1971).

[85] H. J. C. Berendsen, J. P. M. Postma, W. F. van Gunsteren, A. DiNola, and J. R. Haak, *J. Chem. Phys.* **81**, 3684 (1984).

[86] Hans C. Andersen, *J. Chem. Phys.* **72**, 2384 (1980).

[87] S. Nose, *J. Chem. Phys.* **81**, 511 (1984).

[88] S. Nose, *Mol. Phys.* **52**, 255-268 (1984).

[89] W. G. Hoover, *Phys. Rev. A* **31**, 1695-1697 (1985).

[90] D. J. Evans, G. P. Morris, Statistical Mechanics of Nonequilibrium Liquids (Academic Press, London, 1990).

# Chapter 2

# Binary colloidal system in an external potential barrier : Temperature dependence and sub-Arrhenius Behavior

## 2.1 Introduction

Potential energy landscape is a very important concept in physical, chemical and biological sciences and has been widely used to to explain many important physical phenomena[1]. For example, the energy landscape perspective provides a unified framework for describing the thermodynamics and dynamics of supercooled liquids[2, 3, 4]. In studying protein folding phenomenon, the configurational changes are thought as meandering along the reaction coordinate in a funnel-like energy landscape[5, 6]. The lateral motion of proteins bounded to cell membranes is determined by the energy landscape formed by the interaction with surrounding lipids, proteins as well as with the cytoskeleton. Many such examples can be found in the dynamics and kinetics of physical, chemical and biological systems[7, 8]. So there has been an increasing interest to study the dynamics of particles in complex energy land scape. In general, the dynamical behavior of the particles is affected by the important features of the energy landscape; i.e., length scale, shape, amplitude etc. One of the widely used potential to study the equilibrium and dynamics behavior of particles is the sinusoidal potential. Many interesting results are obtained in the case of sinusoidal potential such as

re-entrant melting[9] and laser induced freezing[10]. The dynamics of particles in such potentials shows many similarities with the slowing down dynamics of supercooled liquids, despite being at a much lower density[11, 12]. Similar dynamics has also been found for colloids subjected to random energy landscapes[13].

When particles are subjected to such external potentials, they need to jump over the barriers in the energy landscape. These jumps are thermally activated and occurred not only in the dynamics of particles, but also in many other physiochemical processes, such as crystal nucleation from the melt[14, 15], polymer conformational changes[16, 17], cavitation[18], chemical and nuclear reactions[19, 20] thus spanning a wide range of different processes and fields. The most important measure in these process is the rate constant; reaction rate in the case of chemical reactions and diffusion coefficient in the case of diffusion. One of the most important aspects of rate constants is how they depend on the temperature. One of the most successful equations describing the temperature dependence of rate constant or diffusion coefficient is the Arrhenius equation, according to which the rate constant exponentially depend on the inverse of temperature. Many activated processes follow this temperature dependence and Arrhenius equation is widely regarded as one of the most important equations in the theory of activated processes. However, there are many instances of deviations from Arrhenius equation, especially at low temperatures.

## 2.2 Arrhenius Law

In the late nineteenth century, many scientists addressed the rate constant of thermally activated processes because of the increasing need to describe the temperature dependence of it. The first account of the study of rate constant was attributed to Wilhelmy as early as 1850[21]. While studying the chemical kinetics of sucrose inversion, he derived an equation for the instantaneous rate constant which depends on the instant concentration of the

reactants. Then others such as Berthelot(1862), Warder(1881), Schwab(1883), to name a few, attempted to come up with a working rate equation. In the year 1884, Van't Hoff in his famous text book on chemical dynamics discussed the temperature dependence of equilibrium constant in a chemical reaction in terms of equations[22]. However, it was until 1889 that the correct equation for the basic temperature dependence was proposed by Arrhenius[23]. He considered eight sets of published data on the temperature dependence of rate constants and showed that the dependence of temperature on rate constant can be represented as

$$k(T) = A \ exp\left(\frac{-E_a}{k_B T}\right) \tag{2.1}$$

Here $k$ is the rate constant, A is a constant and $E_a$ is the activation energy. In 1940, Kramers treated the thermally activated escape over a barrier as the escape of a metastable state and obtained the escape rate over the potential barrier subjected to a Gaussian white noise[24]. By solving the Fokker-Plank equation for the Brownian motion in phase space in the presence of nonlinear potential function, Kramers derived the Arrhenius equation for the temperature dependence of escape rate or equivalently for the diffusion coefficient as,

$$D(T) = D_0 \ exp\left(\frac{-E_a}{k_B T}\right) \tag{2.2}$$

Here $D_0$ is a constant, $E_a$ is known as the activation energy and $T$ is the absolute temperature. In Arrhenius equation, the activation energy $E_a$ is considered to be independent of temperature. Taking the logarithm of this equation:

$$lnD(T) = ln(D_0) - \frac{E_a}{k_B T} \tag{2.3}$$

i.e., the plot between $lnD$ and $1/T$ is linear and the activation energy can be obtained from the slope of the curve,

$$E_a = -\frac{\mathrm{d}lnD(T)}{\mathrm{d}(1/k_B T)} \tag{2.4}$$

The Arrhenius law is found to be very successful in describing the temperature dependence of many activated barrier crossing problems including particle diffusion in solids and liquids[25, 26], diffusion in microporous materials[27, 28], elementary chemical reactions[29, 30], enzymatic catalysis[31, 32], electrical conductivity in ionic liquids and super ionic conductors[33, 34] etc. This conspicuous success of Arrhenius law in describing these barrier crossing problems has elevated it to a canonical status for more than a century. However, it was soon realized that deviations from Arrhenius equation can occur because the mechanisms for these processes can have quite different dependencies on temperature. In general these deviations are observed at low temperatures. For example, in many chemical reactions where the mechanism involve quantum tunneling[35, 36, 37] or concurrent reactions[38, 39, 40] strong deviations from Arrhenius behavior is observed. In general the deviations from Arrhenius behavior can be classified in to two depending on the shape of the $lnD$ $vs.$ $1/T$ curve(Arrhenius plot). When the Arrhenius plot features a concave deviation, it is referred as a sub-Arrhenius process and for convex deviation, it is called super-Arrhenius process. Both of these observations are encountered in the experimental as well as the theoretical studies. These deviations correspond to a temperature dependent activation energy in contrast to the normal Arrhenius picture, where activation energy is treated as a constant independent of temperature.

## 2.3 Deformed Arrhenius equation

Recently a simple formalism was proposed to include the non-Arrhenius behavior in a unified manner[36, 41, 42, 43, 44]. This was inspired by the Tsallis's treatment of nonextensive statistical mechanics[45]. Tsallis proposed a probability distribution function instead of Boltzmann distribution as a generalization of entropy to cover the cases of non-extensivity.

$$P(E) = \left(1 - d\frac{E}{k_B T}\right)^{1/d} \tag{2.5}$$

Note that in the limit $d \to 0$, Boltzmann distribution is recovered. In fact, the basis of this formalism is Euler's discovery that the exponential function can be expressed as the limit of succession

$$exp(x) = \lim_{n \to \infty} \left(1 + \frac{x}{n}\right)^n \tag{2.6}$$

Now replacing $n$ with $1/d$ and identify $d$ as the continuous generalization of $1/n$, we can define a $d$-exponential function:

$$exp_d(x) \equiv (1 + dx)^{\frac{1}{d}} \tag{2.7}$$

Inspired by the Tsallis's distribution, Aquilanti *et al.* proposed a $d$-Arrhenius equation by replacing the deformed exponential in the Arrhenius equation

$$D(T) = D_0 \, exp_d\left(\frac{-E_0}{k_B T}\right) \tag{2.8}$$

Using the expression for $d$-exponential, this becomes

$$D(T) = D_0 \left[1 - \frac{dE_0}{k_B T}\right]^{1/d} \tag{2.9}$$

This is a unified formula representing both Arrhenius and non-Arrhenius behavior of diffusion. Note that in the limit $d \to 0$ it becomes Arrhenius equation. Here $E_0$ is the height of the potential barrier and $d$ is known as the deformation parameter, the sign of which will determine the nature of deviations from Arrhenius behavior. By taking the logarithm in both sides of equation 2.9:

$$lnD(T) = lnD_0 + \frac{1}{d}ln\left(1 - d\frac{E_0}{k_B T}\right) \tag{2.10}$$

The activation energy can be obtained by taking the negative of the derivative of this equation, as

$$
\begin{aligned}
E_a = -\frac{\mathrm{d}lnD(T)}{\mathrm{d}(1/k_B T)} &= E_0\left(1 - \frac{dE_0}{k_B T}\right)^{-1} \\
&\cong E_0 + d\frac{E_0^2}{k_B T} \quad \text{(for small } d\text{)} \tag{2.11}
\end{aligned}
$$

In this picture, $E_a$ is no longer a constant, but varies with temperature. The parameter $d$, known as "deformed parameter", basically determines the nature and shape of Arrhenius plot. As $d \to 0$, we recover Arrhenius equation and $E_a \to E_0$. For positive values of $d$, Arrhenius plots are convex and we get super-Arrhenius diffusion and for negative values of $d$, they are concave and sub-Arrhenius behavior is observed. From equation 2.11 , it is clear that the activation energy depends on temperature for both sub-Arrhenius and super-Arrhenius processes; however, the dependence is contrasting due to the sign of $d$. For super-Arrhenius behavior, activation energy increases with decrease in temperature, while for sub-Arrhenius behavior it decreases with decreasing temperature.

Super-Arrhenius behavior of diffusion is mainly found in systems where collective or cooperative dynamics is predominant such as dynamics of supercooled liquids[46, 47], diffusion through membranes[48, 49], macroscopic sliding of bacteria[50] etc. Meanwhile, sub-Arrhenius behavior is mainly seen in chemical reactions[41, 51, 52] and quantum tunneling was proposed to be responsible for such behavior. In fact, Bell model for incorporating tunneling in chemical kinetics was extended to correlate the deformation parameter $d$ with the parameters of the energy barrier[53, 54]. Therefore in the literature, there is a consensus that super-Arrhenius behavior occurs in classical systems, while sub-Arrhenius behavior occurs at processes where quantum tunneling plays a significant role. To the best of our knowledge, there has been no investigations reported in the literature of a classical system exhibiting sub-Arrhenius diffusion. However, sub-Arrhenius behavior has been observed in the sedimentation of weekly-aggregated colloidal gels[55] and in complex reactions[39, 40]. In this chapter we investigate the dynamics of a binary colloidal mixture of disparate sizes which is subjected to an external potential barrier using canonical ensemble molecular dynamics simulations. We show that one of the components in the binary mixture undergoes sub-Arrhenius diffusion, while the other component exhibits normal Arrhenius diffusion. This contrasting behavior of different components in the mixture

can be attributed to the attractive depletion interaction[56, 57, 58] between the potential energy barrier and the larger component in the mixture.

## 2.4    Model and Simulation details

We have carried out canonical ensemble molecular dynamics simulations of a binary mixture of colloids, consisting of large($l$) and small($s$) spherical particles, subjected to an external potential barrier. The particles interact through a purely repulsive potential in a periodically repeated cubic simulation box, at the center of which an external symmetric Gaussian potential is present along one of the spatial direction($z$). The interaction potential, $V_{ab}(r_{ij})$, between these particles is soft-sphere repulsion, given by

$$V_{ab}(r_{ij}) = \epsilon_{ab}\left(\frac{\sigma_{ab}}{r_{ij}}\right)^{12}$$

(2.12)

where $r_{ij}$ is the interparticle separation between two particles $i$ and $j$ and the indices $a$, $b$ correspond to $l$(large), $s$(small) colloidal particles. The interaction parameters are chosen as $\sigma_{ss} = 1.0$, $\sigma_{ll} = 2.0$, $\epsilon_{ss} = 1.0$ and $\epsilon_{ll} = 4.0$, all being expressed in reduced units. The Lorenz-Berthelot mixing rules are used to determine the interaction parameters between the large and small particles, i.e., $\sigma_{sl} = (\sigma_{ss} + \sigma_{ll})/2.0$ and $\epsilon_{sl} = \sqrt{\epsilon_{ss}\epsilon_{ll}}$. The external potential, in the form of Gaussian barrier at the center of the simulation box along the $z$-direction, is given by[57, 58],

$$V_{ext}(z) = \epsilon_{ext} \; e^{-\left(\frac{z-(L/2)}{w}\right)^2}$$

(2.13)

Here $\epsilon_{ext} = 3.0$ is the height of the potential barrier which the particles have to overcome during their motion and $L$ is the simulation boxlength. We chose the width of the external potential to be $w = 3.0$. Recent advances in experimental techniques make it possible to realize such external potential in colloidal systems[59]. Since we are interested in the depletion interactions and their effect on the dynamics of the system, the masses of both the

species of particles are kept equal. In this simulation,by using the algorithm of fifth order Gear predictor-corrector method[60], the equations of motions are solved in the presence of a thermostat determined by the Gaussian principle of least constraint[61]. Then the trajectories obtained from the simulations are recorded with a time step of $dt = 0.001$ in the reduced units of $([m\sigma_{ss}^2/\epsilon_{ss}]^{1/2})$. As in ref.[58], here also we use an equivolume mixture of both the species of the particles with a total volume fraction of $\phi = 0.20$. We have carried out the simulations for three different simulation boxlengths, i.e., $L = 13.0$, 15.0 and 17.0 to study the finite size effects on the dynamics. Keeping the total volume fraction to be fixed at $\phi = 0.20$ and varying the box lengths, the number of particles changes. These particles have to cross the barrier along the $z$-direction periodically at a distance equal to the box length as the periodic boundary conditions are applied along all the three directions. By varying the boxlengths we actually vary the periodicity of the external potential barrier along the $z$-axis. There are 52 large particles and 420 smaller particle in the case of $L = 13.0$, 81 large particles and 645 smaller particles for $L = 15.0$ and 117 large particles and 938 small particles for $L = 17.0$. For each box length, the simulation runs for a total of $5 \times 10^6$ timesteps with each timestep being $dt = 0.001$ in reduced units, out of which the first $1 \times 10^6$ steps are considered for equilibration of the system and remaining steps are used in calculating the equilibrium and dynamic properties. The simulations are repeated three times for different temperatures, varying from low to high ($T \in (0.25, 3.00)$), and the dynamical properties are averaged over these production runs.We have also carried out two sets of simulations in which only one of the components are present; i.e. either the small particles or the larger particles. The details for these simulations are same as that of binary mixtures except that they are single component simulations and volume fractions are kept 0.10 for both large and smaller particle systems. Hence the number density of the smaller particles systems is eight times higher than that of the larger particle systems.
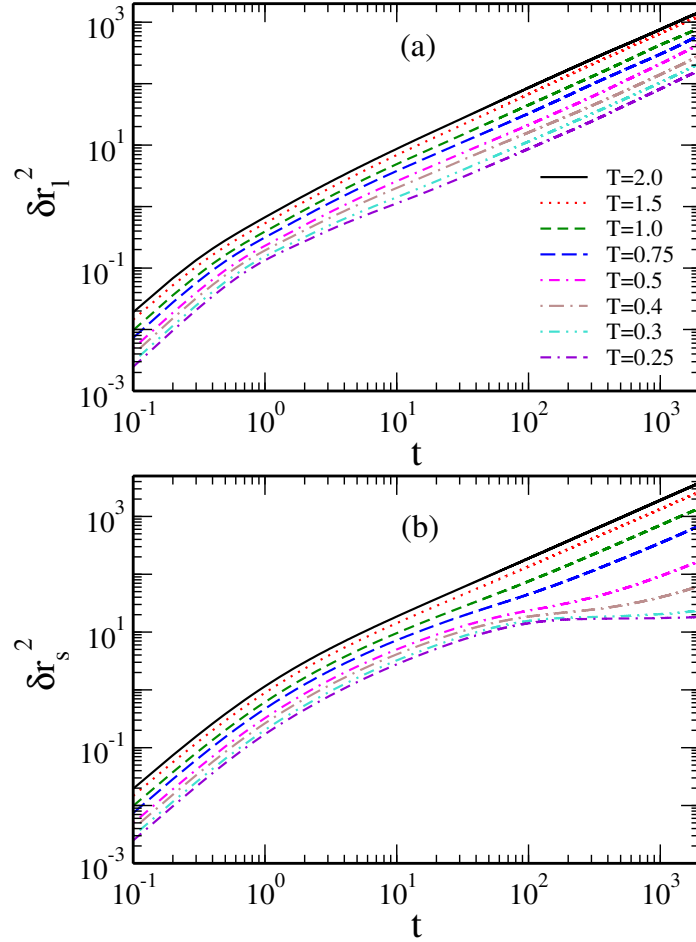
Figure 2.1: Mean squared displacement (MSD) of (a) large and (b) small particles at various temperatures in a binary mixture. MSD of large particles shows a linear relationship with time at all temperatures studied while that of small particles shows a slowing down in dynamics as temperature decreases.

## 2.5 Results and discussion

### 2.5.1 Mean squared displacement

The trajectories obtained from the MD simulations of a binary colloidal mixtures of soft spheres, in the presence of an external repulsive potential barrier of Gaussian form, are used to calculate the dynamical properties of the particles. To investigate the effect of depletion interaction on the constituent particles of the binary mixture, we have calculated the mean
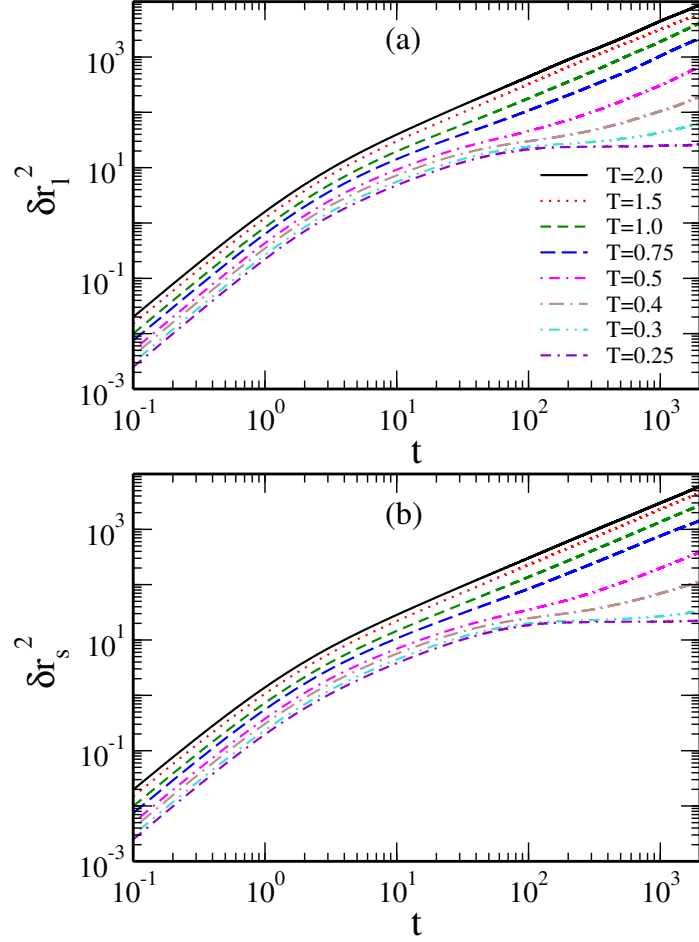
Figure 2.2: Mean squared displacement (MSD) of (a) large and (b) small particles at various temperatures in the single component systems. MSD of large particles also shows slowing down as temperature decreases.

squared displacement(MSD) of the constituent particles in both binary colloidal system and in single component system for temperatures ranging from $T= 0.25$ to $2.00$. The mean squared displacement(MSD) at time $t$ is defined as,

$$\delta r^2 = \frac{1}{N} \sum_{i=1}^{N} \langle (r_i(t) - r_i(0))^2 \rangle \tag{2.14}$$

The evolution of MSD with time for binary mixture is plotted in Figure 2.1. As reported earlier[12, 58], the MSD for the smaller particles is linear at higher temperatures, but shows a slowing down as the temperature decreases as manifested by an emerging plateau

at intermediate times before it regains the linear behavior. The smaller particles gets localized between the external potential barriers (multiple barriers occur because of the periodic boundary conditions) for a long time before it jumps over the barriers. This localization becomes stronger at lower temperatures as the particles possess lower kinetic energy to jump over the barriers. However, the behavior of MSD of larger particles is in stark contrast; it retains its linear behavior even at the lowest temperatures simulations. This behavior is attributed to the attractive depletion interaction between the external potential barrier and the larger particles. This attraction effectively reduces the energy barrier for the diffusion of larger particles and hence the dynamics of larger particles do not show any localization between the barriers unlike smaller particles. Here our results are in very good agreement with ref. [58]. Further these behaviors should be contrasted with the MSD of single component systems in the presence of the external barrier. In these simulations, we have either the smaller particles or larger particles with the external barrier and MSD was calculated from the MD trajectories. These are plotted in Figure 2.2. The MSD for smaller particles shows qualitatively similar behavior as in the case of binary mixture system, while that of larger particles shows very contrasting behavior compared to its counterpart in the binary mixture. Here the dynamics of larger particles also undergoes a slowing down as evidenced by the plateau in the MSD at intermediate times as temperature decreases. Since no smaller particles are present in the simulations here, there is no depletion interactions between the repulsive barrier and the larger particles. So the dynamics of larger particles here is essentially same as the smaller particle system (or the smaller particles in the binary mixture); they get localized between the barriers before escaping over the barrier.

## 2.5.2   Self diffusion coefficient and activation energy

We can get further evidence about how depletion interaction alters the dynamics of particles from the diffusion coefficient along the direction of external potential. Self diffusion coef-
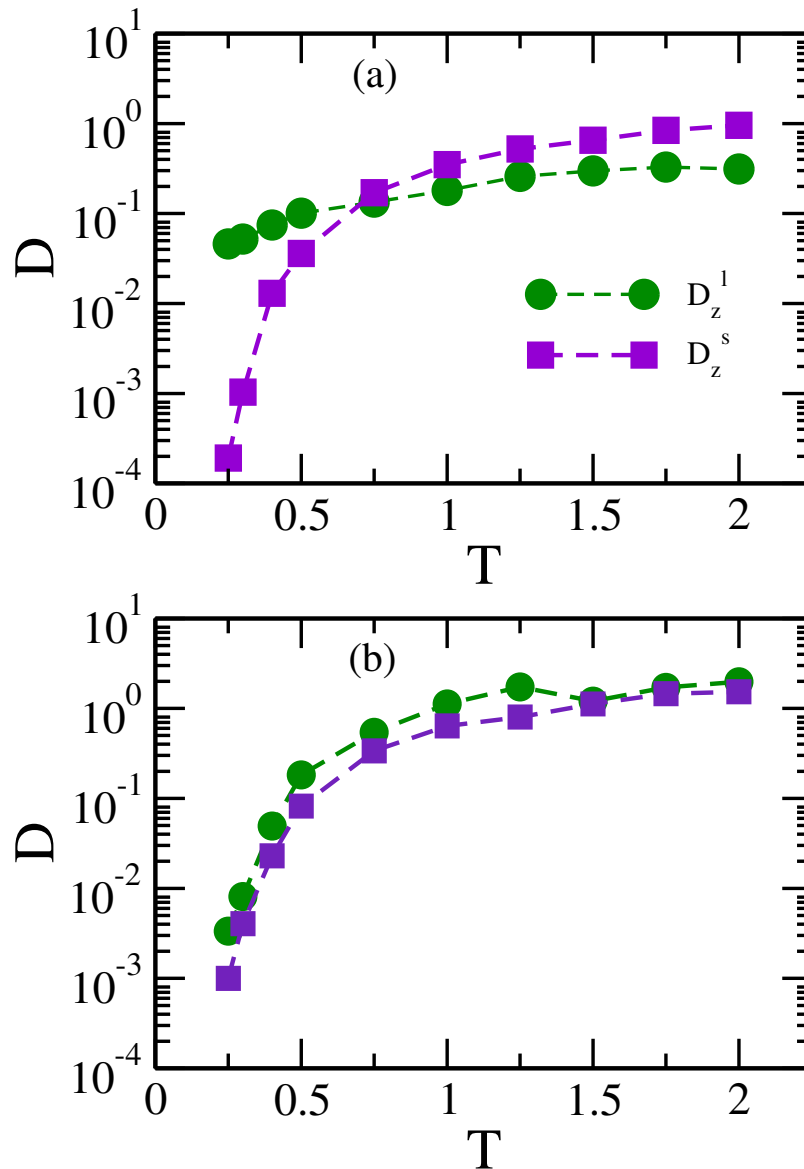
Figure 2.3: Self diffusivity of large and small particles in (a) binary system and (b) single component system, against temperature. (a) In case of binary mixtures, at higher temperatures, smaller particles diffuses faster than larger particles as expected. However, as temperature decreases, they undergoes a dynamic slowing down while larger particles diffuse faster, in agreement with reported results. (b) In single component system the diffusivities of both large and small particles decreases rapidly at lower temperatures.
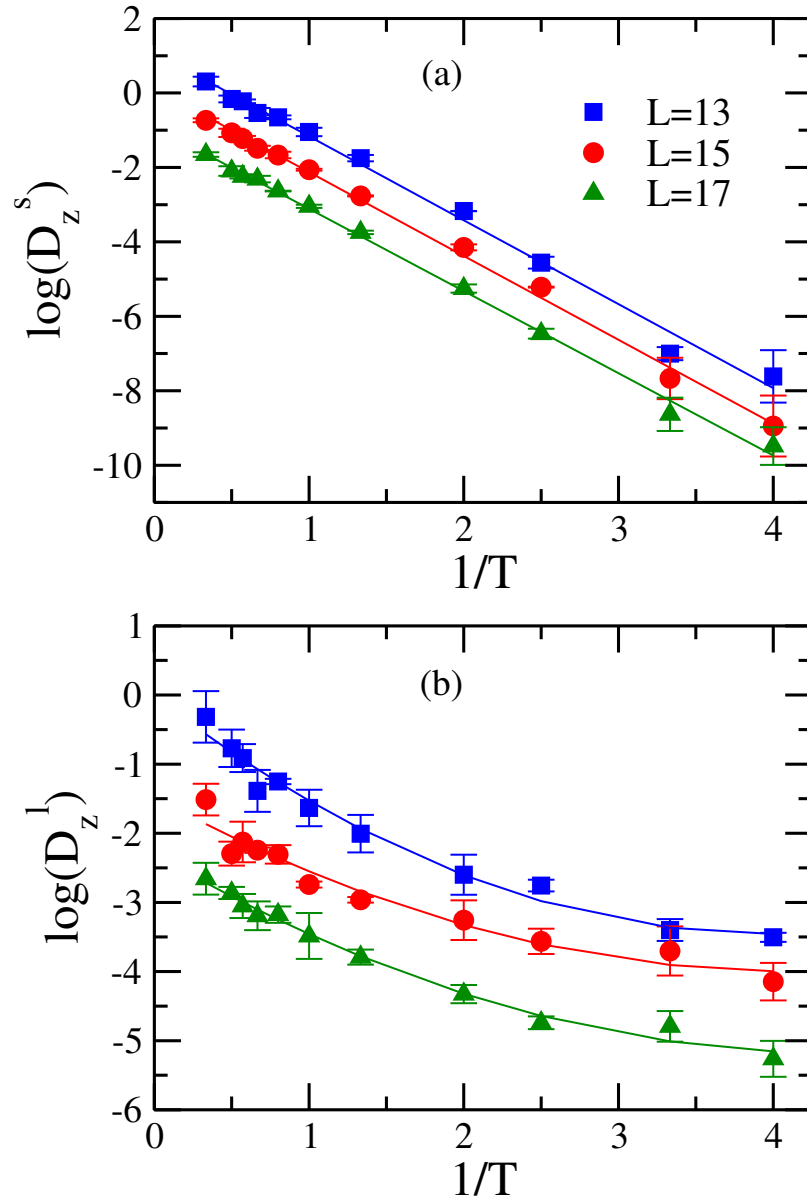
Figure 2.4: Arrhenius plot for (a) small particles and (b) large particles. Small particles follow Arrhenius law, while larger particles follow sub-Arrhenius behavior. The points are from simulation data and the lines are fits to Arrhenius or $d$-Arrhenius law. The data points for L = 15 and L = 17 shifted by 1 and 2 orders of magnitude. The activation energy for the smaller particles is found to be 2.24 and the $d$-parameter values in the case of larger particles are found to be -0.1453, -0.1983 and -0.1735 for L = 13, L = 15 and L = 17.0 respectively

ficient or diffusion constant or diffusivity can be obtained using Einstein's proportionality relation for the mean squared displacement in the long time limit as

$$\delta r^2 = 2nDt \tag{2.15}$$

where $n$ is the dimension of the system and $t$ is the time when the particles are in diffusive regime. We calculated the diffusion constant of both the species of particles along $z$- direction both in the case of binary mixture as well as single component systems. Figure 2.3 shows (a) the diffusion coefficients of small($D_z^s$) and large($D_z^l$) particles in the binary mixture; (b) diffusion coefficients of small and large particles in the single component system at different temperatures. In the binary mixture, at higher temperatures the small particles have enough thermal energy to overcome the barrier, hence diffuse faster than the large particles. However, as the temperature decreases, we observe a drastic fall in the diffusivity of small particles below $T = 0.75$, as evident from figure 2.3(a). This sharp decrease in diffusivity is not observed in the case of larger particles. Hence, at lower temperatures, the larger particles diffuses faster than the smaller particles. This contrasting behavior in the diffusivity of the components in the mixture can be explained in terms of the attractive depletion interaction between the external potential barrier and larger particles. Since the larger particles are getting attracted towards the barrier because of this depletion interaction, as evident from the density profile of the larger particles oulined in the next section, the effective barrier for them to cross over decreases which will enhance their dynamics. This is also manifested by the mean force of the potential , which is described later in this chapter. Meanwhile, because of this depletion interaction, the smaller particles stay away from the region of external potential barrier(see the density profile in next section) and effectively face a higher barrier to cross over. Thus the depletion interaction acts opposite for the two components in their dynamics and causes the larger particles to diffuse faster than the smaller counterparts. This behavior should be contrasted with dynamics of these
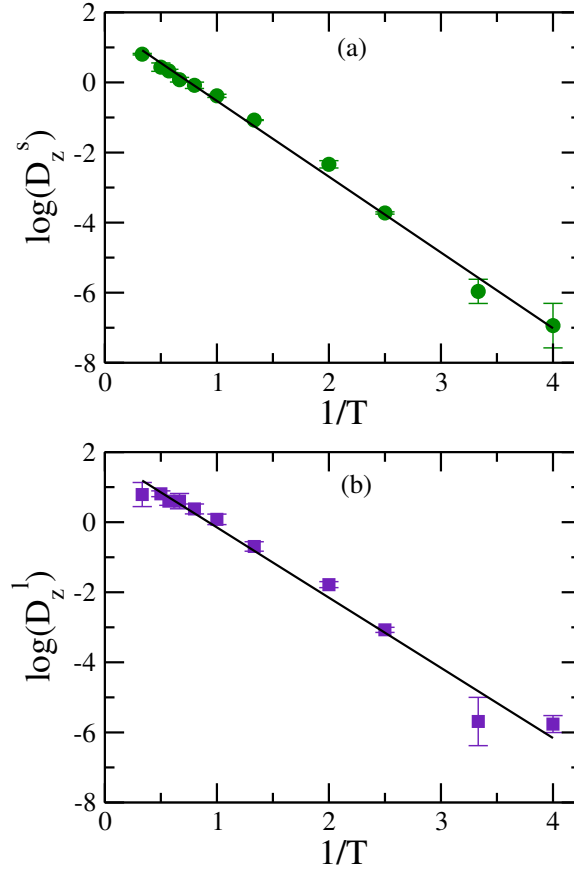
Figure 2.5: Arrhenius plot for (a) small particles and (b) large particles in single component systems for L = 15. Both the plots are linear and can be fitted with Arrhenius equation(solid lines).

particles in the single component case. In single component systems, there is no depletion interaction and both smaller as well as larger particles face the same energy barrier for their dynamics. So, the diffusivity of both small and large particles decreases rapidly at lower temperatures due to the localization of the particles between the barriers (see figure 2.3(b)).

As shown in figure 2.3(a), there is a sharp decrease in the self diffusivity of smaller particles below $T = 0.75$, while the diffusivity of larger particles decrease slowly below $T$=0.75. The slow change in the self-diffusion coefficient of larger particles suggests that the activation energy for their dynamics may be temperature dependent and the diffusion can be non-Arrhenius. In order to further verify this, we have plotted the $ln\ D$ versus

$1/T$ in figure 2.4 to show the Arrhenius plot for both the species of particles for different values of simulation box lengths. Please note that the data for $L = 15.0$ and $L = 17.0$ are shifted downwards by one and two orders of magnitude respectively for clarity. In fact the values of diffusivity at these three boxlengths overlap, suggesting the diffusivity does not depend on the boxlength. However, we have found that if we decrease the boxlengths to smaller values(i.e., as the periodicity of the external potential decreases), the dynamics of larger particles changes. This will be discussed in a later chapter in this thesis. From the figure, it is clear that that the diffusivity of small particles follow Arrhenius behavior for all boxlengths. But the Arrhenius plot for larger particles show a deviation from the linear behavior, and assumes a concave shape, indicating that they show a sub-Arrhenius behavior of temperature dependence. As mentioned earlier in this chapter, sub-Arrhenius behavior is observed mostly in systems where quantum tunneling is the main mechanism behind the activated process. But the results of our simulations suggests that a classical system can also show sub-Arrhenius behavior in the diffusion process. Moreover, the two components in the binary mixture follows different temperature dependence in their diffusional behavior. The Arrhenius plot of large particle diffusion is found to obey the d-Arrhenius equation as revealed by the nonlinear fits to the diffusivity data shown in Figure 2.4(b). The values of $d$ parameter obtained from the fitting are -0.1453, -0.1983 and -0.1735 for boxlengths 13.0, 15.0 and 17.0 respectively. The negative sign of $d$ indicates that the diffusion of larger particles are sub-Arrhenius[62]. Comparing it with the Arrhenius plot of single component systems under the influence of an external potential barrier which is given in Figure 2.5, it is seen that both large and small particles follow Arrhenius behavior in their temperature dependence of diffusivity. The diffusion coefficient of large particles is larger than that of small particles at all temperatures for single component systems, as the number density of larger particles is less than that of small particles.

Since the diffusion of larger particles is sub-Arrhenius, the activation energy should be

depending on temperature. This temperature dependent activation energy can be calculated by substituting the $d$ values obtained above in equation 11. This has been plotted at Figure 2.6 for the three different boxlengths.
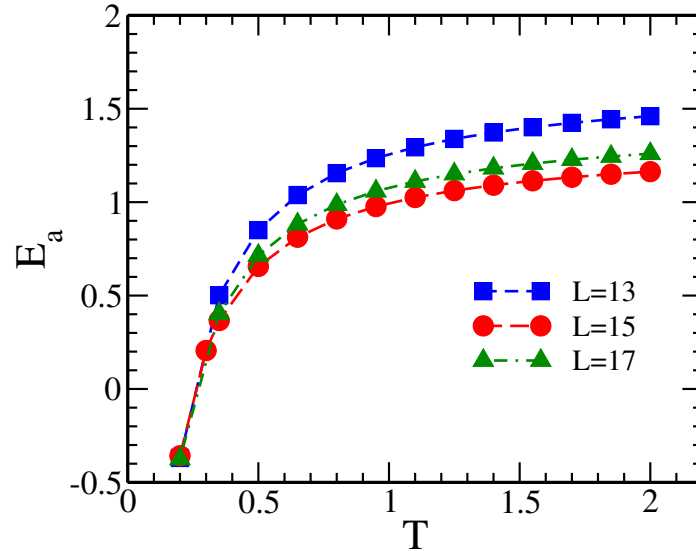


Figure 2.6: Activation energy of larger particles against temperature for L=13,15,17.

The first point to be noted is that the activation energy for diffusion is less than the external potential barrier at all temperatures. This is in contrast with the activation energy of smaller particles which is greater than the external barrier (2.1066 in single component systems and 2.24 in the binary mixture). This agrees with the earlier results that the depletion interaction effectively increases the barrier for smaller particles as they are driven away from the barrier. However, the attractive depletion interaction between the potential barrier and larger particles effectively lowers the barrier for the larger particles. The activation energy for the diffusion of larger particles is found to be 1.8984 in the single component systems, while in the binary system it is temperature dependent and decreases as the temperature decreases. The reduction in the activation energy is larger as the temperature is lowered. This essentially means the depletion interaction is temperature dependent and become more and more prominent as temperature decreases. This also explains why the diffusion coefficient

51

remains same or changes very slowly as temperature is lowered. The diffusivity depends on two factors here; namely activation energy and temperature or more precisely the ratio of activation energy to temperature. In case of smaller particles the activation energy remains constant; so the ratio of activation energy to temperature becomes larger as temperature decreases. This reduces the diffusivity rapidly. In case of larger particles, the activation energy decreases as temperature lowers so that the ratio changes very little at different temperature. This in turn ensures that the diffusivity of larger particles remains more or less same irrespective of the changes in temperature. Please note that the activation energy is negative at the lowest temperature studied. The effective activation energy comprises of two parts: the repulsive external potential and the attractive depletion interaction between the barrier and large particles. The depletion interaction becomes stronger as temperature decreases and at the lowest temperature it is strong enough that larger particles encounter an effective potential well rather than a potential barrier. This is manifested by the negative value for activation energy. As mentioned before, sub-Arrhenius behavior is observed so far only in systems where quantum tunneling is observed and believed to be a quantum phenomena. To the best of our knowledge, this is the first classical system to be reported to have a sub-Arrhenius behavior in the diffusion. Our results suggests that more than classical or quantum nature of the systems, it is the temperature dependence of activation energy which determines the sub-Arrhenius or super-Arrhenius deviations from the Arrhenius law of diffusion. It should be noted that an apparent sub-Arrhenius behavior has been observed in case of binary Lennard-Jones systems at high volume fractions[63]. However, when the mean squared displacement is corrected for the negative correlations for successive displacements, the diffusion is turn out be super-Arrhenius. Since the binary colloidal system we are investigating is at a much lower density, the successive displacements will not be negatively correlated and will not change the nature of diffusional process.

### 2.5.3 Density profile

It has been shown above that the depletion interaction causes the particles to experience the external potential barrier differently for smaller and larger particles. Further insight can be provided by calculating the density profile of both the species in binary and single component system. Figure 2.7 shows the density profile of binary mixture at various temperatures. The depletion induced attraction of larger particles towards the barrier at low temperatures can be visualized here in terms of split peaks around the barrier(see figure 2.7(a)).These peak height increases with decrease in temperatures which is consistent with the results we obtain in the diffusion constant versus temperature plot. In the mean time the smaller particles get depleted from the barrier region, their density is much smaller at the barrier region than the bulk density. The minimum in the density profile of smaller particles becomes more and more pronounced with decrease in temperature, indicating that they prefer to stay away from the region of external barrier and subsequently get localized between the barriers. In the case of single component system, the density profile of both the species of particles looks similar except the larger particles develop very little peak as the temperature goes down (see figure 2.8). Since there is no depletion interaction involved, both large and small particles' density is lower than their bulk density at the region of external potential barrier. This is again consistent with the results we obtained for the dynamics of each species.

### 2.5.4 Free energy and Mean force of interaction

The assertion that the depletion interaction effectively modifies the energy barrier can be further quantified by calculating the free energy of interaction along the z-direction for both components in the binary mixture as well as in the single component system. This is
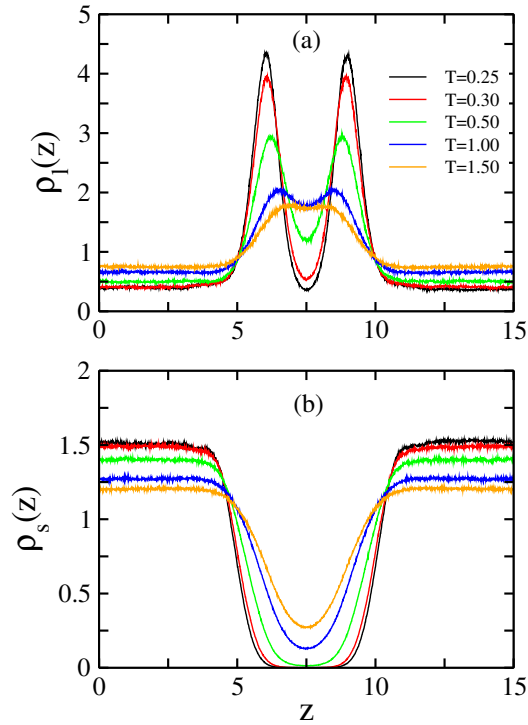
Figure 2.7: Density profile of (a) large and (b) small particles at various temperatures in the binary mixture for L=15.
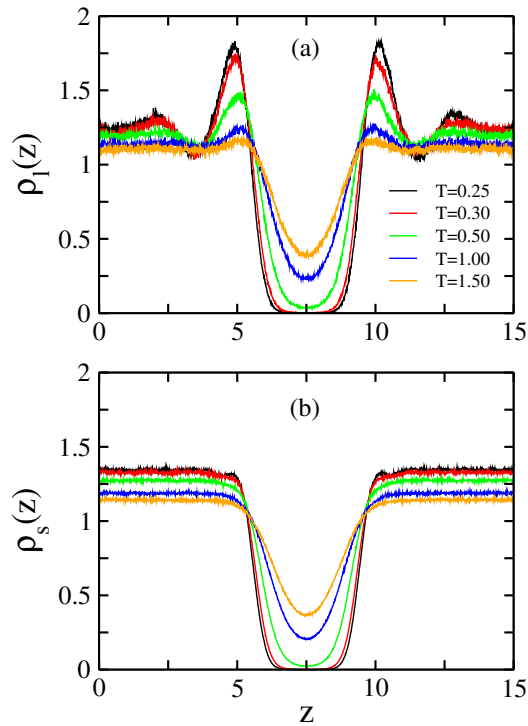


Figure 2.8: Density profile of (a) large and (b) small particles at various temperatures in the single component system for L=15.

obtained from the density profile of each of the components along the $z$-direction, using[64]

$$G(z) = -k_B T \; ln \; \rho_i(z) \tag{2.16}$$

where $\rho_i(z)$ is the density profile for each of the species along the z-direction normalized with respect to the bulk density. Figure 2.9 shows the free energy of interaction for smaller particles in two different systems; namely only smaller particles with the external potential barrier(dashed line) and the binary mixture with external potential barrier (solid lines) at four different temperatures. When only small particles are present, there is no depletion interaction and barrier does not get modified. However, the binary mixture invokes depletion interaction between the barrier and the larger particles. So the density of larger particles near the barrier increases and because of this crowding, the smaller particles will move away further from the barrier. This increases the effective free energy for smaller particles, which is evident in Figure 2.9. However, since the volume fraction is small, this decline in the density of smaller particles from the region of external potential barrier does not depend on temperature and hence the free energy of interaction remains unchanged with respect to temperature. So the effective potential barrier is temperature independent and the diffusion process remain Arrhenius. However at higher volume fractions, the effective barrier become temperature dependent and the diffusion becomes super-Arrhenius[65]. In the single component system when only smaller particles are present, there is no depletion interaction between the particles and the barrier, so the barrier does not get modified.

Figure 2.10 shows the free energy profile of larger particles for two different systems : (1) only larger particles with external potential barrier and (2) the binary mixture with external potential barrier at four different temperatures. There are few points to be noted here. Firstly, for larger particles in the binary mixture, there is a minimum for free energy of interaction at the spatial position of the external potential barrier rather than a maximum observed in the case of single component system or in the case of smaller particles in the
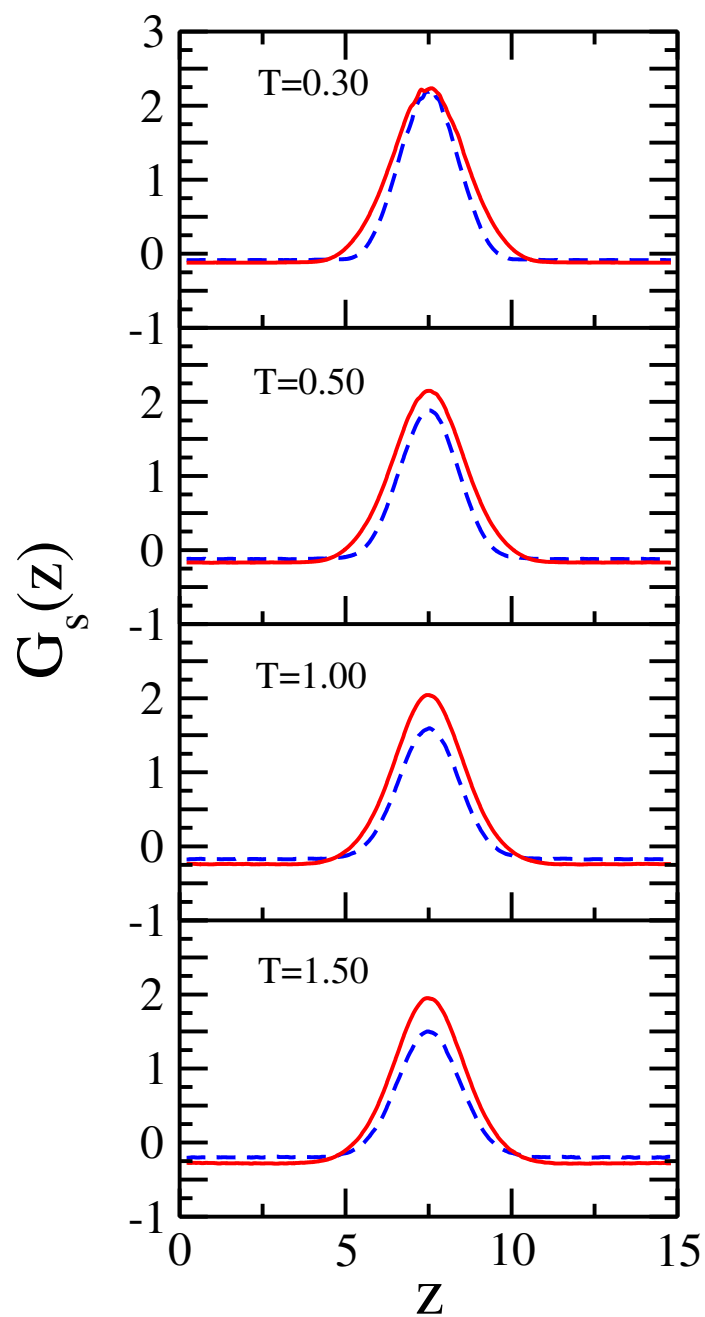
Figure 2.9: Free energy of interaction for the smaller particles along the z - direction when the system has only small particles(dashed lines) and when both large and small particles present (solid lines).
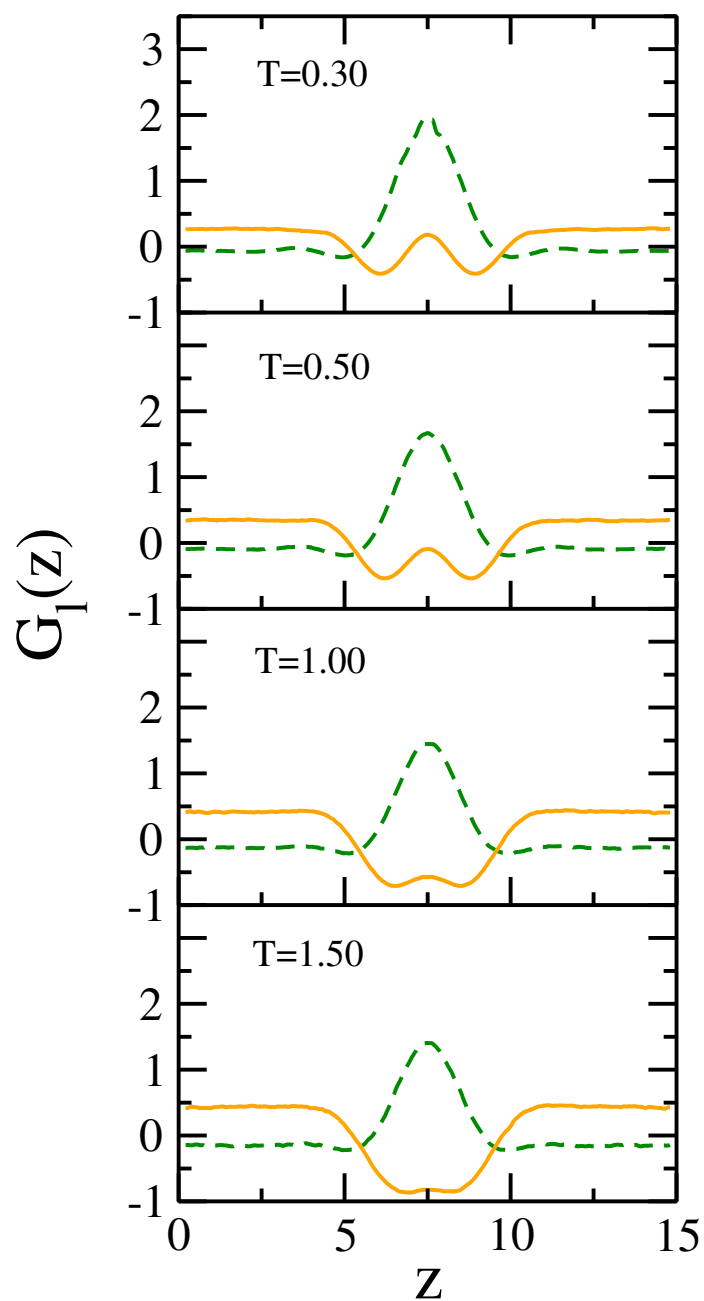
Figure 2.10: Free energy of interaction for the larger particles along the z - direction when the system has only large particles(dashed lines) and when both large and small particles present (solid lines).

binary mixture. So here the free energy barrier that the particles have to face in their dynamics is the difference in free energy between this minimum and that of bulk(free energy value away from the external potential barrier). This barrier height is much smaller compared to the barrier height particles have to cross in single component system. Secondly, for the single component system the barrier height does not change significantly with respect to temperature while the barrier height decreases with decreasing temperature in case of binary mixture. These observations are consistent with the conclusions made based on the activation energy calculations outlined above. The fact that the free energy barrier is temperature dependent for the binary mixture and that the barrier height decreases with decreasing temperature provides an explanation for the sub-Arrhenius diffusion observed in the case of larger particles. It should be noted that $G_s(z)$ is less than zero at the edges of the simulation box while $G_l(z)$ is closer to zero in the single component systems. This difference occurs due to different number density of single component systems.

From the density profile, we can also calculate the mean force as[64]

$$F(z) = k_B T \frac{d(ln\,\rho_i(z))}{dz} \qquad (2.17)$$

along the direction of the potential barrier. Here $F(z) = F_+(z) - F_-(z)$, where $F_+(z)$ is the mean force of interaction along positive $z$ direction and $F_-(z)$ is the mean force along negative $z$ direction. These are plotted in Figure 2.11 and 2.12 for smaller particles and larger particles respectively. From figure 2.11 it is clear that the force on smaller particles near the potential barrier is repulsive (negative on the left side of the barrier and positive on the right side) both in the single component system and in the binary mixture. Also it is clear that the magnitude of the force does not change significantly with respect to temperature and hence the dynamics remains Arrhenius. However, the effective force in the larger particles shows a very contrasting behavior. The force is mainly attractive towards the barrier (positive on the left of the barrier and negative on the right), and the magnitude
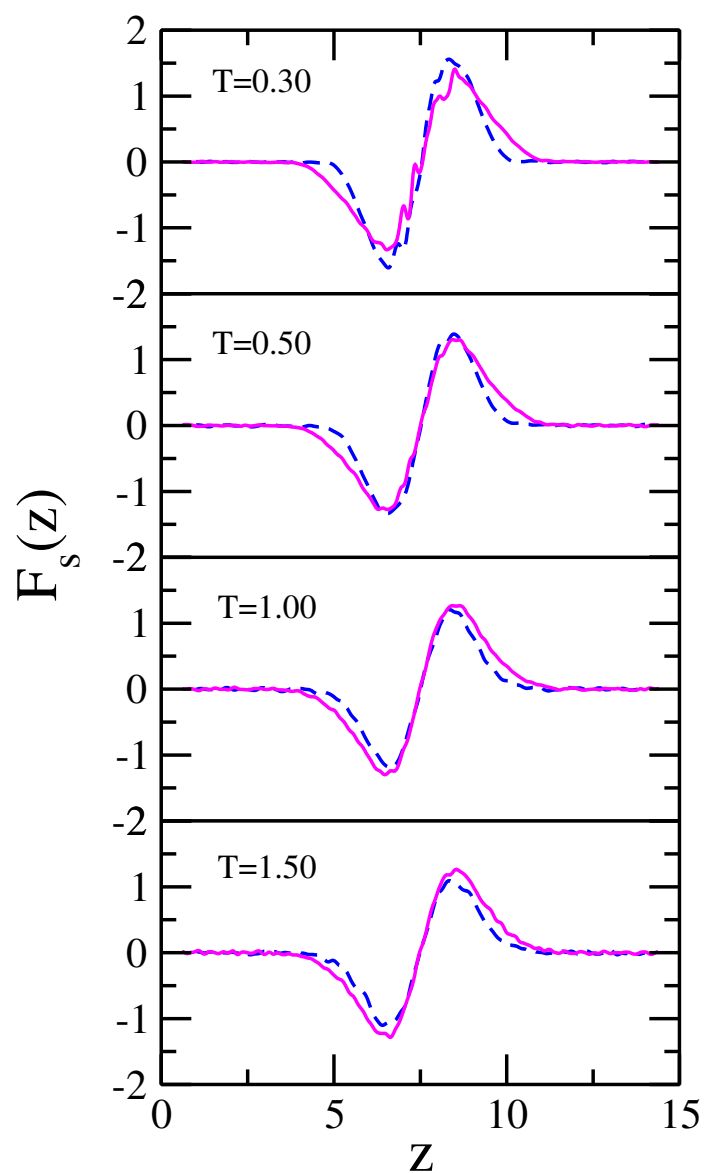
Figure 2.11: Mean force of interaction for the smaller particles along the z - direction when the system has only small particles(dashed lines) and when both large and small particles present (solid lines).
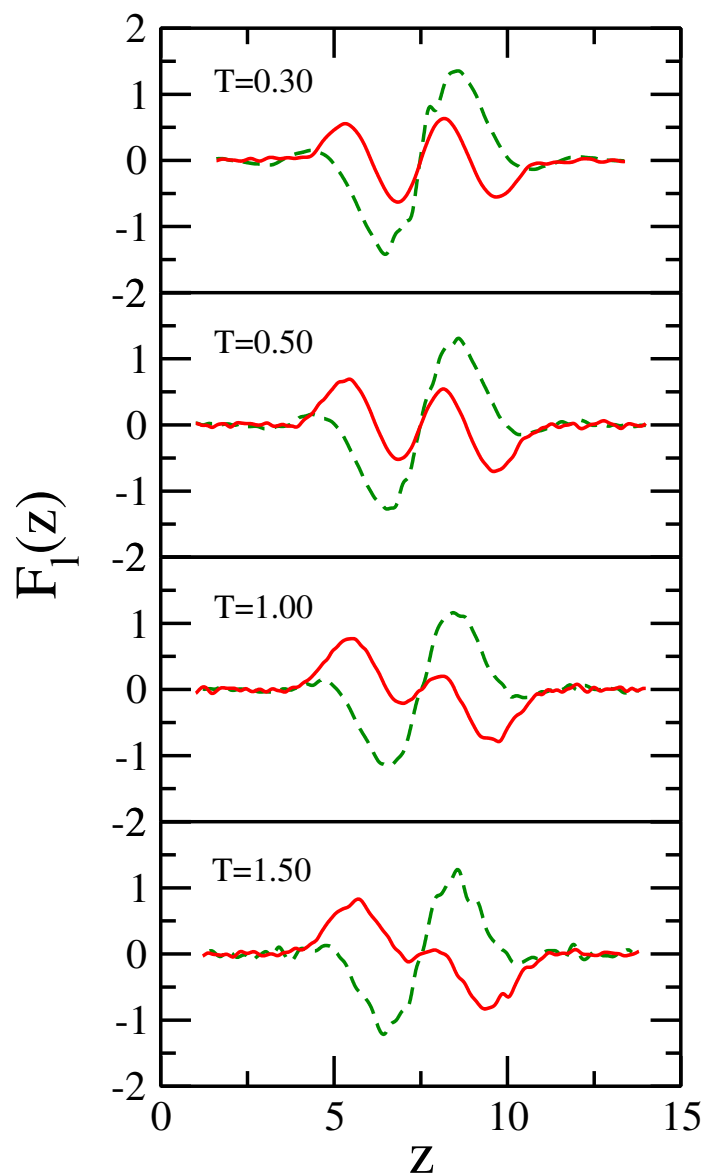
Figure 2.12: Mean force of interaction for the larger particles along the z - direction when the system has only large particles(dashed lines) and when both large and small particles present (solid lines).

of the force changes as the temperature changes. This confirms the sub-Arrhenius behavior observed in the diffusivity of larger particles. It should be noted that the fluctuation in the mean force in the region of potential barrier at low temperatures arises due to the splitting of the peak in density profile at lower temperatures.

### 2.5.5   Waiting time distribution

Waiting time distributions measure the delay times between successive hops of particles in a dynamical process. As mentioned in the methods section, unfolding the trajectories of individual particles will result in trajectories such that each particle has to cross periodically repeated potential barriers. This means each particle spends their time between two barriers during the interval between two successive crossings over barriers. We have also calculated the distributions of these waiting times for both large and small particles from the molecular dynamics trajectories by calculating the delay time between successive jumps of the particles over the barrier. A log-log representation of these waiting time distributions for both the particles has been plotted in Figure 2.13. As temperature decreases, the waiting time distribution for both type of particles flattens out. This is expected as particles will spend more time between two potential barriers before crossing over and their dynamics become more and more localized as the temperature decreases. However, the decay of waiting time distribution of smaller particles is much slower compared to that of larger particles. These distributions can be very well fitted to a sum of two exponentials. This essentially tells us that there are two time scales associated with the barrier crossing of particles. We have plotted the two relaxation times($\tau_1$ and $\tau_2$) for smaller particles and the two relaxation times($\tau_3$ and $\tau_4$) for larger particles against temperature in the inset of Figure 6(a) and 6(b) respectively. One of the relaxation times($\tau_1$ or $\tau_3$) in each case remains mostly unaffected as temperature decreases; while the other ($\tau_2$ or $\tau_4$) increases as the temperature decreases. $\tau_1$ (or $\tau_3$) corresponds to the recrossing occurs near the potential barriers, which explains the
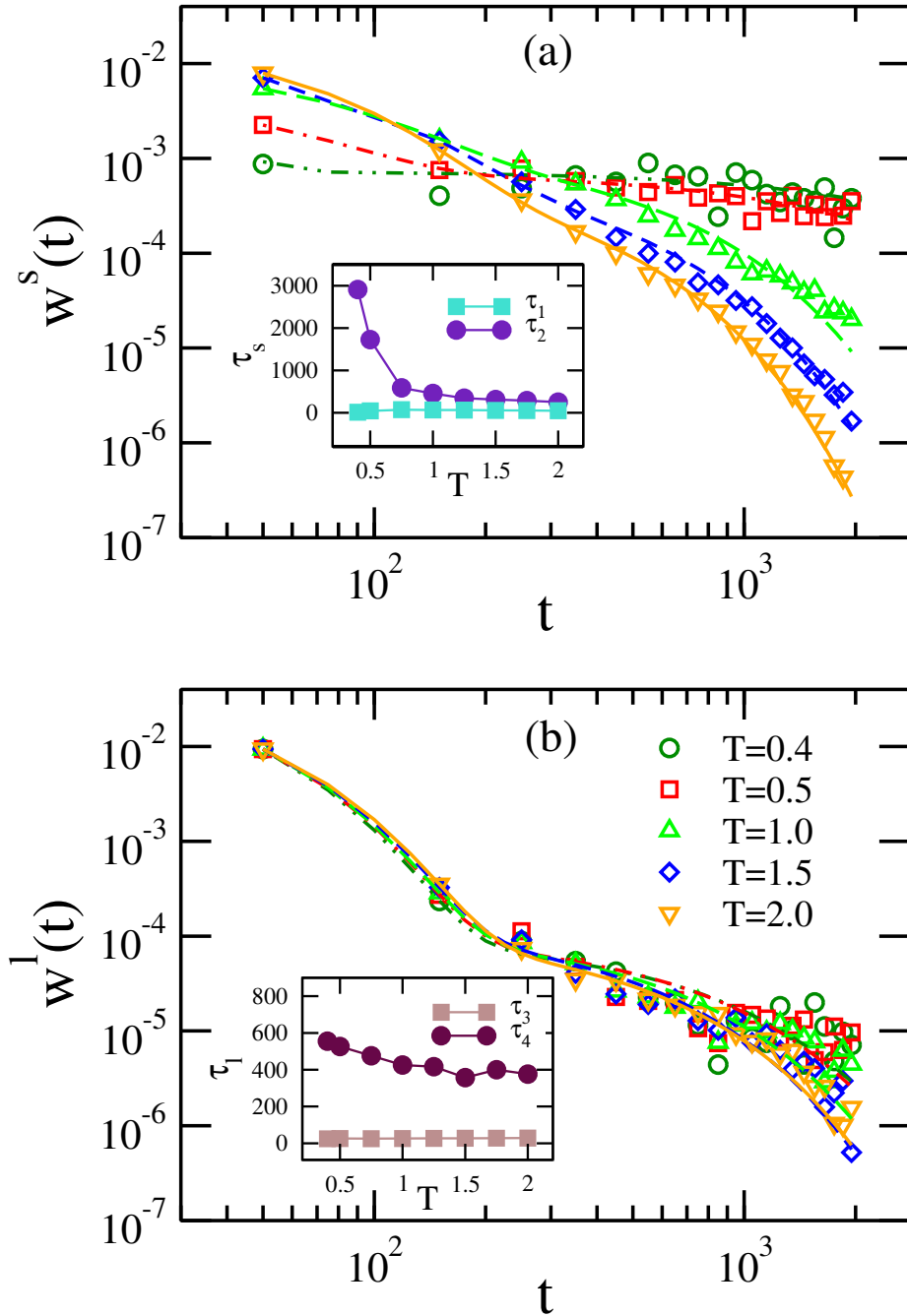
Figure 2.13: Waiting time distribution of (a) small particles and (b) large particles. The symbols are the data from the simulations and the lines are exponential fits. A sum of two exponential fits the data very well for both the species. The corresponding relaxation times are plotted in the inset of both the figures.

weak dependence on temperature. The larger relaxation time, $\tau_2$ (or $\tau_4$) can be attributed to the long time diffusion due to barrier crossing. As evident in the figure, $\tau_2$ increases rapidly with decreasing temperature while $\tau_4$ increases more slowly as temperature decreases. This indicates increasing localization of smaller particles between the repulsive barriers compared to that of larger particles and support the sub-Arrhenius diffusion observed in the dynamics of larger particles.

## 2.6   Conclusion and summary

We performed the canonical ensemble molecular dynamics simulation of binary colloidal system subjected to external repulsive potential. The dynamics of both components in the mixture are strongly influenced in a contrasting manner by the depletion interactions between the larger particles and the potential barrier. This depletion interaction is temperature dependent and changes the effective barrier accordingly. Thus, we observe a sub-Arrhenius diffusive behavior for larger particles, while the smaller particles follow Arrhenius behavior. The effective barrier of the smaller particles increases because larger particles get crowded in the region of external potential barrier and smaller particles gets depleted away from that region. This crowding of larger particles and hence the depletion of smaller particles from the region of potential barrier does not depend on temperature, especially since the volume fraction of the particles is small. So the effective potential barrier for smaller particles remain unchanged with respect to temperature and they follow Arrhenius diffusion. For such system slowing down of dynamics has been reported earlier[12]. The interaction between the particles in our model is purely repulsive. However, there is an effective attraction between the large particles due to the depletion interactions. So, at higher densities, we can expect condensation of the system and change over to super-Arrhenius diffusion[65](will be discussed in the third chapter) . It should also be mentioned that the results are more

general over a wide range of parameters than the set we used in these simulations[65].

We have shown that, contrary to the agreement in literature that sub-Arrhenius diffusion is related to quantum phenomena, a classical system can show a sub-Arrhenius temperature dependence of diffusivity. An increase in the probability of crossing the barrier can lead to sub-Arrhenius behavior irrespective of the nature of the process involved. In this sense, the depletion interactions in the present investigation or quantum tunneling in the earlier reported investigations have similar effects on the barrier crossing. Even though the results we obtained are for a binary mixture of colloids, we believe our findings are applicable to many other systems which involve barrier crossing. Many of the biological transport process which involve more than one components, differing in their dimensions, shows faster diffusivity for bigger components[66, 67]. Similarly, anomalous changes in diffusivity with respect to particle dimensions are reported for particles diffusion in porous materials such as zeolites[68, 69] and metal oxide frameworks[70, 71]. The pathways of transport in these systems involve many bottlenecks, which can be similar to the external potential used in our investigations. Therefore, our results contribute to the understanding of such processes.

# References

[1] P. Hangii, P. Talkner, M. Borkovec, *Rev. Mod. Phys.* **62**, 251 (1990).

[2] S. Sastry, P. G. Debenedetti, F. H. Stillinger, *Nature* **393**, 5545 (1998).

[3] S. Sastry, *Nature* **409**, 164 (2001).

[4] T. B. Schrøder, S. Sastry, J. C. Dyre, S. C. Glotzer, *J. Chem. Phys.* **112**, 9834 (2000).

[5] R. L. Baldwin, *Nature* **369**, 183 (1994).

[6] R. L. Baldwin, *J. Biomol. NMR* **5**, 103 (1995).

[7] F. Zhang, G. M. Lee, K. Jacobson, *BioEssays* **15**, 579 (1993).

[8] K. Jacobson, E. D. Sheets, R. Simson, *Science*, **268**, 1441 (1995).

[9] C. Bechinger, Q. H. Wei, P. Leiderer, *J. Phys.: Condens. Matter* **12**, A425 (2000).

[10] A. Chowdhury, B. J. Ackerson, N. A. Clark, *Phys. Rev. Lett.* **55**, 833 (1985).

[11] B. Vorselaars, A. V. Lyulin, K. Karatasos, M. A. J. Michels, *Phys. Rev. E* **75**, 011504 (2007).

[12] C. Dalle-Ferrier, M. Krüger, R. D. L. Hanes, S. Walta, M. C. Jenkins, S. U. Egelhaaf, *Soft Matter* **7**, 2064 (2011).

[13] R. D. L. Hanes, C. Dalle-Ferrier, M. Schmiedeberg, M. C. Jenkins, S. U. Egelhaaf, *Soft Matter* **8**, 2714 (2012).

[14] T. R. ten Wolde, M. J. Ruiz-Montero, D. Frenkel, *Phys. Rev. Lett.* **75**, 2714 (1995).

[15] S. Auer, D. Frenkel, *Ann. Rev. Phys. Chem.* **55**, 333 (2005).

[16] J. E. Anderson, R. Ullman, *J. Chem. Phys.* **47**, 2187 (1967).

[17] J. Skolnick, E. Helfand, *J. Chem. Phys.* **72**, 5489 (1980).

[18] HK Kim, E. Tuite, B. Norden, *Eur. Phys. J. E* **4**, 411 (2001).

[19] B. G. Harvey, W. H. Wade, P. F. Donovan, *Phys. Rev.* **119**, 225 (1960).

[20] D. Roudil, X. Deschanels, P. Trocellier, C. Jegou, S. Peuget, JM. Bart, *J. Nucl. Mater.* **325**, 148 (2004).

[21] Keith J. Laidler, *J. chem. Edu.* **61**, 6 (1984).

[22] J. H. vant Hoff, *Etudes de Dynamiques Chimiques*, 114 (1884).

[23] S. Arrhenius, *Z. Phys. Chem.* **4**, 226 (1889).

[24] H. A. Kramers, *Physica(Utretch)* **7**, 284 (1940).

[25] K. Hüger *et al.*, *Appl. Phys. Lett.* **93**, 162104 (2008).

[26] M. J. Purdue *et al.*, *J. Chem. Phys.* **124**, 204904 (2006).

[27] J. Kärger, R. Valiullin, S. Vasenkov, *New J. Phys.* **7**, 15 (2005).

[28] J. M. Bermúdez-Garcia *at al.*, *Phys. Chem. Chem. Phys.* **18**, 19605 (2016).

[29] R. Zellner, W. F. Steinert, *Int. J. Chem. Kin.* **8**, 397 (1976).

[30] A. Kohen, J. P. Klinman, *Acc. Chem. Res.* **31**, 397 (1998).

[31] R. S. Swanwick, G. Maglia, L. Tey, R. K. Allemann, *Biochem. J.* **394**, 259 (2006).

[32] S. Gul, G. W. Mellor, E. W. Thomas, Keith Brocklehurst, *Biochem. J.* **396**, 17 (2006).

[33] N. Kamaya *et al.*, *Nature Materials* **10**, 682 (2011).

[34] H. Wagner, R. Richert, *J. Appl. Phys.* **85**, 1750 (1999).

[35] H. H. Limbach, J. M. Lopez, A. Kohen, *Philos. Trans. R. Soc. Lond. B. Biol. Sci.* **361**, 1399 (2006).

[36] V. H. C. Silva, V. Aquilanti, H.C.B. de Oliveira, K.C. Mundim, *Chem. Phys. Lett.* **590**, 201 (2013).

[37] F. O. Sanches-Neto, N. D. Coutinho, V. H. C. Silva, *Phys. Chem. Chem. Phys.* **19**, 24467 (2017).

[38] J. R. Hulett, *Q. Rev. Chem. Soc.* **18**, 227 (1964).

[39] B. Perlmutter-Hayman, Progress in inorganic chemistry : on the temperature dependence of Ea, S. J. Lippard, Ed. (John Wiley & sons, New York, 1976).

[40] S. Vyazovkin, *Phys. Chem. Chem. Phys.* **18**, 18643 (2016).

[41] V. Aquilanti *et al.*, *Chem. Phys.* **398**, 186 (2012).

[42] V. Aquilanti *et al.*, *Chem. Phys. Lett.* **498**, 209 (2010).

[43] V. H. C. Silva, N. D. Coutinho, V. Aquilanti, *AIP Conf. Proc.* **1790**, 02006 (2016).

[44] M. Nishiyama, S. Kleijn, V. Aquilanti, T. Kasai, *Chem. Phys. Lett.* **470**, 332 (2009).

[45] C. Tsallis, *J. Stat. Phys.* **52**, 479 (1988).

[46] G. Stirnemann, D.Laage, *J. Phys. Chem.* **137**, 031101 (2012).

[47] V. K. de Souza, D. J. Wales, *Phys. Rev. Lett.* **96**, 057802 (2006).

[48] C. Rotella, S. Napolitano, M. Wubbenhorst, *Macromolecules* **42**, 1415 (2009).

[49] M. Nishiyama, S. Kleijn, V. Aquilanti, T. Kasai, *Chem. Phys. Lett.* **482** 325 (2009).

[50] J. Chen, J. Neu, M. Miyata, G. Oster, *Biophys. J.* **97** 2930 (2009).

[51] Z.-X. Liang *et al.*, *Proc. Natl. Acad. Sci. USA* **101** 9556 (2004).

[52] J. Braun *et al.*, *J. Am. Chem. Soc.* **118** 11101 (1996).

[53] R. P. Bell, Ser. A, *Math. Phys.* **148** 241 (1935).

[54] R. P. Bell, *Trans. Faraday Soc.*, **55** 1 (1958).

[55] R. Buscall *et. al.*, *Soft Matter* **5**, 1345 (2009).

[56] S. Asakura, F. Oosawa, *J. Polym. Sci.* **22**, 1255 (1954).

[57] A. V. Anil Kumar, *J. Chem. Phys.* **138**, 154903 (2013).

[58] A. V. Anil Kumar, *J. Chem. Phys.* **141**, 034904 (2014).

[59] J. J. Thorn, E. A. Schoene, T. Li, D. A. Steck, *Phys. Rev. Lett.* **100**, 240407 (2008).

[60] M. P. Allen, D. J. Tildesley, Computer Simulation of Liquids (Oxford Univ. Press, USA, 1989).

[61] D. J. Evas, G. P. Morriss, Statistical Mechanics of Nonequilibrium Liquids (Academic Press, London, 1990).

[62] M. Mustakim, A. V. Anil Kumar, *Physica A* **563** 125462 (2021).

[63] V. K. de Souza, D. J. Wales, *Phys, Rev, B*. **74**, 134202 (2006).

[64] K. Nygard, *Curr. Opin. Colloid. Interace Sci.* **22**, 30 (2016).

[65] M. Mustakim, A. V. Anil Kumar, *J. Phys. Chem. B.* **126**, 1, 327–335. (2022).

[66] D. Boda, D. D. Busath, B. Eisenberg, D. Henderson, F. Nonner, *Phys. Chem. Chem. Phys.* **4**, 5154 (2002).

[67] M. L. Lopez, M. Aguilella-Arzo, V. M. Aguilella, A. Alcaraz, *J. Phys. Chem. B* **113**, 8745 (2009).

[68] N. J. Turro, X. Lei, C. C. Cheng, D. R. Korbin, L. Abrams, *J. Am. Chem. Soc.* **107**, 5824 (1985).

[69] S. Sarkar, A. V. A. Kumar, S. Yashonath, *J. Chem. Phys.* **112**, 965 (2000).

[70] J. Liu, J. Tian, P. K. thallapally, B. P. McGrail, *J. Phys. Chem. C* **116**, 9575 (2012).

[71] R. Banerjee *et al.*, *Science* **319**, 939 (2008).

# Chapter 3

# Depletion Induced Crystallization in Binary Colloids in the presence of External Potential

## 3.1 Introduction

Suspensions of colloidal particles exhibit similar phase behaviors as atomic systems[1, 2]. This atom-colloid analogy makes the colloids an important model system to study the phase transitions. The solvent mediated effective interactions between the colloidal particles determine the physical properties of a colloidal dispersion and these effective interactions can be tuned to have different ranges as well as strengths[3]. For example, the interaction can be long-ranged repulsive on one end, while it can be tuned to nearly hard-spheres at the other end. This tunability in interactions enables us to use colloids to study a wide range of phase behaviors and transitions. Crystallization is the most important phase transition in condensed matter system, ranging from atomic and molecular system to colloids and granular matter [4] and freezing and melting are among the most studied phenomena both from fundamental as well as technological points of view. In particular, colloidal crystals are of great interest for developing new novel materials such as optical fibers[5, 6], photonic bandgap materials[7, 8, 9] etc. The volume fraction is one of the most important factors in determining the phase behavior of all the colloidal suspensions. In a suspension of hard spheres, the

volume fraction is the only controlling parameter that determines whether the suspension is in a fluid state or in a solid state. When one increase the volume fraction, the particles tend to form crystal structure. It has been observed that in hard sphere colloids, the transition from a fluid state to a crystalline state occurs at higher volume fractions (the suspension remains in fluid state for $\phi < 0.494$, partially crystalline for $0.494 < \phi < 0.545$ and fully crystalline state for $\phi > 0.545$)[1]. However, at volume fraction beyond $\phi = 0.58$, a glass transition happens which is thermodynamically not a stable state[10]. Crystallisation can also be induced by shear using experiments and simulations[11, 12, 13, 14, 15, 16]. However, in colloidal systems with long-ranged repulsive interactions, crystal phases can be formed at lower volume fractions. These crystals are body centered cubic crystals, named 'Wigner crystals'. However, when the interactions are short ranged, the colloidal suspensions tend to be in a liquid state at lower volume fractions. Crystallization at low volume fractions can be achieved by manipulating the local concentration of colloids by dielectrophoresis[17, 18] and diffusiophoresis[19]. It will be interesting to investigate how the local concentration can be modified making use of the entropic effects such that the colloidal systems with short ranged interactions form crystals at lower volume fractions.

The binary mixture of colloids, where the components differ in their sizes, shows rich phase behavior as well as dynamical properties due to the excluded volume effects. The disparity in the sizes of components entropically favors an effective attraction between the larger particles. This entropically driven effective attraction between the larger($l$) components in the binary mixture is called depletion interactions[20, 21] and leads to interesting structural and dynamical properties, especially crystallization, gelation, and self-assembly of colloidal particles[22, 23, 24]. As discussed in chapter 2, it has been shown that when a binary colloidal mixture is exposed to an external repulsive potential, there exists an attractive depletion interaction between the potential barrier and the larger components in the mixture. This depletion interaction significantly alters the structural and dynamical prop-

erties of the binary mixture and exhibits very interesting behaviors[25, 26, 27, 28]. For example, it favors the demixing of the binary mixture and an $l$-rich phase is formed near the external potential barrier[25]. Also, there have been interesting observations about the dynamics of both components in the mixture. The smaller($s$) particles exhibit a slowing down of dynamics at lower temperatures like in the case of supercooled liquids, even though the volume fraction is quite low[26]. Meanwhile, the larger particles continue to undergo normal diffusion even at low temperatures. The temperature dependence of diffusion is also interesting. The smaller particles follow an Arrhenius behavior even though their dynamics has slowed down. However, the diffusion of larger particles deviates from Arrhenius behavior and shows a sub-Arrhenius temperature dependence[27]. These results are outlined in chapter 2. All these results are obtained at a total volume fraction of $\phi = 0.2$.

In this chapter, we extend these investigations to higher volume fractions using molecular dynamics simulations. The effect of volume fraction on the structural and dynamical properties have been studied. The demixing becomes stronger as volume fraction increases and the $l$-rich phase forms crystals of larger particles about $\phi$=0.40. This crystalline phase, which is formed at the region of the external potential barrier moves perpendicular to the barrier with a non-zero diffusion coefficient. This seems to be surprising since the local volume fraction is large enough so that the particle motion is very much hindered. Such moving crystals have been observed earlier in the nonequilibrium systems, where the crystals are subjected to heating or cooling or exposed to light[29, 30, 31, 32]. However, in our model system, there are no driving forces present and the whole system is in equilibrium. It has been also found that the temperature dependence of the diffusion of larger particles along the direction of external potential changes from sub-Arrhenius to super-Arrhenius when the crystal formation occurs in the system.

## 3.2  Model and simulation details

We have carried out molecular dynamics simulations on a model system of colloidal mixture, comprising of small and large spherical colloids with diameters $\sigma_{ss}$ and $\sigma_{ll}$ respectively. These colloidal particles interact via a soft sphere repulsion which is given by

$$V_{ab}(r_{ij}) = \epsilon_{ab}\left(\frac{\sigma_{ab}}{r_{ij}}\right)^{12} \tag{3.1}$$

where $r_{ij}$ is the inter-particle distance and $(a,b) \in (l(large), s(small))$. We chose $\epsilon_{ss} = 1.0$, $\epsilon_{ll} = 4.0$, $\sigma_{ss} = 1.0$ and $\sigma_{ll} = 2.0$ in reduced units. The cross interaction parameters are obtained using Lorentz-Berthelot mixing rule; i.e., $\epsilon_{sl} = \sqrt{\epsilon_{ss} * \epsilon_{ll}}$ and $\sigma_{sl} = (\sigma_{ss} + \sigma_{ll})/2.0$ (The values are $\epsilon_{sl} = 2.0$ and $\sigma_{sl} = 1.5$). The masses of two species are kept same since we do not want the effect of mass difference to be coupled with the effect of depletion interaction in the dynamics of the binary mixture. The phase behavior and dynamics of the single component system of our soft sphere model has been studied extensively by Hoover et al.[33, 34] using molecular simulations and also by Lutsko and Baus using perturbation theory[35]. They have found out that the single component system undergoes a freezing transition from liquid state to face centered cubic system when the dimensionless parameter $\rho\epsilon/k_BT = 0.813$. Here $\rho$ is defined as $\rho = (N * \sigma^3)/(\sqrt{2}V)$. This value corresponds to $\phi/T = 0.602$ in our model system. We take the simulation box of length, $L = 17$, and periodic boundary conditions are applied in all the three spatial directions. In addition to the interaction among the constituent particles, they are also subjected to an external repulsive barrier of Gaussian form at the center of the simulation box along $z-$ direction only[25],

$$V_{ext}(z) = \epsilon_{ext}\ e^{-\left(\frac{z-(L/2)}{w}\right)^2} \tag{3.2}$$

The width and height of the barrier are $w = 3.0$ and $\epsilon_{ext} = 3.0$ respectively. These model system has been extensively studied in low volume fractions and found that the depletion

| $\phi$ | $N$ | $n_s$ | $n_l$ |
|--------|------|-------|-------|
| 0.20 | 1055 | 938 | 117 |
| 0.25 | 1320 | 1173 | 147 |
| 0.30 | 1583 | 1407 | 176 |
| 0.35 | 1847 | 1642 | 205 |
| 0.40 | 2112 | 1877 | 235 |
| 0.425 | 2243 | 1994 | 249 |
| 0.45 | 2375 | 2111 | 264 |
| 0.50 | 2639 | 2346 | 293 |

Table 3.1: Total number of particles, $N$, number of small particles, $n_s$ and number of large particles, $n_l$ at different volume fractions at which simulations are carried out.

interactions between the large particles and the potential barrier causes the mixture to phase separate. The height and width of the barrier determines the extent of this phase separation. In general, depletion interaction increases as the height of the barrier increases. However, the dependence of width of the barrier on demixing shows a nonmonotonous behavior. The extent of demixing increases at low values of $w$ and goes though a maximum at $w = 2.0$[25]. It has also been shown that the depletion interaction is maximum when the volume fraction of small and large particles are equal[25]. Therefore in our simulations, we always took an equivolume mixture of large and small colloidal particles.

We have carried out molecular dynamics simulations on our model system at different volume fractions and temperatures. The simulation details are same as in chapter 2. The simulations were done for different total volume fractions of $\phi = 0.20$, $\phi = 0.25$, $\phi = 0.30$ $\phi = 0.35$, $\phi = 0.40$, $\phi = 0.425$, $\phi = 0.45$, and $\phi = 0.50$ to observe the changes in the structure and dynamics of the system when the volume fraction increases. The number of particles corresponding to each volume fractions are given in table 1.

A series of simulations are performed for 8 different temperatures in the range $T \in (2.00, 0.25)$ for each total volume fraction. Each simulation runs for a total $5 \times 10^6$ steps for volume fraction upto $\phi = 0.40$ with a time step of $dt = 0.001$. For higher volume fractions we have increased the length of simulation to $1 \times 10^7$ steps with a timestep of

$dt = 0.005$ for better statistics. It is repeated for three times for each state point and the average value of dynamical properties are calculated after the equilibration of the system.

## 3.3 Spatial distributions and crystallization

It has been shown earlier that this model system at low volume fractions exhibits interesting structural properties due to the depletion interaction between the external potential barrier and larger particles[25]. The effective attraction between the potential barrier and larger particles results in an increased density of larger particles near the barrier, suggesting that a demixing can occur and the local concentration of larger particles near the barrier can be increased above the threshold for crystallization. Therefore, we systematically investigated the structural properties of the binary mixture at different total volume fractions as well as at different temperatures. Please note that we simulated equi-volume binary mixtures at all volume fractions.

### 3.3.1 Density Profile

In order to characterize the demixing in the system, we have calculates the density profile of both large and smaller particles along the direction of the potential barrier. This is done by dividing the simulation box in to a number of smaller compartments along the z-direction and counting the number of smaller and larger particles separately in these compartments. The number density thus obtained for each of the compartment is normalized with respect to the average density of the respective components. These normalized density profiles of smaller and larger particles at different volume fractions and temperatures are shown in figures 3.1 and 3.2 respectively. The density profile of smaller particles shows a minimum at the region of the external repulsive potential, as expected. This minimum in the density profile becomes sharper and sharper as we decrease the temperature. As evident from figure 3.1, there are no significant changes in the density profile of smaller colloids as we
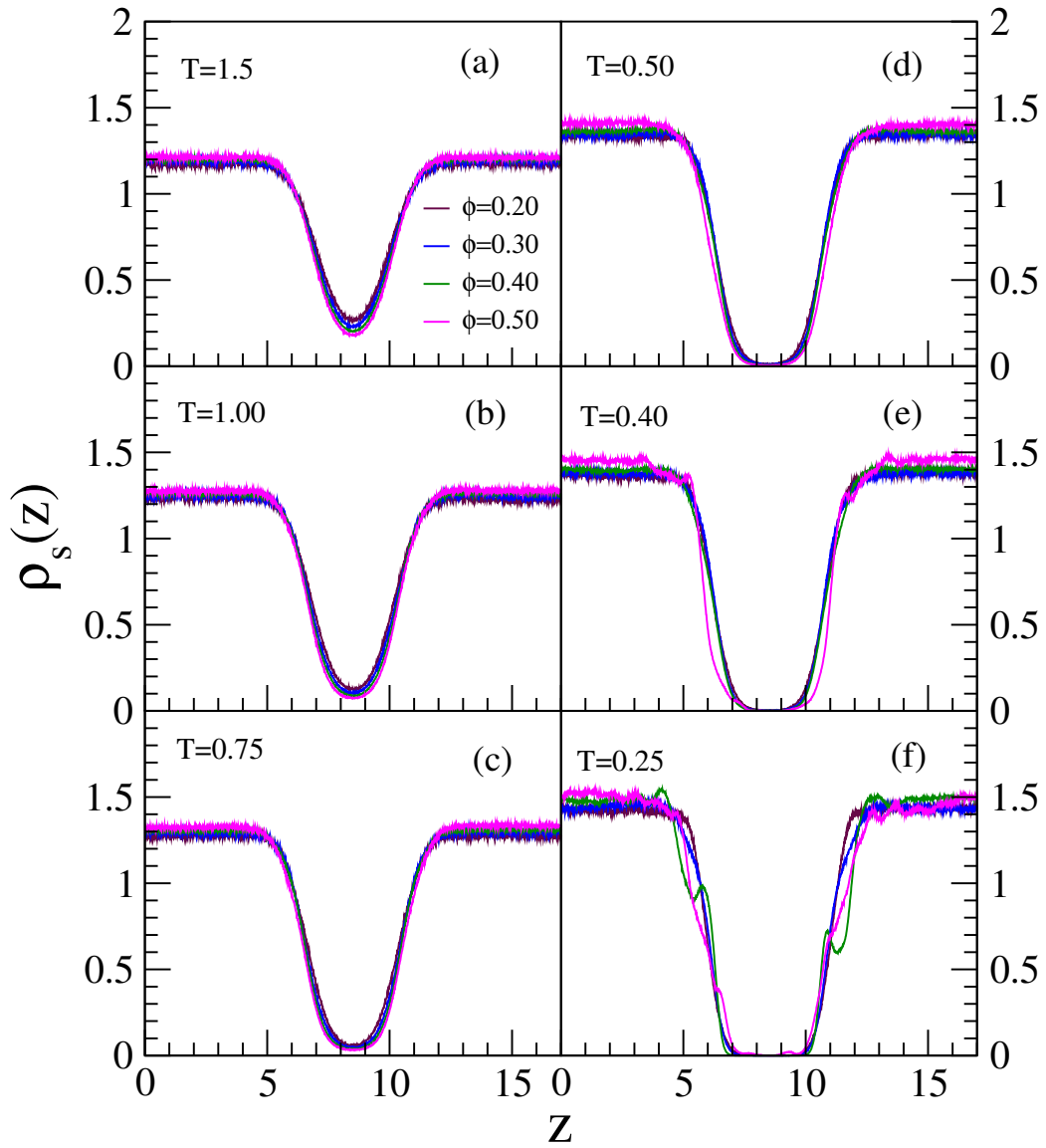
Figure 3.1: Density profile of smaller particles at four different volume fractions $\phi = 0.20$, 0.30, 0.40 and 0.50 and at different temperatures (a) $T=1.5$, (b) $T = 1.0$, (c) $T = 0.75$, (d) $T = 0.50$, (e) $T = 0.40$ and (f) $T = 0.25$.
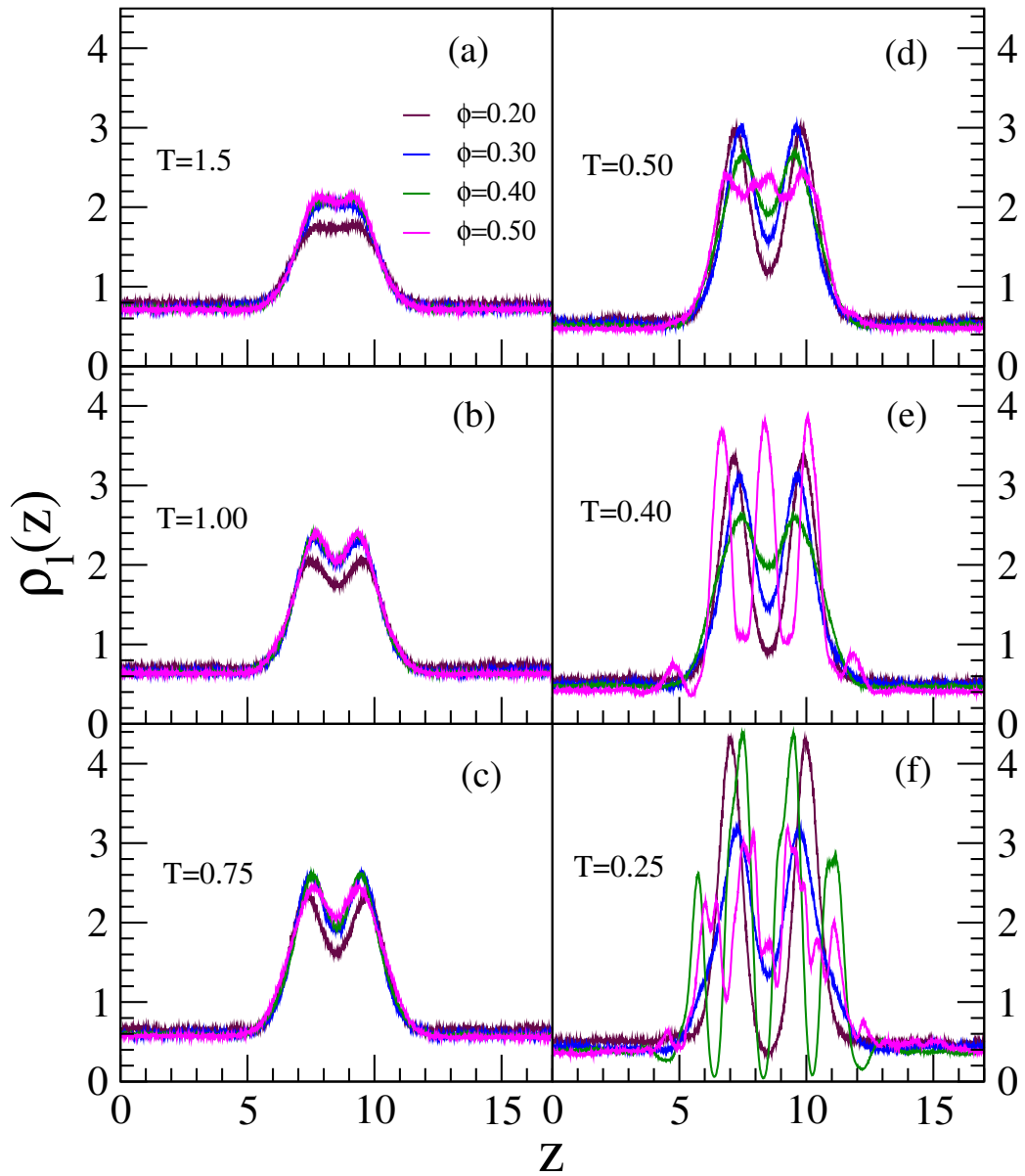
Figure 3.2: Density profile of larger particles at four different volume fractions $\phi = 0.20$, 0.30, 0.40 and 0.50 and at different temperatures (a) $T=1.5$, (b) $T = 1.0$, (c) $T = 0.75$, (d) $T = 0.50$, (e) $T = 0.40$ and (f) $T = 0.25$.

increase the volume fraction of the mixture. However, the density profile of larger particles shows interesting changes with the decrease in temperature as well as with the increase in volume fraction. It is clear from the figure 3.2 that the larger particles get attracted to the region of the potential barrier at all temperatures, as indicated by the peak(s) in the region of the potential barrier. This is in agreement with earlier results for lower volume fractions, outlined in chapter 2[26, 27]. At high temperatures, the normalized density profile does not show any significant changes with respect to the changes in volume fractions, except that the height of the peak increases with volume fraction. However, as we decrease the temperature, the density profile starts developing multiple peaks in the region of potential barrier at higher volume fractions. This indicates the layering of larger particles in the region of the external potential barrier. This layering increases as we increase the volume fraction at low temperatures. The density profiles of smaller and larger particles clearly show that demixing occurs because of the depletion interaction between the potential barrier and larger particles. It also indicates that this phase separation becomes stronger as we decrease the temperature and increase the volume fraction.

### 3.3.2   Phase separation and Phase diagram

To quantify the extent of phase separation, we divided the simulation box into a number of rectangular boxes along the $z$-direction and calculated the difference in the number of large and small particles in each of the rectangular boxes. This difference in the number of large and small particles in the $i^{th}$ box is given by[28, 36]

$$\chi = \frac{n_l^i - n_s^i}{n_l^i + n_s^i} \tag{3.3}$$

Figure 3.3 shows the distribution $P(\chi)$ of $\chi$ at different volume fractions and at different temperatures. At high temperatures, $P(\chi)$ shows a single peak around $\chi = 0$ at all volume fractions, which shows the demixing is negligible. As the temperature decreases to 0.50,
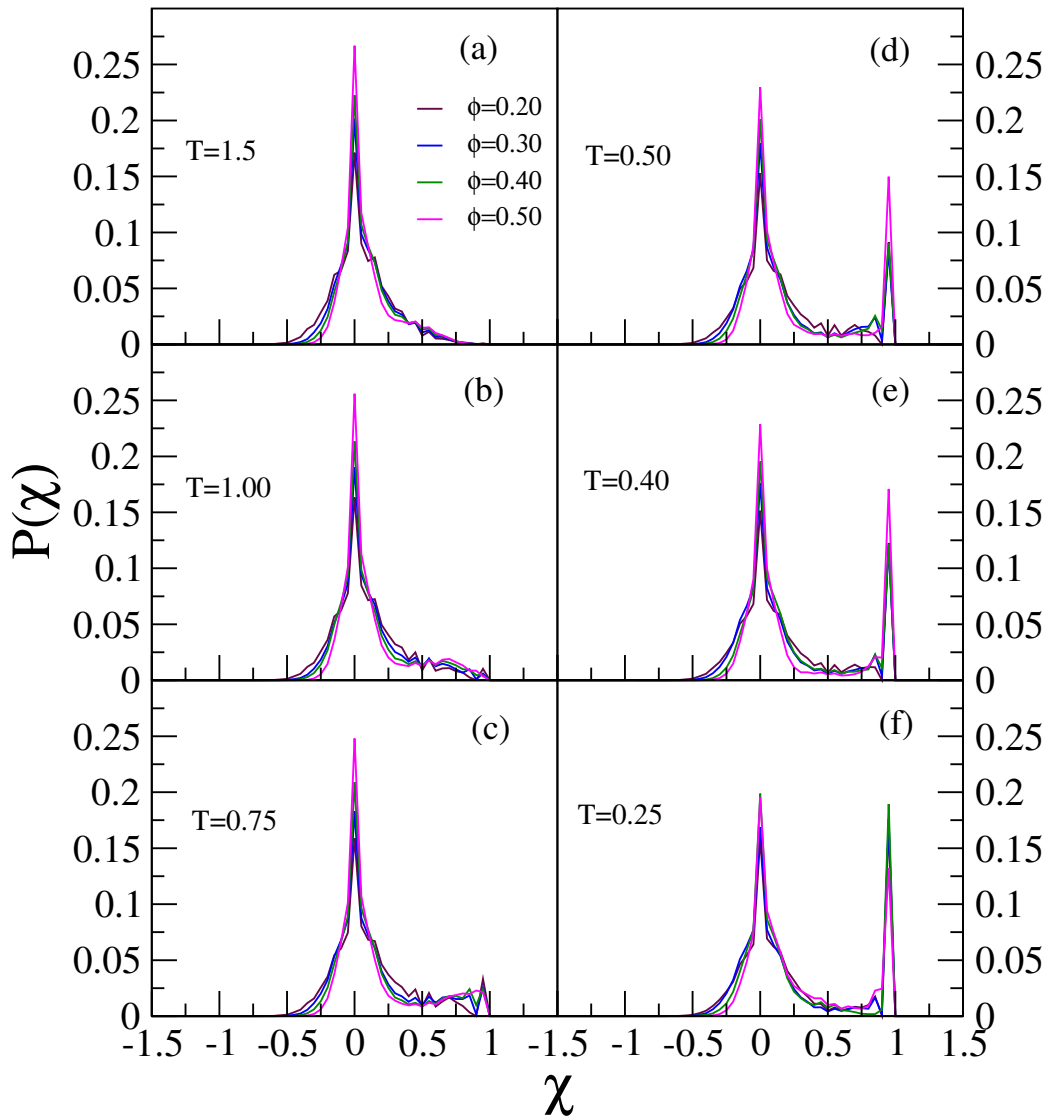
Figure 3.3: Distribution, $P(\chi)$ of difference between the number of larger and smaller particles at different volume fractions and at different temperatures. Development of a peak at $\chi = 1$ indicates the phase separation and formation of a region near potential barrier predominantly of larger particles.
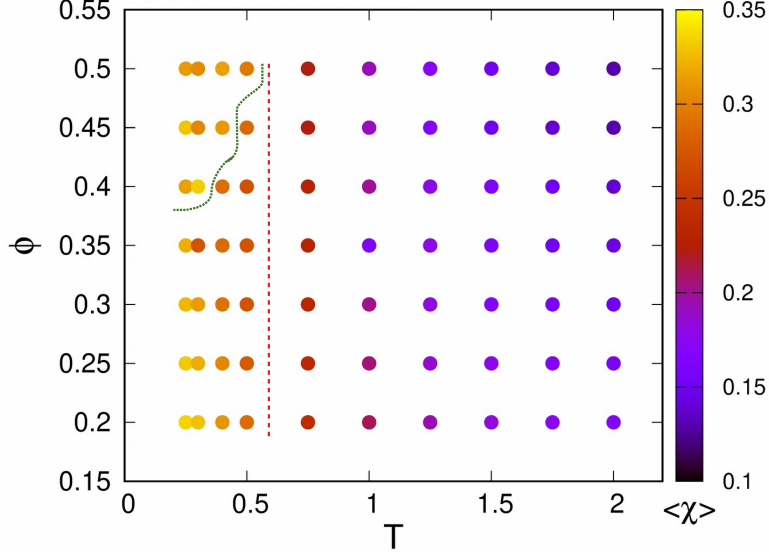
Figure 3.4: $\phi$ $vs.T$ phase diagram of the model system. The dashed line separates out the mixed and phase separated configurations and the dotted line separates out the fluid and crystal configurations.

the height of this peak starts decreasing. The decrease in the peak height of $P(\chi)$ at $\chi = 0$ is accompanied by the appearance of another peak at $\chi = 1.0$ at higher volume fractions. The appearance of this peak at $\chi = 1.0$ means that larger particles are getting accumulated in the region of the external potential barrier. The height of this second peak increases with decreasing temperature as well as increasing density or volume fraction. This indicates that the system phase separates into two: a mixed phase with both large and small particles and another phase with mostly large particles. This single component phase with large particles forms in the region of the external potential barrier. We have defined the average of $\chi$ as[36]

$$\chi_{av}(T, \phi) = \frac{1}{N_{box}} \left\langle \frac{|n_l^i - n_s^i|}{n_l^i + n_s^i} \right\rangle \tag{3.4}$$

where $N_{box}$ is the total number of rectangular boxes, the simulation box is divided into. We consider the value of $\chi_{av}(T, \phi)$ at which the peak at $\chi = 1$ starts developing as the onset value of phase separation. Figure 3.4 shows the values of $\chi_{av}(T, \phi)$ at different temperatures and volume fractions. At higher volume fractions and low temperatures, we get two phases
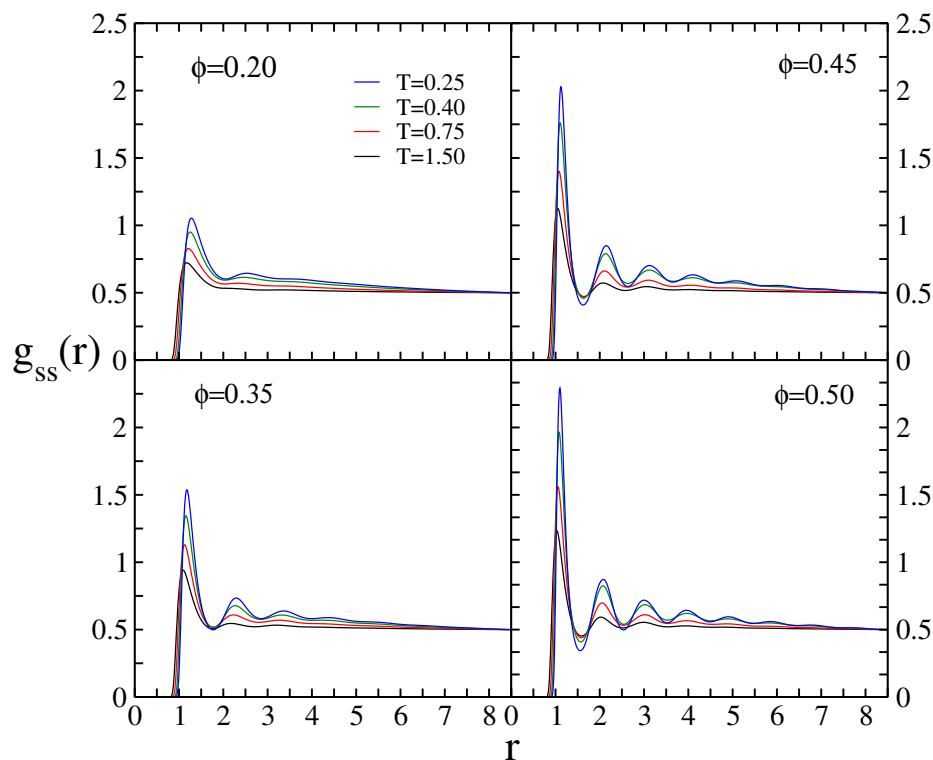
Figure 3.5: Radial distribution function of smaller particles for $\phi = 0.20, 0.35, 0.45, 0.50$ and for T=0.25, 0.40, 0.75, 1.50.

where one of the phases is dominated by the larger particles and the other is a mixed phase with both large and small particles. The left of dashed line in the figure 3.4 indicates the phase points where the phase separation occurs.

### 3.3.3 Radial distribution function

The radial distribution function, $g(r)$ is the most useful measure of the "structure" of a fluid at molecular length scales. For a homogeneous and isotropic system, $g(r)$ is defined as the ratio of the average local density at a distance $r$ from an arbitrary molecule to the average density of the fluid in bulk. In a dense system, $g(r)$ starts at zero, rises to a peak at the distance characterizing the first shell of particles surrounding the reference particle, and approaches 1 for long distances (large r) in isotropic media. This expresses the fact that a fluid possesses no long distance order as does a crystal. Thus the ordering influence of a

specified molecule on its surrounding diminishes with increasing distance and the average local density approaches the average density of bulk as the distance from the molecule becomes large.

Since the density profile and $P(\chi)$ show that there is demixing at higher volume fractions and at low temperatures, it will be interesting to look at the structure of larger particles in the layers formed in the region of the external potential barrier. We have calculated the radial distribution function $g(r)$ of large and small particles at different volume fractions and different temperatures. The radial distribution functions of smaller particles at different temperatures and volume fractions are plotted in figure 3.5. The $g(r)$ of smaller particles shows that they are in the liquid state at all volume fractions and temperatures. As the volume fraction increases, more layering occurs around the particles, which is expected. The radial distribution functions of larger particles at different volume fractions and temperatures are shown in figure 3.6. The $g(r)$ of larger particles changes significantly at higher volume fractions. At low volume fractions, larger particles are in a liquid state at all temperatures. As we increase the volume fraction to 0.35, they undergo crowding at low temperatures as indicated by the split in the second peak in $g(r)$. This is because more and more large particles are getting accumulated in the region of the external potential barrier. Further increase in the volume fraction results in the development of several peaks in $g(r)$ at low temperatures. This indicates that the crystallization of larger particles in the central region is due to the depletion interaction. This is interesting since the volume fraction of large particles is much lower than the volume fraction ($\sim$ 20 %) required for crystallization in single component systems. The attractive depletion interaction between the potential barrier and larger particles effectively confines a significantly large fraction of them in the region of the repulsive potential barrier. Thus the local volume fraction of the pure phase, comprised of only large particles, becomes high enough to form crystals. The periodic boundary conditions make it possible for the system to realise periodic repulsive
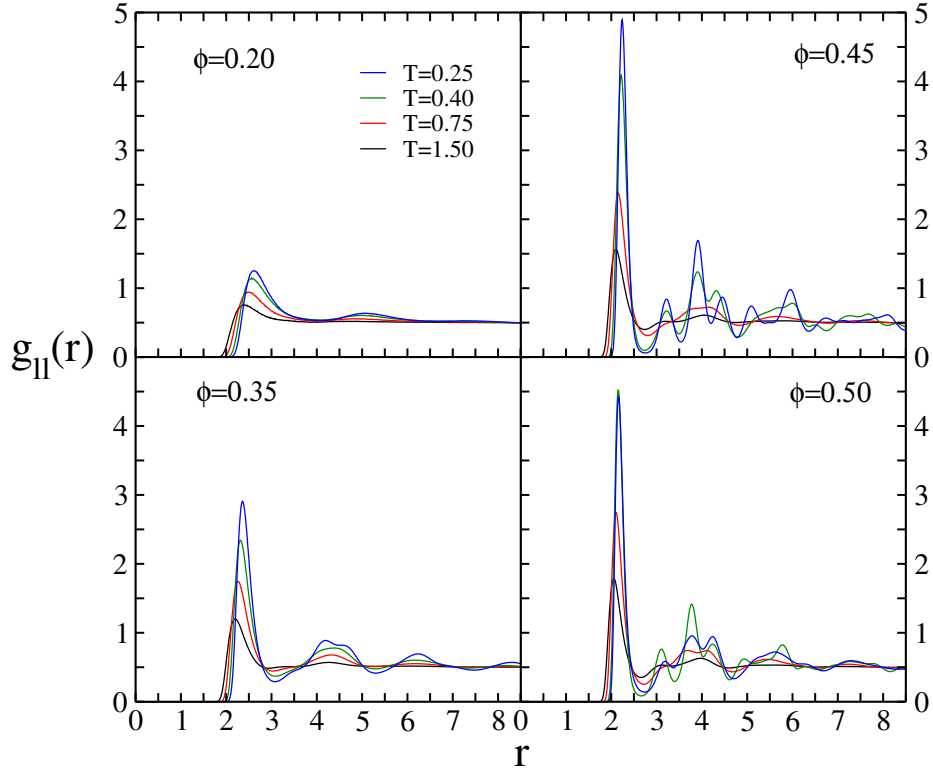
Figure 3.6: Radial distribution function of larger particles for $\phi = 0.20, 0.35, 0.45, 0.50$ and for T=0.25, 0.40, 0.75, 1.50. The peaks in rdf at high volume fractions and low temperatures corresponds to an fcc lattice.

barriers, which can be achieved experimentally, as shown by Dalle-Ferrier *et al.*[37] We expect that experimental realization of our model with such periodic potentials will realise periodic crystalline domains separated by fluid phases. The position of the peaks in the $g(r)$ indicates that the crystal formed is of face centered cubic structure. Also, it should be noted that since the particles are interacting through the soft sphere potential, the effective diameter of the particle and hence the volume fraction changes with temperature.

Our results suggest that crystallization can be achieved at low volume fractions by making use of depletion interaction between the larger particles and external repulsive potential. Earlier, crystallization has been achieved for colloidal systems with long range repulsion at low volume fractions(Wigner crystals). However, the crystallization obtained in our simu-

lations is distinctively different both in structure as well as the mechanism. In Wigner crystals, the long ranged interactions make the particles spaced farther. In the present study, the inhomogeneity in the system due to the depletion interactions enhances the local volume fractions above the threshold for crystallization. However the spacing between the particles in the crystalline environment is much smaller than in the system with long-ranged interactions. In our model system, the interactions between the particles are of the form $r^{-12}$, which is a much shorter range. This essentially means that the volume fraction required for crystallization can be brought down by making use of the depletion interaction between the external potentials and larger particles to manipulate the local volume fraction. The volume fraction of the larger particles to crystallize may be brought down further by increasing the strength of depletion interaction.

### 3.3.4  Coordination number

As our system is anisotropic and heterogeneous due to the presence of the external repulsive barrier, the analysis based on $g(r)$ may not be accurate enough to assert the crystalline nature of the pure phase. In order to further assert the phase separation and subsequent crystallization, we have calculated the coordination number, $N_{nni}$, of each of the large particles. In a face centered crystalline phase, each particle ideally should have 12 nearest neighbors. We have employed the solid-angle based nearest neighbor algorithm(SANN) to calculate the number of nearest neighbors of each particle[38, 39, 40]. Figure 3.7(a) depicts the probability distribution of the nearest neighbors $P(N_{nni})$ for the larger particles for a total volume fraction of $\phi = 0.5$ at different temperatures. As evident from the figure, at high temperatures the distribution is peaked around 9, which indicates the particles are in fluid phase. As the temperature is decreases to $T = 0.5$, the intensity of the peak at 9 decreases and a new peak appears at 12, which indicates the formation of crystalline domain. This peak at 12 becomes more prominent as temperature is decreased further. To make this
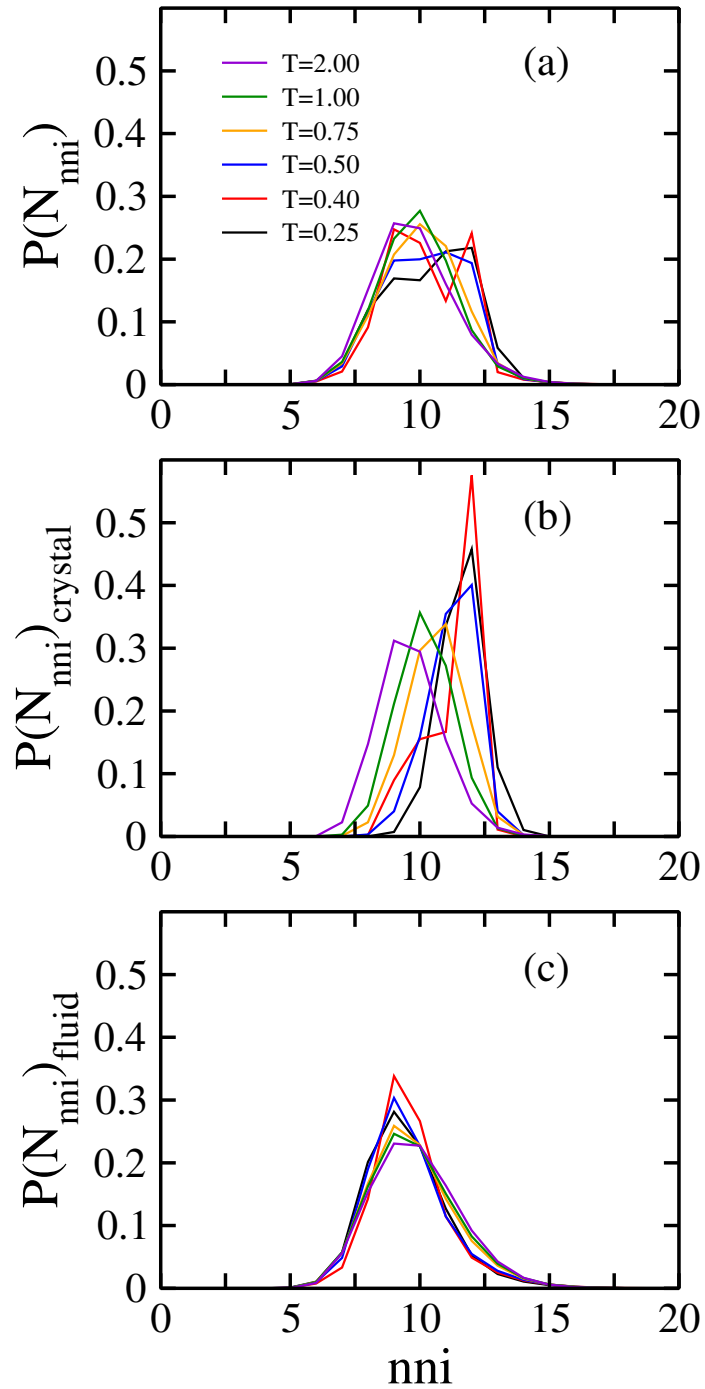
Figure 3.7: Probability distribution function, $P(N_{nni})$ of the coordination numbers of larger particles; (a) total, (b) crystal phase and (c) fluid phase
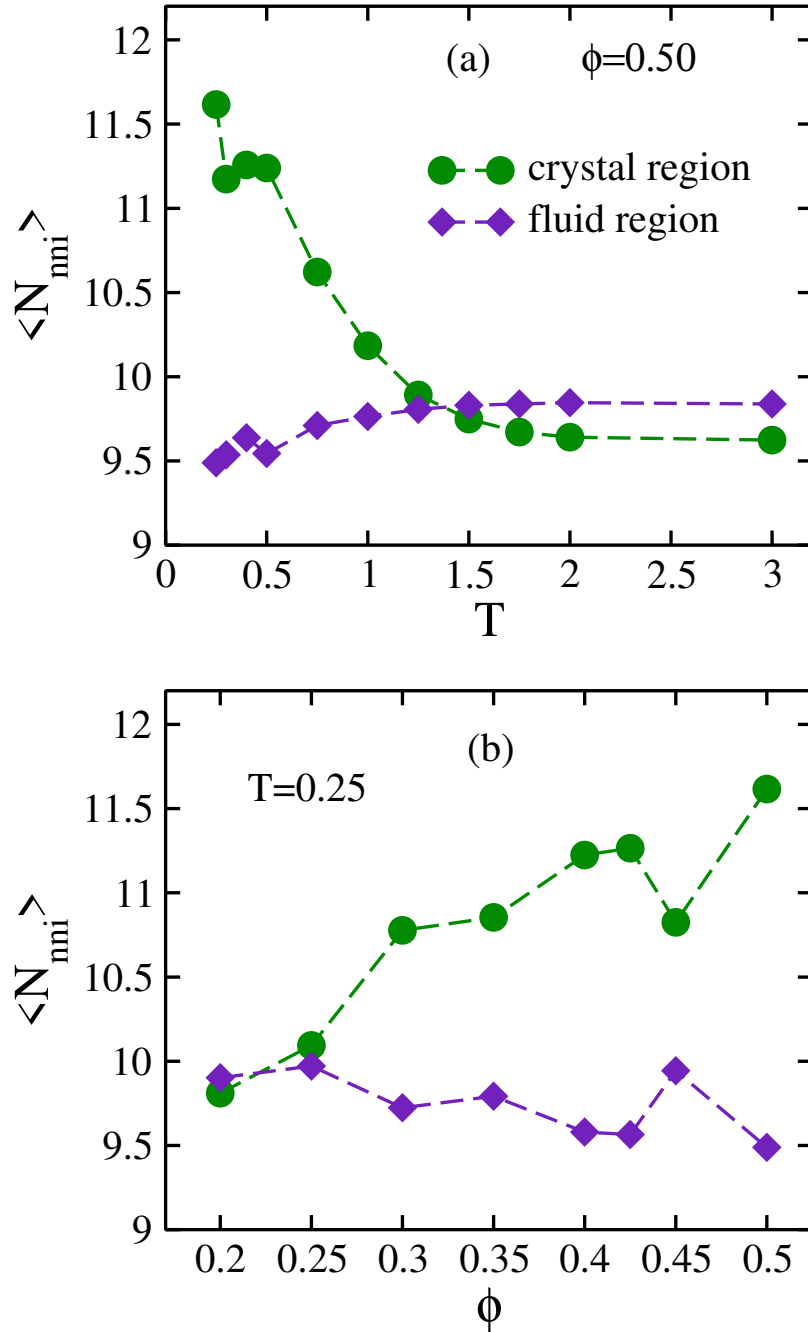
Figure 3.8: Average coordination number $< N_{nni} >$, of larger particles in crystal and fluid environment against (a) temperature and (b) total volume fractions. The average coordination number does not change significantly with temperature and volume fraction in the fluid region. However, in crystal region, $< N_{nni} >$ increases with decrease in temperature or increase in volume fraction and reaches close to 12, indicating crystallization.

more clear, we have calculated the probability distribution of coordination numbers separately for (i) the region of potential barrier and (ii) every where else. This are shown in figure 3.7(b) and (c). These distributions are single peaked at all temperatures. However the peak of the distribution changes from 9 to 12 as temperature decreases. This indicates that formation of crystal domain by the large particles in the region of potential barrier. However, the $P(N_{nni})$ for the regions excluding the potential does not change significantly as temperature decreases, confirming the larger particles are in fluid phase in this region. We have also calculated the average coordination number of larger particles, $< N_{nni} >$, in these two regions. This is shown in Figure 3.8(a). At high temperatures, the average coordination numbers in both regions are between 9 and 10. However, as $T$ decreases to 1.25, the average coordination number in the region of external potential barrier start increasing sharply, indicating the onset of phase separation. At temperatures below 0.5, $< N_{nni} >$ goes above 11. Since the surface atoms of the crystalline domain is also included in the calculation, the average value does not attain the ideal value of 12. In Figure 3.8(b), we plotted the average coordination number against total volume fractions at temperature $T =$ 0.25. At the low volume fractions, the average coordination number of large particles both in the region of potential barrier as well as in the bulk are close to 10, indicating that they are in fluid phase at both the regions. As volume fraction increases, the $< N_{nni} >$ does not change significantly for the large particles in the bulk region and the particles remains to be in fluid phase. However, the average coordination number of larger particles in the region of external potential barrier and reaches above 11 for volume fractions higher than 0.40. This confirms that fcc crystals are formed in this region in consistent with the behavior of radial distribution functions.
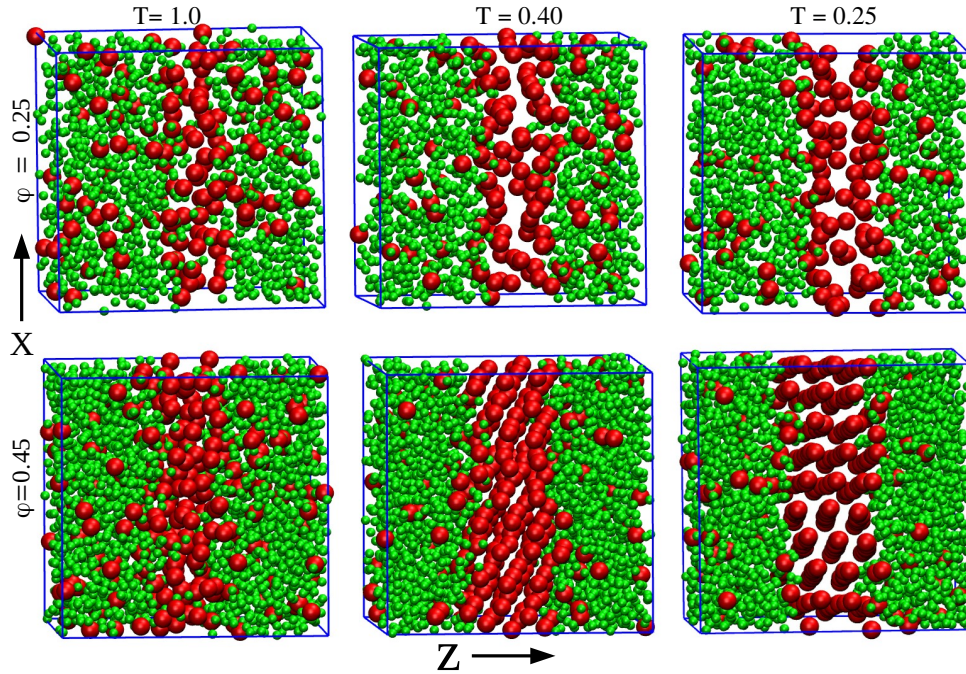
Figure 3.9: Snapshots of instantaneous configurations at two different volume fractions and 3 different temperatures

### 3.3.5 Instantaneous configurations

In order to visualize how the demixing and subsequent crystallization happens in our model system, we have plotted few representative configurations in Figure 3.9. Typical configurations at two different volume fractions ($\phi$=0.25 and 0.45) and 3 different temperatures ($T$= 0.25, 0.40, 1.0) are shown. At lower volume fractions, there is no ordering of larger particles, even though larger particles prefers to get attracted towards the barrier and the demixing is not complete. However, at higher volume fractions, as temperature decreases, it is more evident that the region where potential barrier is present gets occupied more and more by larger particles. The larger particles' local density at the barrier increases and they tend to form ordering as visible from the picture. As discussed in the previous sections, at higher volume fractions and lower temperatures, the larger particles form an fcc crystalline structure.

## 3.4   Dynamics

As discussed earlier in this thesis, it has been shown earlier that this model at low volume fractions shows intriguing dynamical properties of both the smaller and the larger particles. For example, the dynamics of smaller particles at a lower temperature are similar to that of supercooled liquids, even though the volume fractions are very small[26]. This is manifested by the appearance of a plateau in the mean squared displacement at intermediate times, stretched exponential decay of intermediate scattering function, nonzero values of non-Gaussian parameters, etc. Hence it will be interesting to investigate the dynamics of the components in the mixture and study the changes in their dynamical properties when demixing and subsequent crystallization happen. So we have calculated different dynamical properties of the binary colloidal system from the simulated trajectories.

### 3.4.1   Mean squared displacement

Figure 3.10 shows the mean squared displacement(MSD) of smaller particles along $z$-direction for different temperatures at four different volume fractions. At higher temperatures, the MSD is ballistic at earlier times, crossing over to a diffusive regime at longer times. As we decrease the temperature, the dynamics of smaller particles slow down, developing a plateau at intermediate times before crossing over to diffusive dynamics. These results are in agreement with earlier investigations at low volume fractions[26, 27]. However, at high volume fractions and low temperatures, MSD reaches the plateau and continues to stay there even at very large times. This is related to the crystal formation of larger particles in the region of the external potential barrier. Once the larger particles form a compact crystal, the smaller particles find it impossible to penetrate through this structure and remain completely localized between two crystalline domains (crystalline domains are repeated along the $z$-direction because of the periodic boundary conditions). This com-
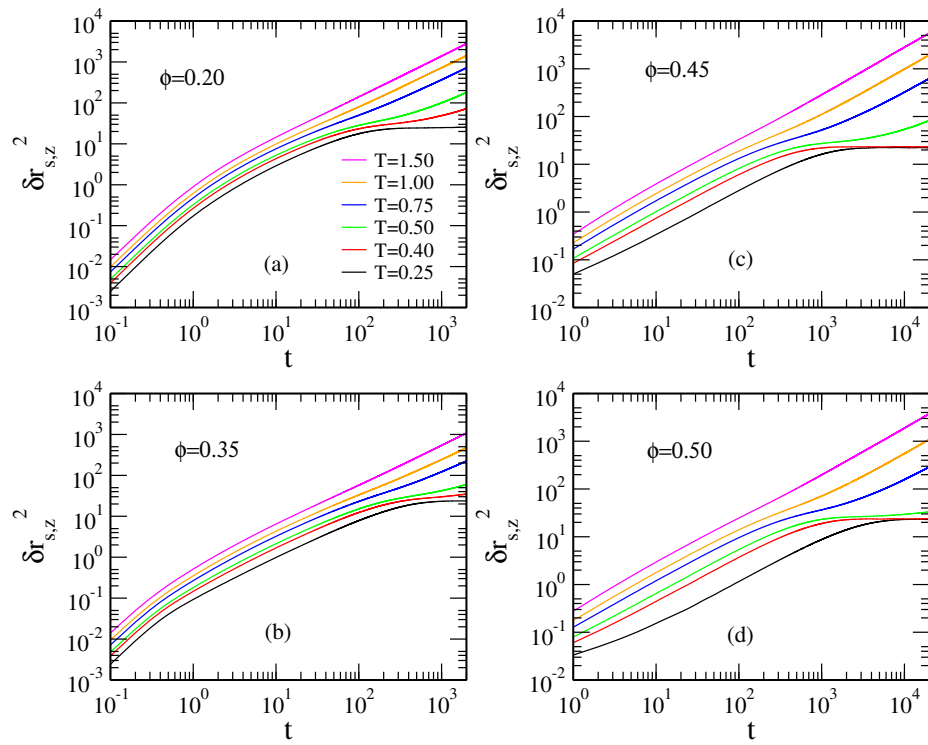
Figure 3.10: Mean squared displacement of smaller particles along the $z$-direction for $\phi = 0.20, 0.35, 0.45, 0.50$ and for T=0.25, 0.4, 0.5, 0.75, 1.0 and 1.5. At low temperatures, MSD shows a plateau at larger times.
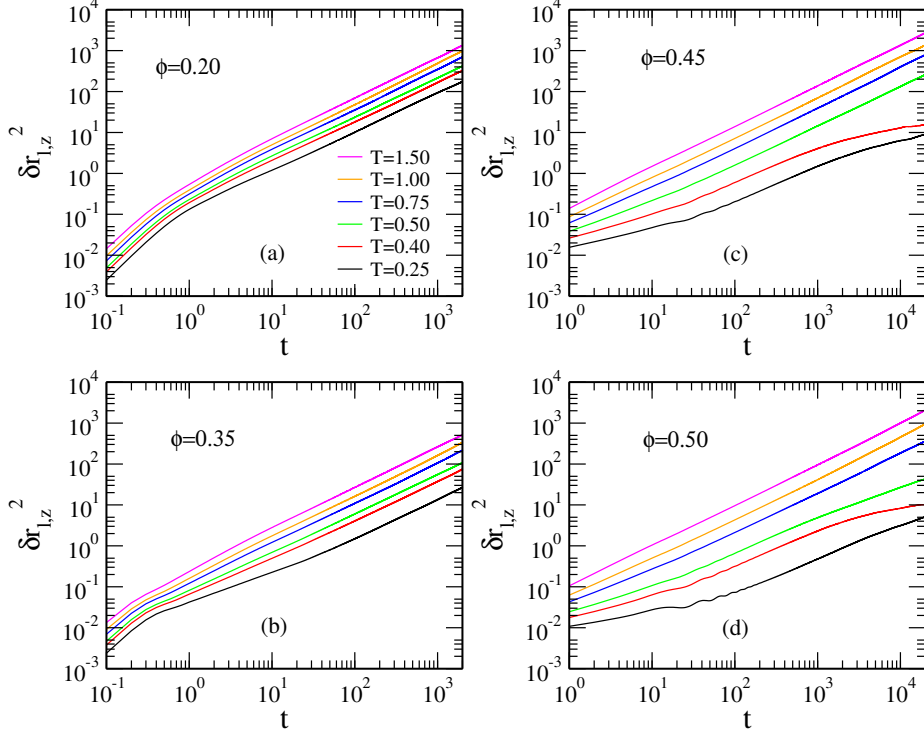
Figure 3.11: Mean squared displacement of larger particles along the $z$-direction for $\phi = 0.20, 0.35, 0.45, 0.50$ and for T=0.25, 0.4, 0.5, 0.75, 1.0 and 1.5. MSD is linear except for those phase points where crystalline formation occurs.

plete localization of smaller particles is reflected in the saturated value of mean squared displacement.

The dynamics of larger particles at low volume fractions is found to be completely contrasting compared to that of smaller particles. Because of the depletion interaction between the external potential barrier and larger particles, MSD of larger particles remains linear at very low temperatures, thus does not show any slowing down of dynamics. We found that our results are matching with these results till the total volume fraction is 0.4. Figure 3.11 depicts the MSD of larger particles along $z$-direction at different volume fractions and at different temperatures. As evident from figure 3.11, at volume fractions larger than 0.4, the mean squared displacement of larger particles deviates from the linear behavior and shows signs of slowing down at lower temperatures. Here again, the demixing and formation of
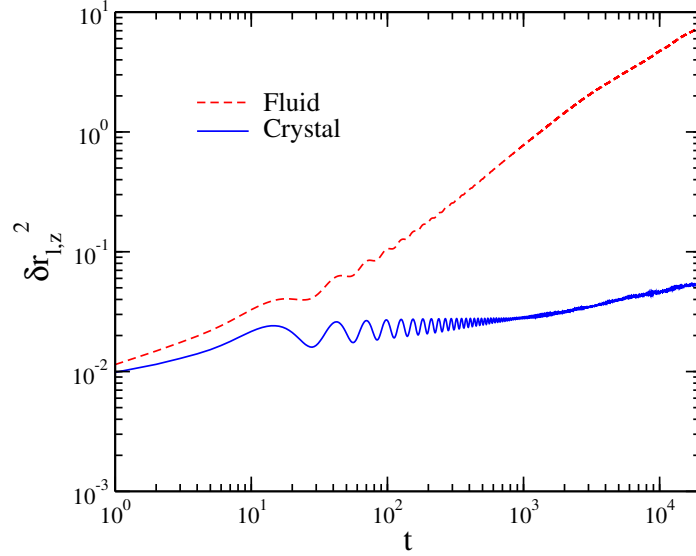
Figure 3.12: Mean squared displacement of larger particles which are in the crystalline phase(solid line) and fluid phase(dashed line) at $\phi$=0.50 and $T$=0.25 along $z-$direction. MSD's at other phase points where a crystalline domain present are similar.

the crystalline phase cause this slowing down behavior of dynamics. It should be noted that the mean squared dispalcement shows a subdiffusive behaviour at small and intermediate times when the volume fraction is close to 0.40, but smaller and at very low temperatures. At these volume fractions and temperatures, the volume fraction of large particles near the potential barrier is very close to the freezing density so that they will start forming clusters. This in turn slows down the dynamics of the system, which is manifested as subdiffusive at small and intermediate times. It will be interesting to observe the dynamics of larger particles that are in the crystal phase and in the fluid phase separately. So we have separated out the mean squared displacement of larger particles that are participating in the crystal formation and that are in the fluid phase along the $z$-direction. This is shown in figure 3.12 for one phase point ($\phi = 0.50$ and $T = 0.25$). We get similar graphs for other phase points where a crystalline domain is present. The mean squared displacement of particles in the crystalline environment reaches a plateau within a very short time, which is as expected. Please note that a very small increase in MSD occurs at very large times. This is due to

92

the surface atoms which get detached from the crystalline phase and enter into the fluid region. However, we found that such occurrences are very small in number and do not alter the average value of MSD significantly. Also please note that the MSD is oscillatory at intermediate time scales. Two reasons can be attributed to this: one, the crystalline structure are formed only in the region of external potential barrier which is very narrow. So the particles in the crystals are not tightly bound as we expect in the case of larger crystals. This will in turn make the particles, especially near the surface to oscillate more. Secondly, since the crysalline region is of narrow width, the crystal as a whole can oscillate along the direction of external pontetial barrier. This can result in oscillatory behaviour of mean squared displacement[41]. The MSD of larger particles in the fluid phase increases with time linearly. The fluctuations from the linear behavior in their MSD is due to the fact that the number of larger particles in the fluid phase is quite small leading to poor statistics.

We have also investigated the dynamics of larger particles perpendicular to the direction of external potential barrier. Since particles do not have to encounter the external potential barrier in these directions, there will not be any direct effect of depletion interaction in their dynamics in these directions, i.e., the consequence of depletion interactions on dynamics in these directions occurs via the demixing and subsequent crystallization of the system. In figure 3.13, the MSD of larger particles along the perpendicular direction of the external potential barrier is given. As expected, the MSD is linear in time and does not show any signatures of slowing down. As in the case above, we separated out the mean squared displacements of larger particles in the crystalline and fluid environment separately. This is plotted for the phase point($\phi = 0.50$ and $T = 0.25$) in figure 3.14. The MSD of larger particles in the fluid phase increases with time linearly as expected. However, interesting behavior occurs in the dynamics of larger particles in the crystal phase. Their MSD also increases linearly with time and shows a nonzero diffusion coefficient. This shows that while the crystalline domain remains intact in its structure, it diffuses as a whole in the direc-
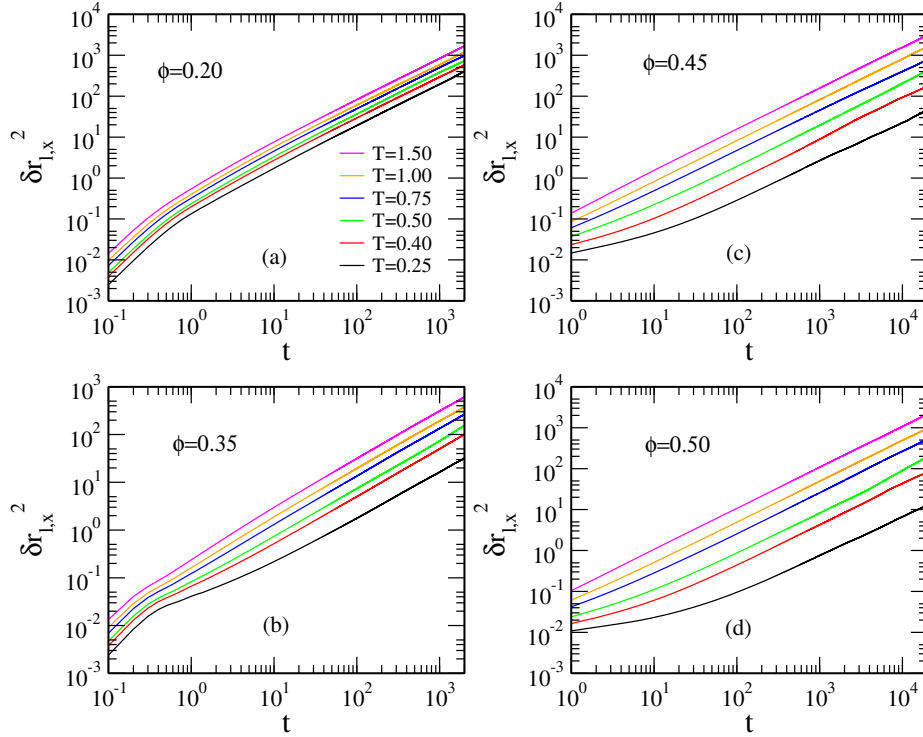
Figure 3.13: Mean squared displacement of larger particles perpendicular to the external potential barrier for $\phi = 0.20, 0.35, 0.45, 0.50$ and for T=0.25, 0.4, 0.5, 0.75, 1.0 and 1.5.
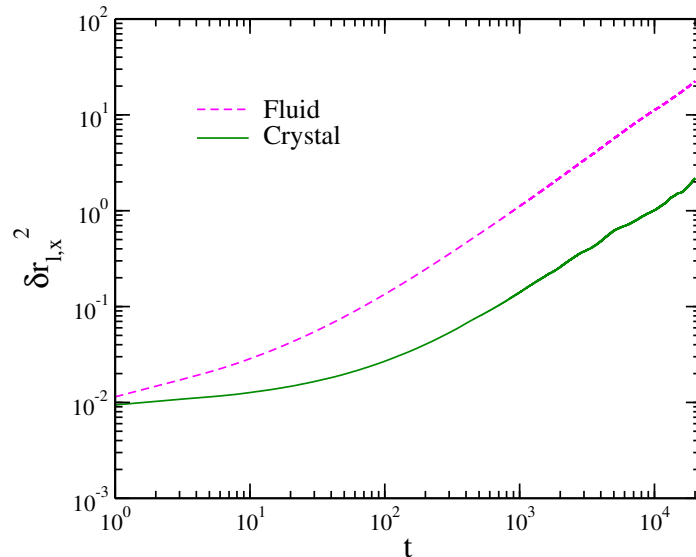


Figure 3.14: Mean squared displacement of larger particles perpendicular to the external potential barrier which are in the crystalline phase(solid line) and fluid phase(dashed line) at $\phi$=0.50 and $T$=0.25. MSD's at other phase points where a crystalline domain present are similar.

tion perpendicular to the external potential barrier (see figure 3.14). Note that this diffusive dynamics along the $x$ and $y$ directions is perpendicular to the crystal-fluid boundary and periodic boundary conditions makes the crystal phase extended along these directions. Such moving crystals have been reported before, but predominantly in nonequilibrium systems where the crystals are exposed to heat or light[29, 30, 32]. These thermosalient and photosalient crystals can sense and respond to such external stimulus and undergo translation and rotation. Dynamic crystals have also been reported in the case of active colloids[42], where racemic mixture of colloids show a hexatic order with diffusive dynamics. However, our model system is an equilibrium system with an external potential involved. Hence the diffusive dynamics we observe in our system is different from the moving crystals observed earlier with external stimuli. Recently, a dynamical crystal phase has been reported in a soft crystal with interstitial dopants near their melting point[43]. To the best of our knowledge, this is the only equilibrium system where a dynamic crystal phase was reported. Although, here the body centered cubic structure of the soft crystal remains intact on average, but the instantaneous structure shows significant deviations from the perfect lattice. However, we have not observed such larger deviations in our system. This warrants further investigation on this diffusive behavior of the crystalline domain to ascertain the physical reasons behind it.

### 3.4.2 Temperature dependence of diffusivity

The temperature dependence of the self diffusion coefficient of fluids usually follows an Arrhenius behavior[44, 45]. However, deviations from Arrhenius behavior are reported in many cases, especially at lower temperatures. Aquilanti and coworkers proposed a formalism based on Tsallis' nonextensive statistical mechanics[46] to include these deviations also into the framework of Arrhenius equation[47, 48, 49, 50, 51]. They have proposed a
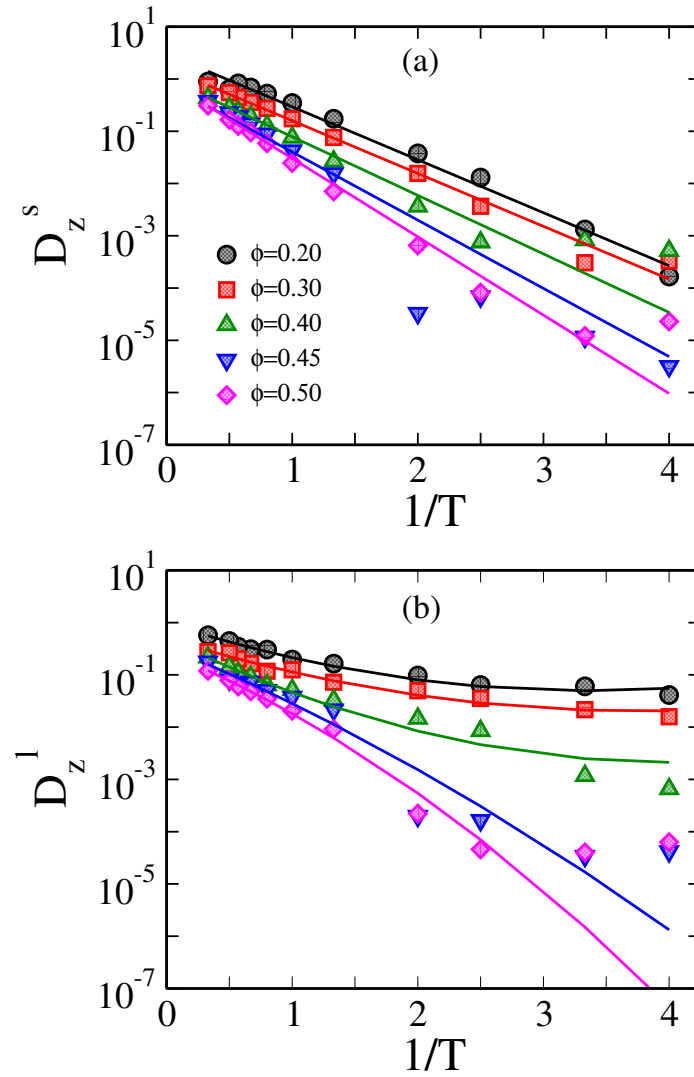
Figure 3.15: $log(D_z)$ versus inverse temperature curve for (a)smaller and (b)larger particles at different volume fractions. The points are from simulations and the curve is a fit to the (a) Arrhenius and (b) $d$-Arrhenius equation(eqn. 5)
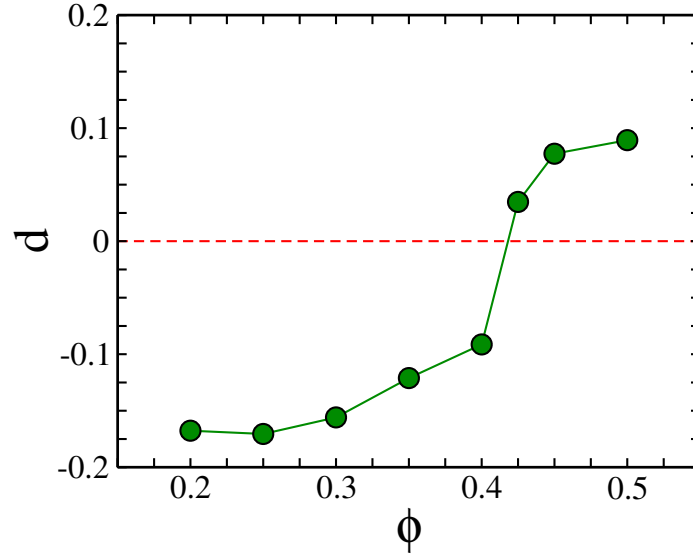
Figure 3.16: The deformation parameter $d$ versus the total volume fraction $\phi$. The sign of $d$ changes from negative to positive at $\phi = 0.425$, indicating the crossover from sub-Arrhenius to super-Arrhenius diffusion.

deformed Arrhenius equation as

$$D(T) = A\Big[1 - d\frac{E_0}{k_B T}\Big]^{1/d} \tag{3.5}$$

which includes Arrhenius behavior as well as the deviations from it. Here $E_0$ is the height of the potential barrier. $d$ is the parameter, known as 'deformation parameter', which will determine the behavior of $D$ with respect to temperature. If the diffusion is Arrhenius in nature, then $d = 0$. For positive values of $d$, the temperature dependence of diffusion is termed as 'super-Arrhenius', where we get convex curve for $log(D)$ $vs.1/T$. When the $log(D)$ $vs.1/T$ curve is concave, the value of $d$ is negative and diffusion is said to be 'sub-Arrhenius'. In most of the observed deviations, super-Arrhenius behavior occurs in classical systems where correlated motion plays an important role as in the case of su-percooled liquids[52, 53]. Sub-Arrhenius behavior is mostly found in processes where quantum effects play an important role as in the case of tunneling effect during chemical reactions[47, 54, 55]. However, we have shown in chapter 2 that self-diffusion of larger par-

ticles in a binary mixture subjected to an external potential barrier at low volume fractions is found to be sub-Arrhenius in nature with a negative $d$ parameter[27]. Hence, we have investigated the temperature dependence of self-diffusion of larger particles at different volume fractions. Figure 3.15 shows the $log(D_z)$ versus inverse temperature curve for different volume fractions. It is evident from the figure that at low volume fractions $log(D_z)$ $vs.1/T$ curve is concave and the diffusion of large particles follows a sub-Arrhenius behavior. However, as we increase the volume fraction, the concavity of the $log(D_z)$ $vs.1/T$ curve decreases and, above $\phi = 0.4$, the curve becomes convex. This means that at higher volume fractions, there is a cross over from sub-Arrhenius to super-Arrhenius behavior in the diffusion of larger particles. To make it more quantitative, we have fitted the $log(D_z)$ $vs.1/T$ curves with the deformed Arrhenius equation and extracted the values of $d$ parameter for different volume fractions. These are plotted in figure 3.16. At low volume fractions, $d$ is negative indicating the sub-Arrhenius nature. At $\phi = 0.425$, $d$ suddenly changes the sign and becomes positive, indicating a cross over to super-Arrhenius behavior. It should be noted that this crossover coincides with the crystallization of larger particles in the region of the potential barrier. As we have seen earlier, when the crystallization happens in the barrier region, most of the larger particles participate in crystal formation and, the number of larger particles in the fluid region becomes much smaller. So the overall diffusion of larger particles becomes suppressed and this is manifested as the super-Arrhenius behavior.

## 3.5   Conclusion and summary

We have investigated the demixing of a binary colloidal mixture subjected to an external potential barrier. The attractive depletion interaction between the potential barrier and larger particles in the binary mixture causes it to phase separate into two regions: one a pure phase comprised of only larger particles in the region of the potential barrier and another a mixed

phase elsewhere. This phase separation allows one to manipulate the local volume fraction of large particles high enough that they undergo crystallization into an fcc structure. In general, such manipulations of local density are done by nonequilibrium processes like dielectrophoresis and diffusiophoresis. However, the binary colloidal mixture we have investigated is in equilibrium and, the changes in the local density of colloidal particles are done through the depletion interaction. The crystal domain, formed in the region of the external potential barrier, moves perpendicular to the external potential. Again such moving crystals are generally observed in nonequilibrium systems, where the crystallites are subjected to driving forces. Our model system does not have any such driving forces and the physical reasons behind these dynamics is unclear. The formation of this crystalline phase coincides with a change over from sub-Arrhenius to super-Arrhenius diffusion of larger particles. It has been concurred that sub-Arrhenius behavior occurs in processes where quantum effects such as tunneling are predominant while super-Arrhenius diffusion occurs in classical systems where particles undergo correlated dynamics such as in supercooled liquids. However, our model system of binary colloids is purely a classical system, where both types of behaviors occur. At low densities, the diffusion is sub-Arrhenius because the depletion attraction between the barrier and the larger particles effectively reduces the activation energy for diffusion and makes it temperature dependent. At higher densities, depletion interaction causes phase separation and subsequent crystallization of larger particles, hindering their diffusion. Thus the diffusive behavior changes from sub-Arrhenius to super-Arrhenius. Finally, the interaction between the colloidal particles in our model system is purely repulsive. However, in real systems, attractive interactions of Van der Waals nature are present. These attractive interactions will further enhance the demixing and the effects we observed in our model system will be more pronounced if we include attractive interactions in out model system.

# References

[1] P. N. Pusey, W. Van Megan, *Nature* **320**, 340-342 (1986).

[2] N. Asherie, A. Lomakin, G. B. Bendek, *Phys. Rev. Lett.* **77**, 4832-4835 (1996).

[3] A. Yethiraj, *Soft Matter* **3**, 1099-1115 (2007).

[4] M. Ledesma-Motolinía, J. L. Carrillo-Estrada, F. Donado, *Sci. Rep.* **11**, 16531 (2021).

[5] S. H. Park, Y. Xia, *Langmuir* **15**, 266-273 (1999).

[6] L. Gonzalez-Urbina, K. Baert, B. Kolaric, J. Pérez-Moreno, K. Clays, *Chem. Rev.* **112**, 2268-2285 (2012).

[7] A. P. Hynninen, *et al.*, *Nat. Mater.* **6**, 202-205 (2007).

[8] D. Wan, S. C. Glotzer, *Phys. Rev. Lett.* **126**, 208002 (2021).

[9] H. Pattabhiraman, G. Avvisati, M. Dijkstra, *Phys. Rev. Lett.* **119**, 157401 (2017).

[10] P. N. Pusey, in: Liquids, Freezing and Glass Transition, Les Houches Session LI, D. Levesque, J. P. Hansen, J. Zinn-Justin, eds. (Elsevier, Amsterdam, 1991).

[11] L. B. Chen, C. F. Zukoski, B. J. Ackerson, H. J. M. Hanley, G. C. Straty, J. Barker, C. J. Glinka, *Phys. Rev. Lett.* **69**, 688–91 (1992).

[12] Y. L. Wu, D. Derks, A. van Blaaderen, A. Imhof, *Proc. Natl. Acad. Sci. USA* **106**, 10564–9 (2009).

[13] A. V. Mokshin, J. L. Barrat, *Phys. Rev. E* **77**, 021505 (2008).

[14] B. J. Ackerson, P. N. Pusey, *Phys. Rev. Lett.* **61**, 1033–6 (1988).

[15] P. Panine, T. Narayanan, J. Vermant, J. Mewis, *Phys. Rev. E* **66**, 022401 (2002).

[16] B. J. Ackerson, *J. Phys.: Condens. Matter* **2**, SA389–SA392 (1990).

[17] M. E. Leunissen, M. T. Sullivan, P. M. Chaikin, A. van Blaaderen, *J. Chem. Phys.* **128**, 164508 (2008).

[18] M. T. Sullivan, *et al.*, *Phys. Rev. Lett.* **96**, 015703 (2006).

[19] A. Reinmuller, *et al.*, *J. Chem. Phys.* **136**, 164505 (2012).

[20] S. Asakura, F. Oosawa, *J. Chem. Phys.* **22**, 1255-1256 (1954).

[21] A. Vrij, *Pure Appl. Chem.* **48**, 471-483 (1976).

[22] A. J. Kim, P. L. Biancaniello, J. C. Crocker, *Langmuir* **22**, 1991-2001 (2006).

[23] K. N. Pham, S. U. Egelhaaf, P. N. Pusey, W. C. K. Poon, *Phys. Rev. E.* **69**, 011503 (2004).

[24] J. Y. Walz, *J. Colloid Interface Sci.* **178**, 505-513 (1996).

[25] A. V. Anil Kumar, *J. Chem. Phys.* **138**, 154903 (2013).

[26] A. V. Anil Kumar, *J. Chem. Phys.* **141**, 034904 (2014).

[27] M. Mustakim, A. V. Anil Kumar, *Physica A* **563**, 125462 (2021).

[28] J. Singh, A. V. Anil Kumar, *Phys. Rev. E* **101**, 022606 (2020).

[29] M. K. Panda, T. Runcevski, A. Husain, R. E. Dinnebier, P. Naumov, *J. Am. Chem. Soc.* **137**, 1895-1902 (2015).

[30] M. K. Panda, *et al.*, *Sci. Rep.* **6**, 29610 (2016).

[31] T. Shima, *et al.*, *Angew. Chem. Int. Ed.* **53**, 7173-7178 (2014).

[32] P.Commins, *et al.*, *Chem. Comm.*, **52**, 13941-13954 (2016).

[33] W. G. Hoover, *et al.*, *J. Chem. Phys.* **52**, 1931-4941 (1970).

[34] W. G. Hoover, S. G. Grey, K. W. Johnson, *J. Chem. Phys.* **55**, 1128-1136 (1971).

[35] J. F. Lutsko, M. Baus, *J. Phys.:Condens. Matter* **3**, 6547-6552 (1991).

[36] S. S. N. Chari, C. Dasgupta, P. K. Maiti, *Soft Matter* **15**, 7275-7285 (2019).

[37] C. Dalle-Ferrier, *et al.*, *Soft Matter* **7**, 2064-2075 (2011).

[38] J. A. van Meel, L. Filion, C. Valeriani, D. Frenkal, *J. Chem. Phys.* **136**, 234107 (2012).

[39] V. Lolito, T. Zambelli, *Adv. Colloid Interface Sci.* **284**, 102252 (2020).

[40] V. Lolito, T. Zambelli, *Langmuir* **34**, 7827-7843 (2018).

[41] K. M. Aoki, *Solids* **2**, 249-264 (2021).

[42] Z. Shen, A. Wurger, J. S. Lintuvuori, *Soft Matter* **15**, 1508-1521 (2019).

[43] J. Tauber, J. Higler, J. Sprakel, *Proc. Natl. Acad. Sci.* **113**, 13660-13665 (2016).

[44] S. Arrhenius, *Z. Phys. Chem.* **4**, 226-248 (1889).

[45] H. A. Kramers, *Physica(Utretch)* **7**, 284-304 (1940).

[46] C. Tsallis, *J. Stat. Phys.* **52**, 479-487 (1988).

[47] Aquilanti, V. *et al. Chem. Phys.*, **398**, 186-191 (2012).

[48] V. Aquilanti, *et al.*, *Chem. Phys. Lett.* **498**, 209-213 (2010).

[49] V. H. C. Silva, V. Aquilanti, H. C. B. de Oliveira, K. C. Mundim, *Chem. Phys. Lett.* **590**, 201-207 (2013).

[50] V. H. C. Silva, N. D. Coutinho, V. Aquilanti, *AIP Conf. Proc.* **1790**, 02006 (2016).

[51] M. Nishiyama, S. Kleijn, V. Aquilanti, T. Kasai, *Chem. Phys. Lett.* **470**, 332-336 (2009).

[52] G. Stirnemann, D. Laage, *J. Chem. Phys.* **137**, 031101 (2012).

[53] V. K. de Souza, D. J. Wales, *Phys. Rev. Lett.* **96**, 057802 (2006).

[54] Z. X. Liang, T. Lee, K. A. Resing, N. G. Ahn, J. P. Klinman, *Proc. Natl. Acad. Sci. USA* **101**, 9556-9561 (2004).

[55] J. Braun, *et al.*, *J. Am. Chem. Soc.* **118**, 11101-11110 (1996).

# Chapter 4

# System size effects on the dynamical properties of binary colloidal mixture

## 4.1 Introduction

In chapter 2, we have investigated the dynamics of our model binary colloidal mixture under an external potential and found several interesting changes in the dynamics of both species in the mixture. In molecular simulations, we used a system of few thousands of particles which makes the system we are studying microscopic. By employing the periodic boundary conditions we can mimic an infinite system in order to correct the physical properties of finite systems[1]. However, the properties calculated in molecular dynamics simulations can still differ from their macroscopic counterparts due to the neglect of long wavelength fluctuations of corresponding properties. This is more important in the case of phase transitions and critical phenomena as the singularities in thermodynamic functions that are associated with a critical point generally occurs in the thermodynamic limit. If the dimensions of the system remains finite, the behaviour of thermodynamic functions are modified. The modifications are essentially become significant if the system dimensions are comparable to the correlation length of critical fluctuations. This can be overcome by using finite size scaling[2, 3, 4], proposed by Fischer in 1973. The theory of finite size scaling at phase transitions has since then received a lot of attention[5].

The effect of finite system size away from critical points are not that significant. Also, dynamical properties shows less system size effects compared to the thermodynamic functions. However, system size effects are noticed for many dynamical properties even when the system is away from the critical points. For example, diffusion coefficients and shear viscosity of Lennard-Jones fluids exhibit strong system size effects in simulations[6]. The diffusion coefficient is found to be increasing with system size, while shear viscosity decreases with increasing system size. Dynamical properties of systems with long-ranged interactions such as Coulomb interactions are found to be significantly different as the system size is varied[7]. Hydrodynamic interactions, which varies as $1/r$ also can cause significant system size effects[8, 9]. So, in the process of analysing dynamical, the effects of finite system size should be removed.

In our simulations we are studying the effect of external potential of Gaussian form on the dynamics of small and large colloidal particles. These colloidal particles are modelled as soft spheres with short range repulsive interactions. Also, in most of our simulations, we have used low volume mixtures($\phi = 0.20$). So any significant system size dependence of dynamical properties are not expected. However, we have extended the simulation for different system sizes to study the finite size effects, if any and to study how the dynamical properties change with system size. In order to do this, we have simulated the system size using different boxlengths, while keeping the volume fraction (total and of each species) constant. Our results and observations are outlined in this chapter.

## 4.2   Simulation model

We investigated the same model system of binary colloids as described in the earlier chapters (see chapter 2). We have carried out canonical ensemble molecular dynamics simulations of this model system at different temperatures. Since our aim is to study the finite size

effects we performed the simulations for different box lengths $L = 9, 10, 11, 13, 15, 17$ while keeping the total volume fraction of the binary mixture fixed at $\phi = 0.20$. As in the previous studies, we use an equivolume mixture of both small and large colloidal particles. The interaction between the colloidal particles as well as the external potential is kept same as in the earlier chapters. The dynamical properties are averaged over three simulation runs and analysed for possible finite size dependence. One important point to be noted is the width of the Gaussian external potential is not varied and kept at $w = 3.0$ at all simulations irrespective of the change in simulation boxlength.

## 4.3    Results and discussion

As explained in the previous chapters, we investigated this binary colloidal mixture for box length $L = 17$ at low volume fraction of $\phi = 0.20$ and observed that the larger components of the mixture show sub-Arrhenius behavior in their diffusivity which is rarely seen in a classical system[10]. Upon increasing the volume fractions larger particles form fcc crystal structure near the barrier while smaller particles remain in fluid phase. The volume fraction of this binary system is still lower than the volume fraction needed for a monodispersed colloidal system to undergo crystallization[11]. The underlying phenomena is explained through the depletion interaction between the larger particles and the barrier. In this chapter we have extended the simulations for other box lengths to investigate the finite size effects and scaling of the dynamical properties in the system.

### 4.3.1    Mean squared displacements (MSD)

We calculated the MSD of both small and large particles along the z-direction using the trajectories obtained from the MD simulations of the binary colloidal mixture in the presence of external Gaussian potential. In figure 4.1 we have plotted the time evolution of MSD of small particles along the $z$-direction where the external repulsive potential is ap-

Figure 4.1: Mean squared displacement(MSD) of small particles along $z$-direction at various temperatures and for box lengths $L = 9, 10, 11, 13, 15, 17$.

plied at different boxlengths. As described in the earlier chapters, the depletion effects due to the presence of smaller particles in the solution, causes anomalous dynamics for smaller particles at this volume fraction at the lower temperatures. The depletion attraction between the larger particles and the barrier keep the smaller particles away from the barrier and make them diffuse slower than the larger particles. At higher temperature the MSD of smaller particles grow linearly with all time for all the box lengths studied. However, below $T = 0.50$ the smaller particles show plateau at intermediate times after the initial ballistic

diffusion for all box lengths, similar to behavior of a supercooled liquid[12]. As evident from the figure 4.1, this behaviour is observed irrespective of the simulation boxlengths. However, it must be noted that the plateau in the MSD at lower temperature starts at earlier times for smaller wavelengths. Also the value of MSD at the plateau decreases as the boxlength decreases. The presence of the external barrier introduces a new length scale to the system which is comparable to the simulation boxlength. The periodicity of the external potential is also same as the simulation boxlength because of the periodic boundary conditions. When the boxlength becomes smaller and smaller, this lengthscale also decreases which is reflected in the earlier appearance of the plateau in MSD as well as its smaller value. In other words, the smaller particles gets localised between the potential barriers at lower temperatures because the effective barrier they need to cross becomes larger due to the depletion attraction between the barrier and the larger particles. So when the simulation boxlength decreases, the smaller particles get less space between the successive barriers to move around which makes their dynamics more restricted and hence the plateau comes earlier at lower boxlengths compared to higher boxlengths.

On the other hand, the larger particles show completely different dynamics at lower temperatures. In figure 4.2 we have shown the comparison MSD curve for larger particles for different box lengths at different temperatures. At higher temperatures the particles have enough thermal energy to cross the barrier, so we get a linear curve at all times as in the case of smaller particles. However, at low temperatures, because of the attractive depletion interaction between the barrier and the larger particles, they are still able to cross the barrier easily compared to smaller particles. This again results in a linear behaviour of MSD vs. time curve in contrast to that of smaller particles. Different box lengths do not affect this qualitative behavior of larger particles except for $L \leq 10.0$ at lower temperatures. At these boxlengths and temperatures below 0.5, the mean squared displacements of larger particles shows signatures of slowing down. The distance between the successive barriers decreases

Figure 4.2: Mean squared displacement(MSD) of large particles along $z$-direction at various temperatures and for box lengths $L =$9, 10, 11, 13, 15, 17.

as we decrease the boxlength which in turn decrease the space available for smaller particles. Thus the effective density of smaller particles between the barriers increases and makes it difficult for larger particles to navigate through. Thus at lower boxlengths and lower temperatures, their dynamics gets slowed down as evidenced by the appearance of a plateau in the MSD at intermediate times. However, still the dynamics of larger particles is faster than the smaller particles at low temperatures. We have already observed this behavior and explained in details in chapter-2, that the dynamics of larger particles is faster than that of

smaller particles, at lower temperatures, and depletion interaction is the primary cause of this kind of dynamics in the binary colloidal system. This enhanced dynamics of larger particles at lower temperature leads to a sub-Arrhenius diffusion in the system. Now with different system sizes, we observe that the MSD does not change significantly. Further to understand the system size dependence of these dynamical properties, we tried to scale the mean squared displacement with respect to the lengthscales and time scales associated with our model system.

## 4.3.2   Scaling of dynamical properties

We have performed the MD simulations of binary colloidal system in the presence of an repulsive external potential of Gaussian form at the center of the simulation box along $z$-direction and the periodic boundary conditions are applied in all directions. Because of the periodic boundary conditions, the external potential is repeated along the $z$-direction with a periodicity which is given by the simulation boxlength. This periodic potential introduces a length scale in the dynamics of the system which is equal to the boxlength along the $z$-direction. Or in other words, because of the periodicity of the potential barrier, in addition of the normal diffusive lengthscale, a new length scale is introduced in the system which is equal to the inverse of the wave vector associated with the external potential barrier, $q = 2\pi/L$, where $L$ is the simulation boxlength. Accordingly the timescale is set by the time it takes a particle to diffuse a distance $q^{-1}$, which is $(q^2 D_0)^{-1}$, thus the dimensionless time scales as [13]

$$t^* = q^2 D_0 t \tag{4.1}$$

where $D_0$ is the short time diffusivity of the particle. At times smaller than this time scale, the partiles do not feel the presence of the external barrier and will be diffusing with a
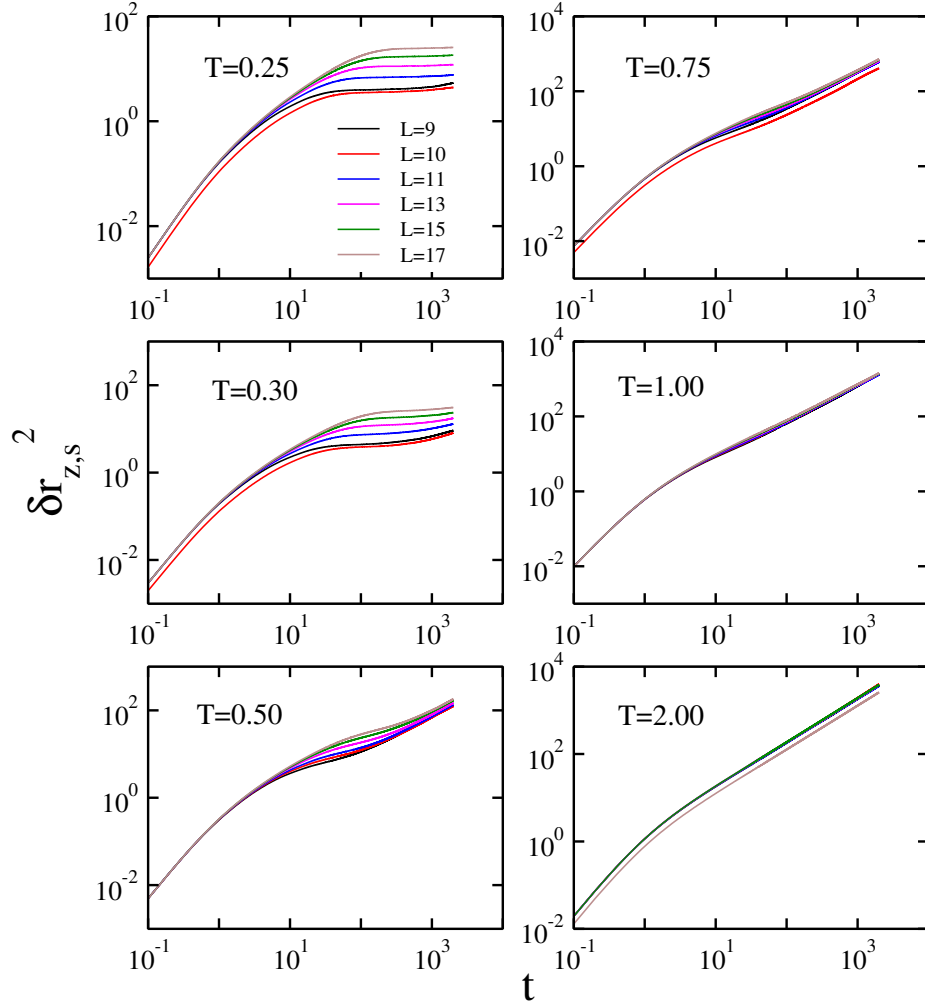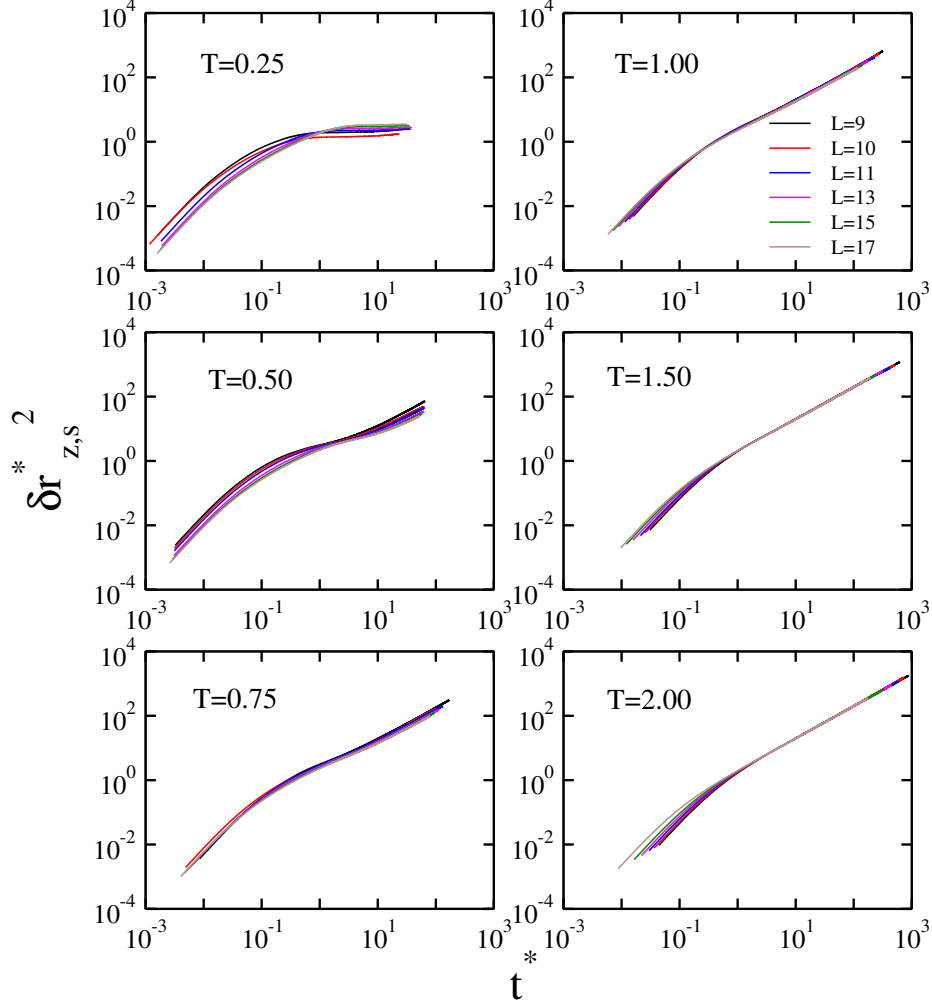
Figure 4.3: Scaled MSD of small particles along $z$-direction at various temperatures and for box lengths $L =$ 9, 10, 11, 13, 15, 17.

diffusion coefficient $D_0$. Similarly the scaled mean squared displacements will be given by

$$\delta r^{*2} = q^2 \delta r^2 \qquad (4.2)$$

We have rescaled the mean squared displacement versus time plot using these two expressions. In figure 4.3 we have plotted the scaled MSD of smaller particles against the scaled time for various temperatures and different box lengths. At higher temperatures the scaled MSD coincides for all the boxlengths. At very low temperatures, there are small deviations which can be attributed to the numerical errors. The scaling can be improved if the simu-
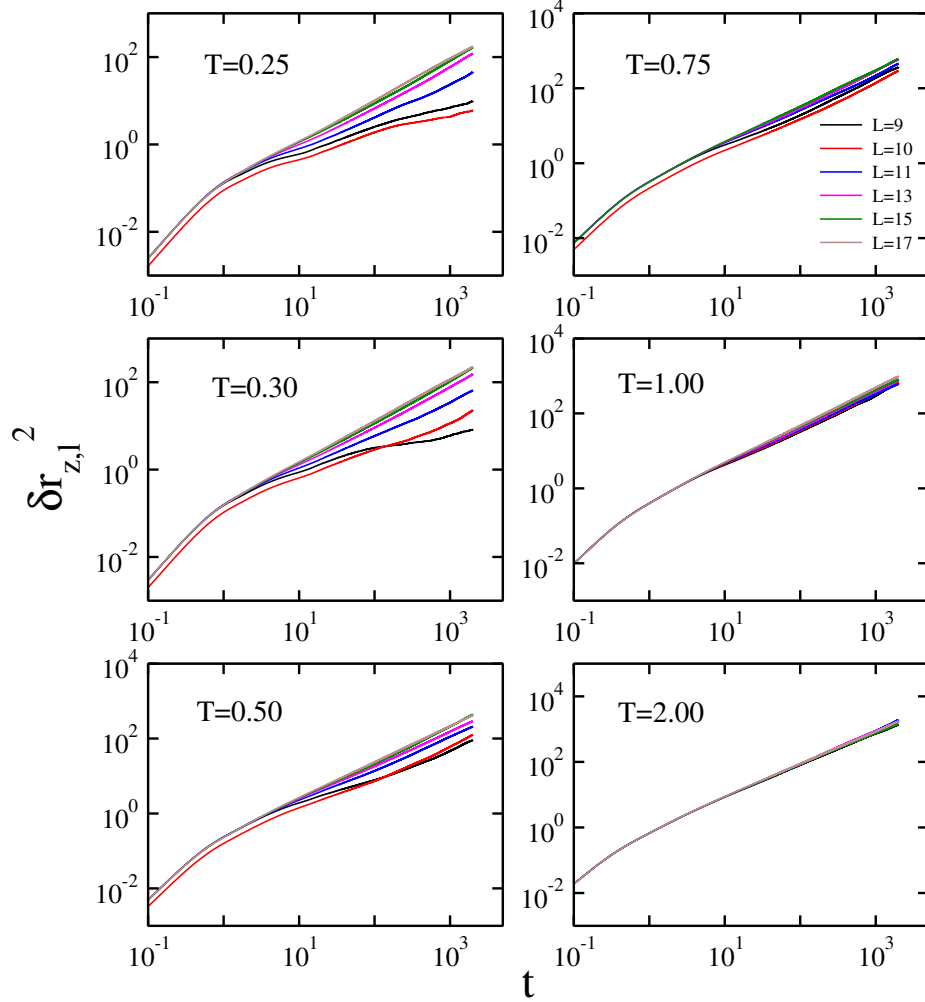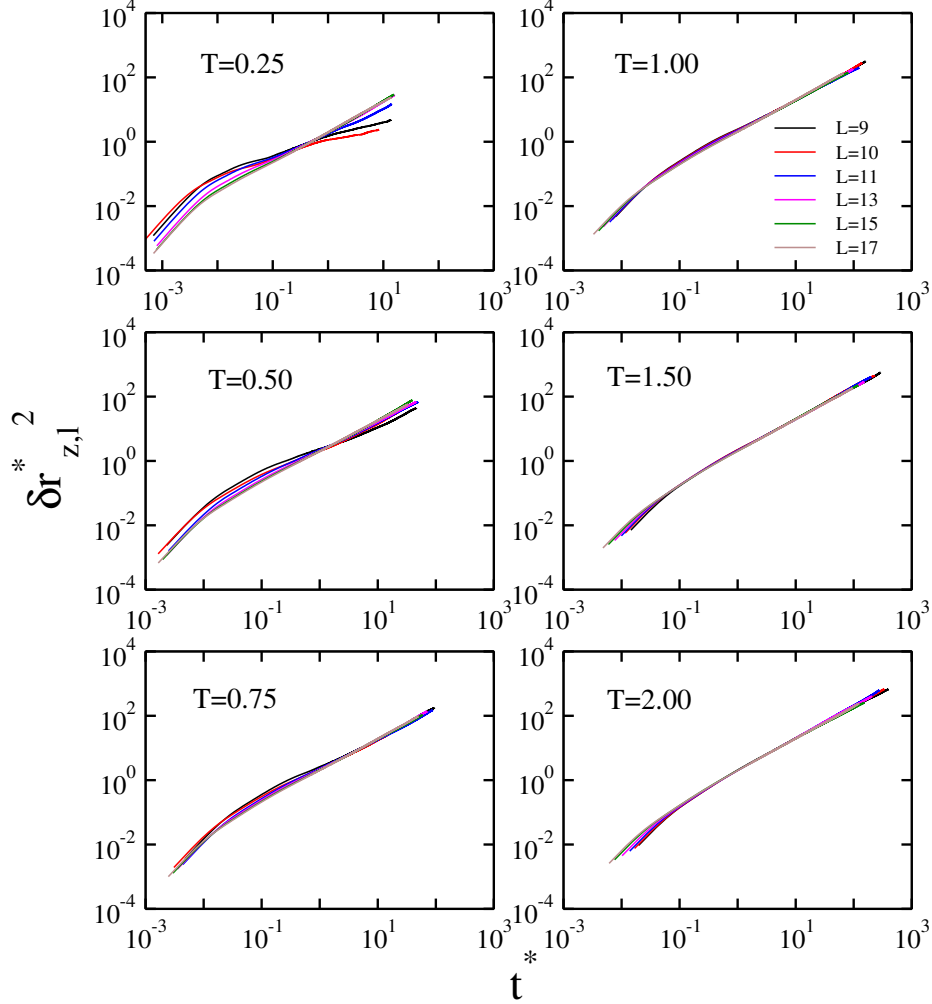
Figure 4.4: Scaled MSD of large particles along $z$-direction at various temperatures and for box lengths $L =$ 9, 10, 11, 13, 15, 17.

lations are carried out for longer times or more simulations runs are carried out. However, there is a very systematic deviation at small times for all temperatures. The scaling is not expected to work at small times, as the particles are undergoing ballistic motion at these times and lengthscale introduced by the external potential does not affect the dynamics of the particles at these small times. The scaling of MSD means that we do not find any significant finite size effects, i.e, the dynamics of smaller particles remain unaffected by the change of system size or box lengths. Also this scaling preserves the qualitative changes

observed in mean squared displacements with respect to temperature.

We have also observed that the scaling works for the mean squared displacement of larger particles in most of the cases. In figure 4.4 we have plotted the scaled MSD of larger particles against the scaled time for various temperatures and different box lengths. As evident from the figure, the scaled MSD matches well for all the box lengths and temperatures except for boxlengths $L \leq 10.0$ at very low temperatures. The scaling fails in those cases where we find that a slowing down of dynamics larger particles. As explained above, at smaller boxlengths and at low temperatures, the smaller particles get crowded in the space between the barriers as the available volume for them decreases. In this case, though the attractive depletion interaction between the external barrier and larger particles still facilitates the larger particles to jump over the barrier, they find it difficult to traverse through the smaller particles confined between the barriers. So the slowing down of larger particles at lower boxlegnths and at lower temperature is characteristically different from that of smaller particles observed at lower temperatures at all box lengths. This difference is the reason why MSD of smaller particles scales even when they exhibit slowing down while the scaling of MSD of larger particles fails when they exhibit slowing down in dynamics.

### 4.3.3 Self Diffusion coefficient

The self diffusion coefficient is calculated from MSD curve by taking the slope at long times. At larger box length like $L = 17$, it is already established that the diffusion coefficient of smaller particles remains higher than that of the larger particles at higher temperature due to high thermal energy, but drastically falls below $T$=0.75 at lower temperatures. On the other hand the diffusivity of larger particles gradually decreases and remain higher than that of smaller particles at lower temperatures. This crossover in the diffusivity of smaller and larger particles is explained on the basis of attractive depletion interaction between the barrier and large particles. Since we have observed that the MSD at different
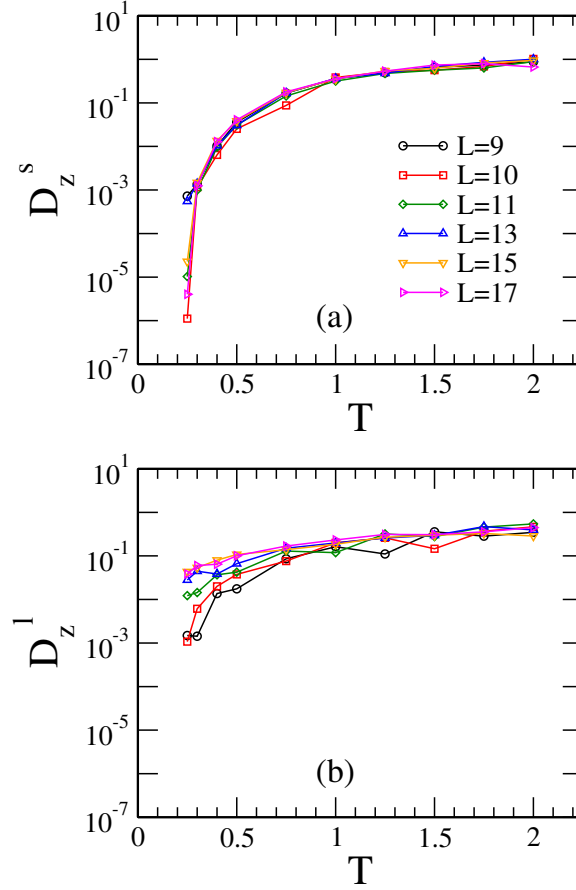
Figure 4.5: Diffusivity of small and large particles along $z$-direction at various temperatures and for box lengths $L =$ 9, 10, 11, 13, 15, 17.

boxlengths can be scaled to coincide with each other, we expect the diffusivity of particles at different boxlengths to be same. We do expect different values of diffusion coefficient in the cases where the scaling fails. In figure 4.5 we have compared the diffusivities of small and large particles for different box lengths along $z$ direction where the barrier is present. In case of smaller particles, the self-diffusion coefficient at different boxlengths are same within the numerical error bars, except the lowest temperature studied. This is expected, as rate determining step for the long time dynamics of the particles is the barrier crossing, especially at lower volume fractions. At $T = 0.25$, the dynamics of smaller particles is very slow such that the mean square displacement is still in the plateau regime even for

the largest time we have calculated. So the error involved in calculating the diffusion co-efficient would be large compared to its value. This results in different values at different boxlengths.
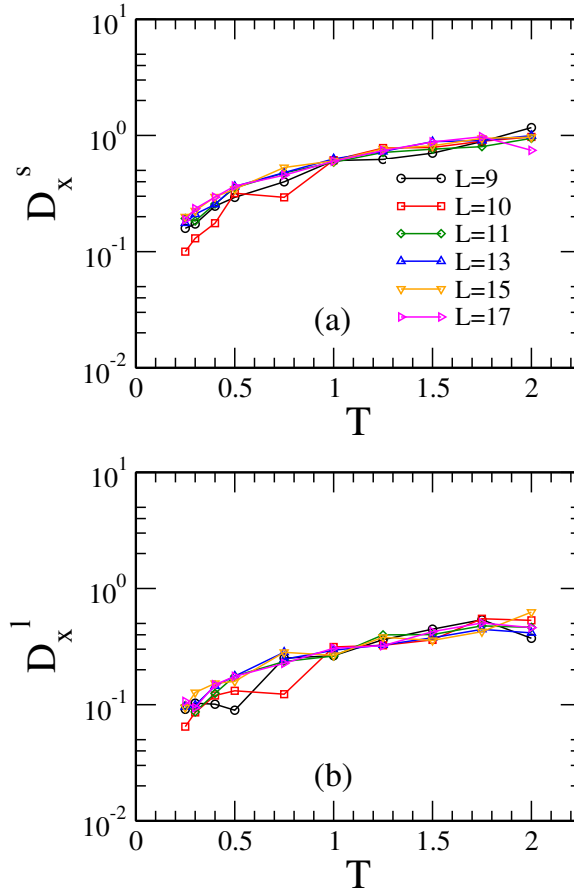


Figure 4.6: Diffusivity of small and large particles along $x$-direction at various temperatures and for box lengths $L =$ 9, 10, 11, 13, 15, 17.

However, the diffusivity of the larger particles varies slightly at different boxlengths. These changes are not very significant in their absolute numerical values. Moreover, they do not show a systematic variations with change in simulation boxlength. Hence they can be attributed to the statistical error during the simulations as well as during further analysis. However at boxlength $L \leq 10.0$ and temperature $T \leq 0.75$, the values of diffusion coeffi-cient are significantly lower than that at corresponding temperatures and larger boxlengths.

It must be noted that the scaling of MSD vs. time curve fails for these boxlengths and temperatures. This is reflected in the values of self diffusion coefficients. Also, the diffusivity of larger particles are still higher than that of smaller particles at lower temperatures even at smaller boxlengths. This suggests that the attractive depletion interaction between larger particles and the external barrier enhances the dynamics of larger particles even at smaller periodicity of the external potential, but the higher density of the smaller particles in the space between successive barriers causes the larger particles to diffuse slower. These two effects are competing each other and we can expect that at even smaller boxlengths, the smaller particles may again start diffusing faster than the larger particles even at low temperatures.

We have also compared the diffusivities along the direction perpendicular to external barrier ($x$ direction) in figure 4.6. Since there is no potential barrier in this direction, the diffusive behavior of both the components show similar trend in their diffusivities. However, the diffusivities of smaller particles remains little higher for all temperatures studied as there is no depletion interaction to cause faster dynamics in case of larger particles. In both the cases, the self diffusion coefficients at different box lengths are within the error bar and show no qualitative change. This is expected as the simulations are carried out at a low volume fraction. However, at higher volume fractions, the degree of confinement induced by the barrier will be larger, especially for the smaller particles and we expect the diffusion coefficients to decrease with decreasing box lengths.

### 4.3.4 Displacement distribution

The external potential at the center of the box along $z$- axis is repeated at the interval of the length equal to the box length because of the periodic boundary condition in the system. So the particles spend some time in between the successive barrier before crossing it. As we decrease the box length, the length in between the barrier also decreases which

in consequent provide less space for particles to move around. As explained earlier, we found interesting changes in the dynamical behavior of larger particles in small box length and at low temperatures. In order to further decipher this behaviour, we have calculated the displacement distributions for both large and smaller particles at different time intervals. Displacement distribution is the probability distribution function of displacement of particles in a particular time interval. It is defined as the probability $P(\Delta r, t)$ that a particles has a displacement $\Delta r$ in a time interval $t$. In figure 4.7 and 4.8 we have shown the these displacement distributions for small and large particles respectively at few representative temperatures and time intervals for $L$=9.0.



Figure 4.7: Displacement distribution of small particles along $z$-direction at various temperatures $T$=0.25, 0.30, 0.50, 1.00 and for box length $L$ =9.

For smaller particles, the displacement distribution is always Gaussian irrespective of the temperature and time intervals. As time interval increases, this Gaussian displacement
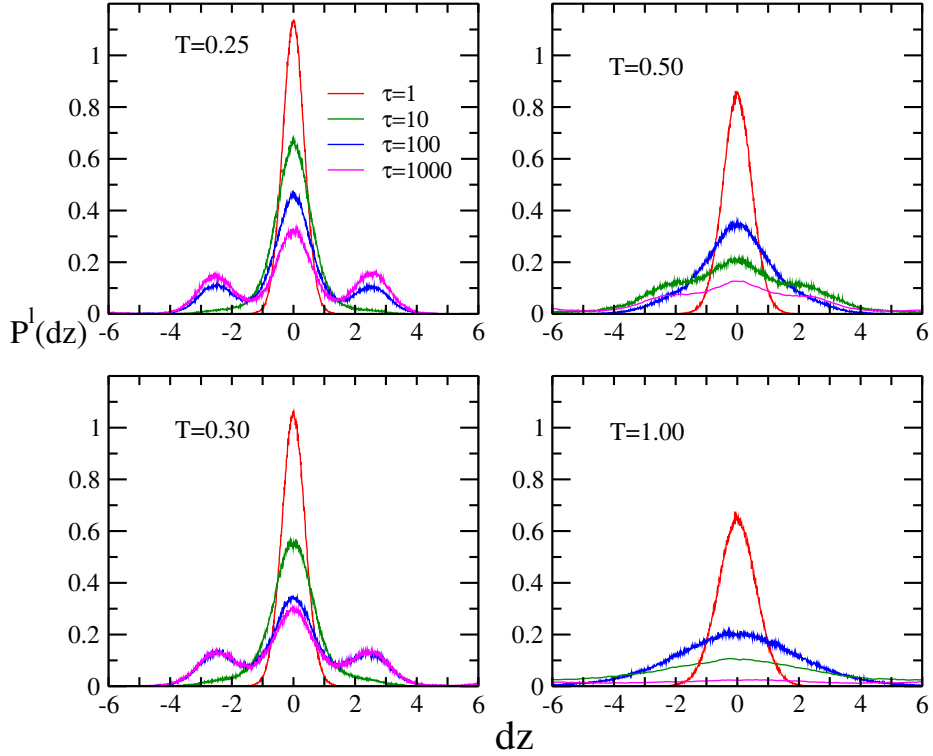
Figure 4.8: Displacement distribution of large particles along $z$-direction at various temperatures $T$=0.25, 0.30, 0.50, 1.00 and for box length $L$ =9.

distribution flattens out as expected in the case of normal diffusion. This flattening is more at higher temperatures, which is again expected. Though the dynamics of the smaller particles slows down at lower temperatures, we do not find any deviations from the Gaussian behaviour of displacement distribution at these temperatures. This is interesting and need to be investigated further. However, in case of larger particles, the displacement distribution exhibit interesting behaviors. At higher temperatures, the distribution is Gaussian suggesting the normal Brownian motion of particles. However, as temperature decreases, displacement distribution further develops two peaks symmetrically placed on both sides of the main peak at $dz = 0.0$. These peaks indicate larger jumps of particles which can be interpreted as the jumps over the barrier. These peaks are at around $dz = \pm 3.0$, which is the width of the external potential barrier. This observation can be viewed along with the two
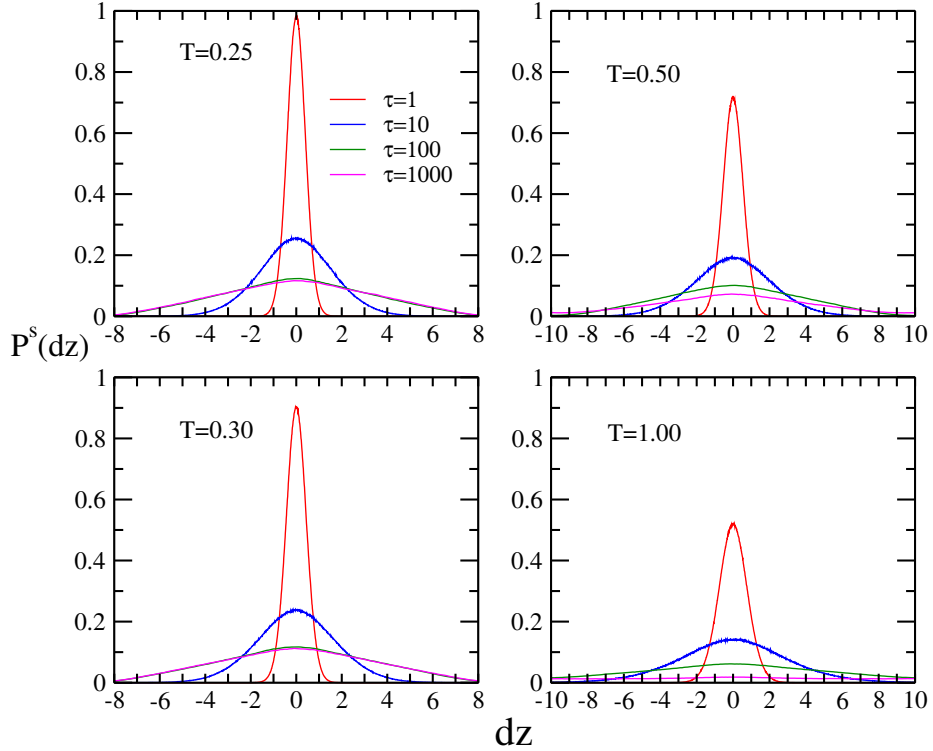
Figure 4.9: Displacement distribution of small particles along $z$-direction at various temperatures $T$=0.25, 0.30, 0.50, 1.00 and for box length $L$ =13.

time scales observed in the waiting time distribution discussed in chapter 2. There we have mentioned that the waiting time distribution can be fitted with two exponentials giving two different timescales for both smaller and larger particles[10]. The smaller time scale remains unaffected as we decrease the temperature for both species of particles. However, the larger time scale increases as we decreases the temperature and this increase is much larger in the case of smaller particles as compared to the larger particles. Now we can associate these two time scales with two different displacement of particles ; the smaller time scale for normal Brownian motion of the particles and the larger one for the jump over the barrier. The jump over the barrier becomes increasingly difficult for the smaller particles as indicated by the increasing timescale as well as the absence of secondary peaks in the displacement distributions. The appearance of secondary peaks in the displacement of larger particles is
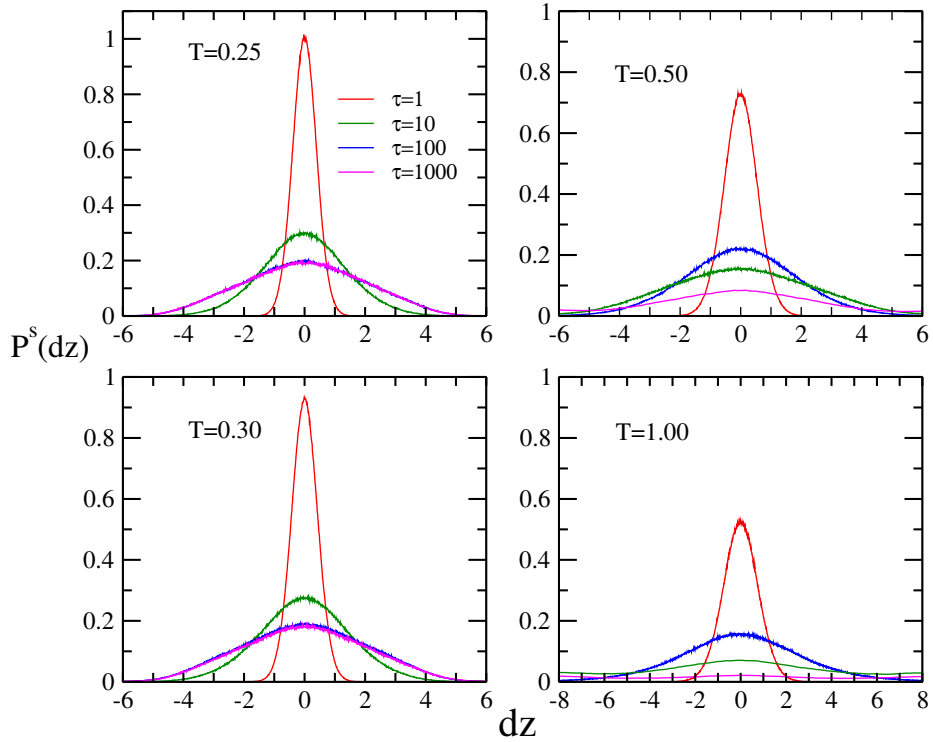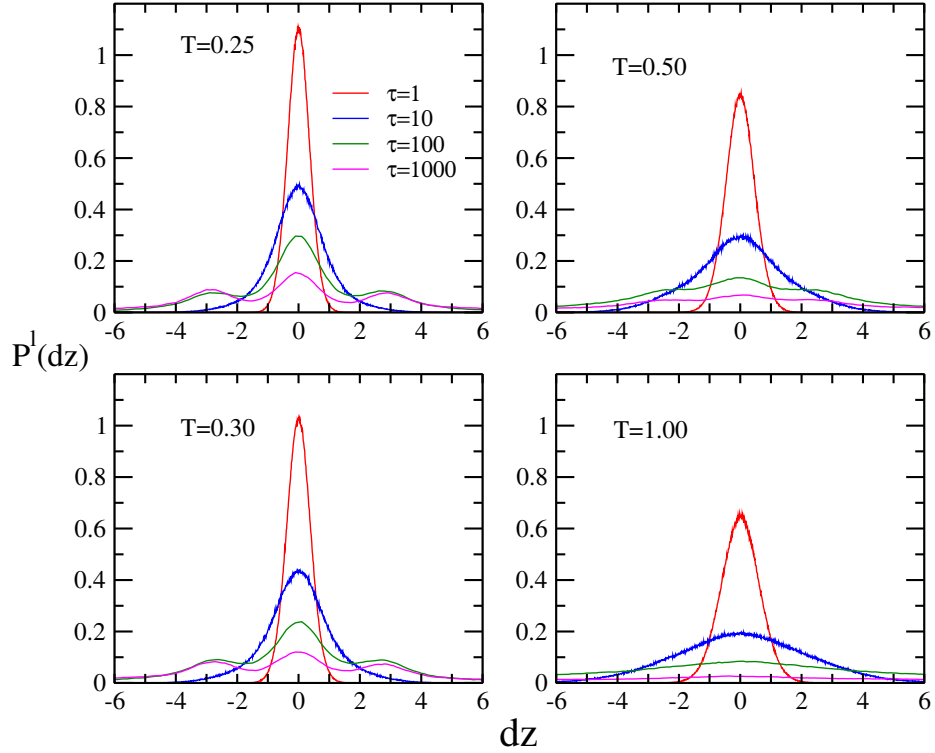
Figure 4.10: Displacement distribution of large particles along $z$-direction at various temperatures $T$=0.25, 0.30, 0.50, 1.00 and for box length $L$ =13.

in agreement with the slowly increasing timescale in the waiting time distribution of larger particles (Chapter 2, Figure 2.13). Thus, it is quite clear that the larger particles undergo a jump diffusion, especially at low temperatures. Dalle-Ferrier *et al.*[13] had carried out experiments on single component colloids subjected to periodic sinusoidal potentials. These experiments could be repeated using the binary colloidal mixtures to test our simulation results. However, it is suggested that the wavelength of the sinusoidal potential, used in such experiments, should not be very small. If the wavelength or the periodicity of the sinusoidal potential is smaller, then there is a possibility of failure of the scaling which is outlined in this chapter, and consequently, the dynamics of both the species in the mixture can be qualitatively very different. Finally, we have also calculated the displacement distributions at larger boxlegnths to rule out that the secondary peaks we obtain in the displacement dis-

tribution of larger particles is an artefact of reducing the simulation boxlengths. These are plotted in the figures 4.9 and 4.10 for smaller and larger particles respectively at boxlength $L = 13.0$. As evident from the figures, there is no qualitative change in these distributions for both the small and large particles.

## 4.4 Conclusion and summary

We have studied the dynamical properties of a binary colloidal mixture of soft spheres subjected to external potential of Gaussian form at different boxlengths to investigate the dependence of dynamics on the system size. It has been already established that the smaller particles show dynamics similar to supercooled liquids at lower temperatures and follow Arrhenius law in their diffusivity; while the larger particles show an enhanced dynamics at low temperatures due to the depletion interaction with the barrier. This results in higher diffusivity for larger particles than the smaller particles at low temperatures and a sub-Arrhenius temperature dependence of diffusion. These results were obtained for larger simulation boxlegnths. In this chapter, we systematically changed the boxlengths and studied the dynamics of our model binary mixture. We found that the dynamical behaviour of both the species in the binary mixture is unchanged for boxlengths greater than 10.0. For boxlengths smaller than or equal to 10.0, the dynamical behavior changes for larger particles at low temperatures. We have scaled the mean squared displacement and time with the lengthscale and timescale associated with the periodicity of the external potential and found them to be coinciding with each other except for the cases where the dynamics are different. This reveals that there are no finite size effects on the dynamics of both species for particles for relatively large simulation boxlengths. This is expected as the density of our system is small and the system is not undergoing any critical phenomena. The deviations from the scaling law for the mean squared displacement of larger particles at lower

boxlengths and low temperatures can be attributed to the increased effective density of smaller particles in between the successive potential barriers. We have also observed that while the displacement distribution of smaller particles is Gaussian for all the boxlengths and temperatures studied, that of larger particles develop secondary peaks at low temperatures at all boxlengths. The secondary peaks correspond to the jump over the barrier and are in agreement with the observation that the waiting time distribution of particles has two length scales associated with it. The implication of these results is manyfold.

# References

[1] M. P. Allen, D. J. Tildesley, Computer simulation of liquids (Clarendon Press, Oxford, 1987).

[2] M. E. Fisher, Proc. 51st Enrico Fermi Summer School, Green, M. S., Ed. (Academic Press, New York, 1973).

[3] C. Domb, J. L. Lebowitz, Phase Transitions and Critical Phenomena, vol. 8, Eds. (Academic press, London, 1983).

[4] K. Binder, D. P. Landau, *Phys. Rev. B.* **30**, 1477 (1984).

[5] J. Cardy, Scaling and Renormalization in Statistical Physics (Cambridge Univ. Press, Cambridge, 1997).

[6] I, C. Yeh, G. Hummer, *J. Phys. Chem.* **108**, 15873-15879 (2004).

[7] T. Wappler, T. Vojta, M. Schreiber, *Phys. Rev. B* **55**, 6272 (1997).

[8] B. Dunweg, K. Kremer, *Phys. Rev. Lett.* **66**, 2996 (1991).

[9] B. Dunweg, K. Kremer, *J. Chem. Phys.* **99**, 6983 (1993).

[10] M. Mustakim, A. V. Anil Kumar, *Physica A* **563**, 125462 (2021).

[11] M. Mustakim, A. V. Anil Kumar, *J. Phys. Chem. B* **126**, 1, 327–335 (2022).

[12] A. V. Anil Kumar, *J. Chem. Phys.* **141**, 034904 (2014).

[13] C. Dalle-Ferrier, *et. al.*, *Soft Matter* **7**, 2064–2075 (2011).

# Chapter 5

# Structure and Dynamics of Binary Colloidal system in an External Asymmetric Potential

## 5.1 Introduction

In previous chapters, we have investigated a binary colloidal system under the influence of an external potential through the NVT molecular dynamics simulations. These investigations revealed that the attractive depletion interaction between the large particles and the external barrier leads to interesting structural and dynamical behaviour of both components in the binary mixture. As we outlined in the previous chapters, this depletion interaction causes the demixing of the binary mixture[1] and localised crystallization of the larger particles near the barrier[2]. The dynamical properties also exhibit very interesting behaviours. For example, the smaller particles in the mixture at low temperatures gets localised between the barriers and undergo a slowing down of dynamics, very similar to that of supercooled liquids[3, 4]. Also, the temperature dependence of diffusion of larger particles exhibits a sub-Arrhenius behaviour, which is not very common in classical systems[4]. In all these investigations, we used a one-dimensional external potential, which is of symmetric Gaussian form. It will be interesting to investigate how these structural and dynamical properties change when an asymmetry is introduced to the external potential. In this chapter, we out-

line the results when an external potential of asymmetric Gaussian form is applied to a system of binary colloids. We found that the results we obtained are quite distinct from that in the case of symmetric potential.

In recent times, there has been immense interest in the transport properties of particles subjected to asymmetric potentials. One of the main reasons behind this is due to the fact that many of the naturally occurring energy pathways for diffusion and transport of particles in many physical, chemical and biological systems contains asymmetric potential barriers. For instance, it is reported that an asymmetry of cell-membrane channel controls the transport across it by ratchet like mechanism in the presence of non-equilibrium fluctuations [5]. Kolomeisky showed that asymmetry in the external potential alters the molecular transport across cell membrane, even without nonequilibrium fluctuations [6]. This results in asymmetric diffusion across such membrane channels in which diffusion of particles dominates in one direction [7]. Also rectification of particles in asymmetric energy landscapes has attracted much attention in the last decade[8, 9]. Rectification of swimming bacteria has been observed in a system with an array of asymmetric potential barriers[10]. In all these systems, the intuitive picture of diffusive transport of particles in a thermally activated series of jumps over the potential barriers with the thermal noise provides a mechanism by which the particles can crossover the barriers. In general, potential barriers significantly suppresses the diffusion. Now if we can introduce a factor which favours the particles jumps over the barrier, it can cause remarkable changes in their dynamical properties. As we have seen in previous chapters, the depletion interaction between the barrier and larger particles favours the larger particles jumps over the barrier. So we introduce asymmetry in the potential barrier and observe the changes in the dynamics of both components in our binary mixture. We found that as asymmetry in the potential increases, the diffusion of the larger particles change from sub-Arrhenius to super-Arrhenius temperature dependence [11]. This happens due to the crowding of larger particles on the steeper side of the potential barrier. However

the smaller particles gets depleted away from the barrier and follow Arrhenius law in the temperature dependence of diffusion as in the case of symmetric potential barrier. Interestingly, by calculating the self part of the van-Hove correlation function of small and large particles, along the applied external potential, we reveal that the transport of the particles is bidirectional. Our model can be realized in such experiments where the external potential remains asymmetric while maintaining bidirectional transport. It has been shown earlier that the surface diffusive motion of 9, 10-Dithioanthracene on an asymmetrical potential surface, though reduces the diffusivity, maintains the bidirection transport[12]. In the next section we will lay out the model system and the simulation details. Then in the following section we will discuss the results ; both structure and dynamics of the system.

## 5.2 Methodology and Model system

We take a binary mixture of small and large colloidal particle, but with equal masses. These particles interact via a repulsive, but soft potential as in the case of the model system we used to study in the previous chapters. The simulation parameters are: $\sigma_{ss} = 1.0$, $\sigma_{ll} = 2.0$, $\epsilon_{ss} = 1.0$, and $\epsilon_{ll} = 4.0$. Cross interaction parameters are obtained using Lorentz-Berthelot additive mixture rules, i.e., $\sigma_{sl} = (\sigma_{ss} + \sigma_{ll})/2$ and $\epsilon_{sl} = \sqrt{\epsilon_{ss}\epsilon_{ll}}$. We have used an equivolume mixture of large and small colloids with total volume fraction $\phi = 0.20$ in all our simulations with a total volume fraction of $\phi = 0.2$ and temperatures $T = 2.0$ - $0.3$. We performed canonical ensemble molecular dynamics (MD) simulations of this system subjected to an asymmetric external potential at the center of the box along z-direction. The asymmetry in the external potential is achieved by introducing an error function in the previous symmetric Gaussian function [1, 4] given by;

$$V(z) = \epsilon_{ext}\, e^{-\left(\frac{z-z_0}{\omega}\right)^2} \big[1 + erf\{A\left(\frac{z-z_0}{\omega}\right)\}\big] \qquad (5.1)$$
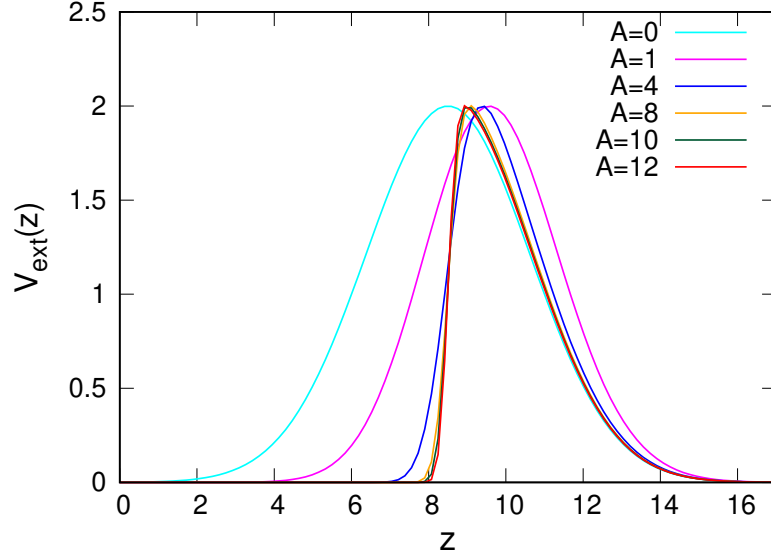
Figure 5.1: External potential along z-direction with different asymmetry parameter $A = 0, 1, 4, 8, 10, 12$. $A = 0$ corresponds to symmetric potential and for $A > 0$, the potential shifts towards right with increase in value of $A$ making it asymmetric around the center of the box.

where $\epsilon_{ext}$, $\omega$, and $A$ are height, width, and asymmetry parameter of the external potential respectively. We have fixed the width $\omega = 3.0$, while varying the $\epsilon_{ext}$ and $A$ in this study. The asymmetry parameter $A = 0$ corresponds to the symmetric external potential [4], while non-zero values of $A$ correspond to the asymmetry in the potential. The simulations are carried out for different asymmetry parameters like $A = 0.0 - 20.00$ and $\epsilon_{ext}$ is adjusted such that the height of the potential remains at $2.0$. Figure 5.1 depicts the external potential for few different values of the asymmetry parameter $A$.

There are two unequal sides of the external potential, we refer them as asymmetric side (left) and symmetric side (coincides with the Gaussian potential) on the right for the reasons of brevity. To check the finite-size effects, we performed simulations of the system at box length $L = 15, 17, 19, 21$ keeping other simulation parameters unchanged. Periodic boundary conditions are imposed in all the three directions, hence the external barrier will have a periodicity of box length in the $z$-direction. Dynamical properties of the system are
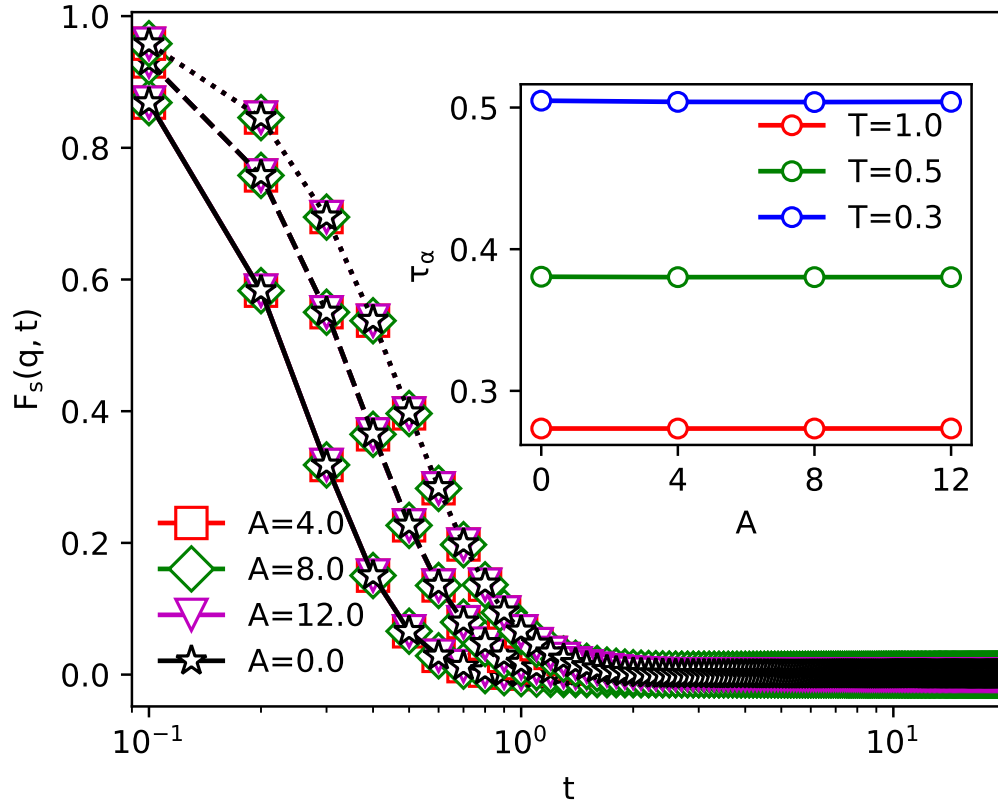
Figure 5.2: Incoherent intermediate scattering function, $F_s(q,t) = N^{-1}\langle \sum_{i=1}^{N} e^{-i\mathbf{q}\cdot\mathbf{r}_i} \rangle$ is plotted against time $t$. Here, $q$ is the wave number corresponding to the main (first) peak of the static structure factor $S(q)$ and $N$ is the total number of particles in the system. Solid, dashed, and dotted lines are corresponding to $T = 1.0$, 0.5, and 0.3, respectively. The $\alpha-$relaxation time increases with lowering temperature, however, it is invariant with $A$; at the same temperature, $F_s(q,t)$ coincides for different $A$. At the lowest temperature, i.e., $T = 0.3$, $\tau_\alpha \simeq 0.5$, and the equilibration time used is $1000\tau_{LJ}$ that is much longer than $100\tau_\alpha$.

computed from the phase space trajectories produced in each production run and averaged over five simulation runs, each starting from a random initial configuration. The system is equilibrated at $T = 3.0$ for $1 \times 10^6$ steps, then this equilibrated configuration is used as the initial configuration for rest of the temperatures. Then for $T=0.75$ and above the system runs for $4 \times 10^6$ after the equilibrium. At temperatures lower than $T = 0.50$, the system is equilibrated till $1 \times 10^7$ steps, followed by $1.5 \times 10^7$ production runs. This is required as the dynamical evolution of the system becomes slower at the low temperatures. Each state point is simulated five times using different initial configurations to achieve better statistics. We monitored the instantaneous values of thermodynamic quantities to ensure that the system has reached the equilibrium before starting the production runs. However, we have also calculated the self intermediate scattering function at various temperature for different asymmetry (see figure 5.2) to ensure that the system has equilibrated properly. $F_s(q,t) = N^{-1}\langle\sum_{i=1}^{N} e^{-i\,\mathbf{q}.\mathbf{r}_i}\rangle$ is plotted against time $t$ in fig.5.2 for various $A = 0, 4, 8, 12$ and for three temperatures $T = 1.0$ (solid), $0.5$(dashed), and $0.3$(dotted). Here, $q$ is the wave number whose value is equal to the distance of first peak of the static structure factor $S(q)$ (see figure 5.12) and $N$ is the total number of particles in the binary colloidal system. We can observe from the figure that $F_s(q,t)$ decays to zero quickly (before $10\tau_\alpha$ ) for all the asymmetry and temperature values. In the inset of the figure we have the $\alpha-$relaxation time for different $A$, at $T = 0.3, 0.5, 1.0$, which is calculated by fitting the function with Kohlrausch-Williams-Watts (KWW) law (see section 5.3.8). However, for a given $T$, $F_s(q,t)$ is invariant with $A$. But with decrease in temperature the value of $\alpha-$relaxation time increases, which happens because of the caging of larger particles near the barrier due to depletion effect (the detail phenomena will be discussed in the coming section). Here the equilibration time used in the simulation for lowest temperature $T = 0.3$ is $1000\tau_{LJ}$ which is much higher than the time taken for the $F_s(q,t)$ to relax to zero ($\tau_\alpha \simeq 0.5$).

## 5.3   Results and Discussion

The structural and dynamical properties of the binary colloidal mixture are calculated from simulated phase space trajectories. These properties are averaged over different production runs. Since the asymmetric potential is applied only in $z$-direction, we expect that the depletion interaction between the barrier and the larger particles affects dynamical properties along the $z$-direction primarily. We will discuss these changes in the dynamical properties of the constituent particles and compare with them with that in the case of symmetric potential. We will also try to interpret how the structural changes are correlated with the changes in dynamical properties.

### 5.3.1   Mean squared displacement

We have calculated the mean squared displacement (MSD) of the colloidal particles from the trajectories obtained from the molecular dynamics simulations of the binary colloidal system. The mean-squared displacement (MSD) of the constituent particles of the system is calculated by using the equation,

$$\delta r^2 = \frac{1}{N} \sum_{i=1}^{N} \langle (r_i(t) - r_i(0))^2 \rangle \tag{5.2}$$

In figure 5.3, the MSD for large and small particles along the $x$-direction (perpendicular to the external potential) for different asymmetry parameters and different temperatures are plotted. Since the external potential barrier is only along the $z$-direction and the volume fraction is low, the MSD of both the species of particles does not show any constrained motion at low temperatures along the directions normal to the applied external potential barrier for the symmetric [3] and the asymmetric case (see Figure 5.3). In figure 5.3 it can be clearly seen that the MSD is linear for both the species for all temperatures and asymmetry parameter. However MSD of both particles shows significant effect of depletion
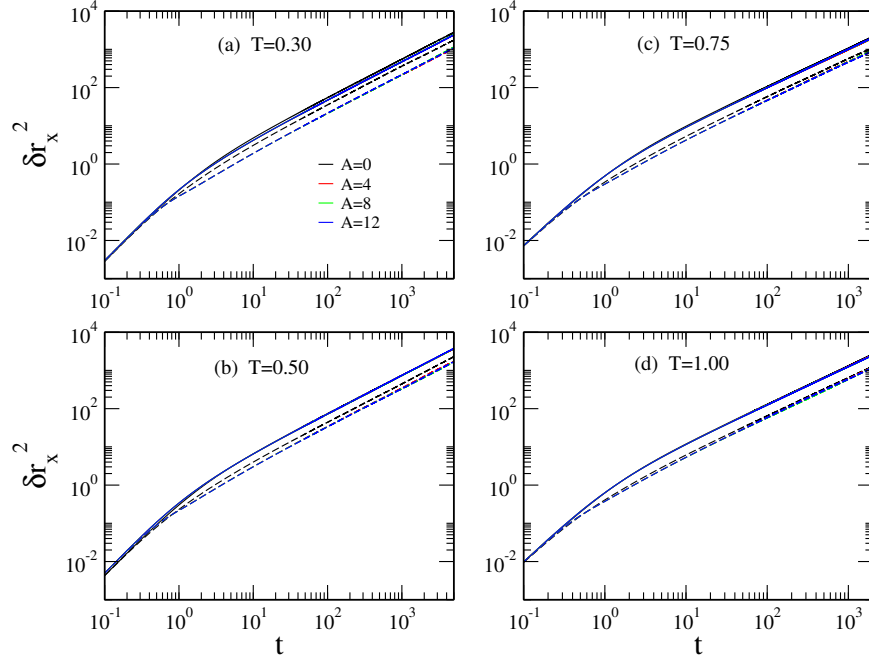
Figure 5.3: MSD for large (dashed line) and small (solid line) particles along x-direction for asymmetry A= 0(black), 4(red), 8(green) ,12(blue) at different temperatures T= 0.30 - 1.00 (a–d)

interactions, especially at lower temperatures.

Figure-5.4 shows the log-log plot of MSD with respect to time of both small (solid line) and large (dashed line) particles along the z-direction. The plot contains the data for four asymmetry i.e, $A$= 0, 4, 8, 12 and for four temperatures $T$= 0.30, 0.50, 0.75, 1.00 (a–d) and $L$=17. At the higher temperatures, both the species in the binary mixture undergo normal diffusion at all values of asymmetry parameter $A$. As expected, the dynamics of the smaller particles is faster than that of the larger particles, as evident from the higher values of MSD for the smaller particles. However, at low temperatures, the MSD of the smaller particles deviates from the linear behavior and develops a plateau at intermediate times. This is due to the localization of the smaller particles between the external potential barriers (multiple barriers arise due to the PBCs), as in the case of symmetric barriers ($A$ = 0). However, the MSD of the larger particles remains linear (at long times) even at the
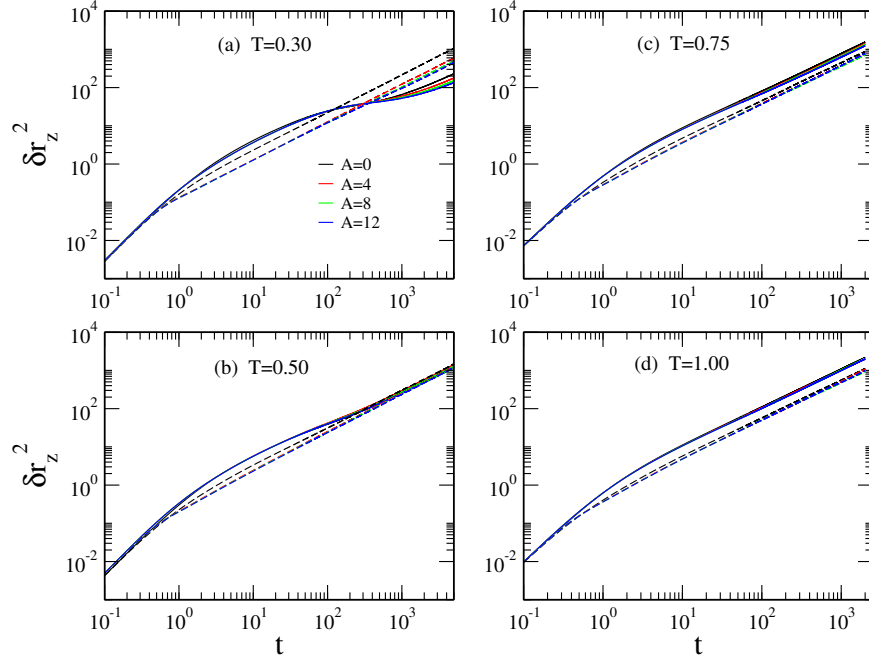
Figure 5.4: MSD for large (dashed line) and small (solid line) particles along z-direction for asymmetry A= 0(black), 4(red), 8(green) ,12(blue) at different temperatures T= 0.30 - 1.00 (a–d)

lower temperatures due to the attractive depletion interaction between the external potential barrier and the larger particles. The asymmetry in the potential barrier does not affect the qualitative nature of MSD of the smaller particles at all temperatures, though it slows down with $A$ that is pronounced at $A = 10$. This slowing down can be dynamical in the sense that the higher asymmetry in the external potential reduces the probability of larger particles crossing over the barrier, thus have to spend a considerably large amount of time near the barrier. This, in turn, increases the probability of large particles reversing the direction of motion near the asymmetric side, therefore, a probability of finding the smaller particles near the barrier increases. This is evidenced in the peak in density profile of the smaller particles near the asymmetric side of the barrier [see Figs. 5.9(a–b)], which will be discussed in the next section. However, the MSD of the larger particles decreases with increasing $A$. This is expected as the depletion interaction is between the potential barrier and the larger

particles and any change in the potential will be mainly affecting the dynamics of the larger particles.

## 5.3.2   Temperature dependence of diffusivity

The diffusion of particles through the potential barrier show some interesting behavior at low temperatures and higher asymmetry, as observed from the MSD curves. Calculating self diffusion coefficient or diffusivity of the particles can give further insight to the dynamical behavior of the particles. The long time diffusion coefficient or diffusivity of the constituent particles of the mixture can be calculated by the expression $D_z = \lim\limits_{t\to\infty} \frac{\delta r_z{}^2}{2t}$, where $\delta r_z{}^2$ is the MSD along z-direction. As temperature decreases, the diffusion coefficient of the smaller particles decreases rapidly. Here again the asymmetry in the potential barrier does not affect the diffusivity of the smaller particles, except for very large values of $A$, namely 10 and 12. To understand the temperature dependency of diffusivity, we plot $ln\,D$ versus $1/T$ for both the species of particles for different $A$ values in figure 5.5. The diffusion coefficient of the smaller particles fit linearly (see figure 5.5(a)) with the Arrhenius equation

$$D = D_0 \exp(-E_a/k_B T) \tag{5.3}$$

where $E_a$ is the activation energy of the diffusion process.

Since the smaller particles follow Arrhenius law, the activation energy for the diffusion is essentially temperature independent. The activation energy for smaller particles $E_a^s$ for different asymmetry is plotted in figure 5.6(a). Increase in asymmetry causes marginal increase in the activation energy for smaller particles and it is always higher than the effective activation energy of larger particles. However, the diffusion coefficient of the larger particles decreases rather slowly with temperature, which suggests a non-Arrhenius behavior. As asymmetry in the potential barrier increases, $D_z^l$ starts decreasing faster with decreasing temperature, but the numerical values are still larger compared to $D_z^s$. As we have dis-
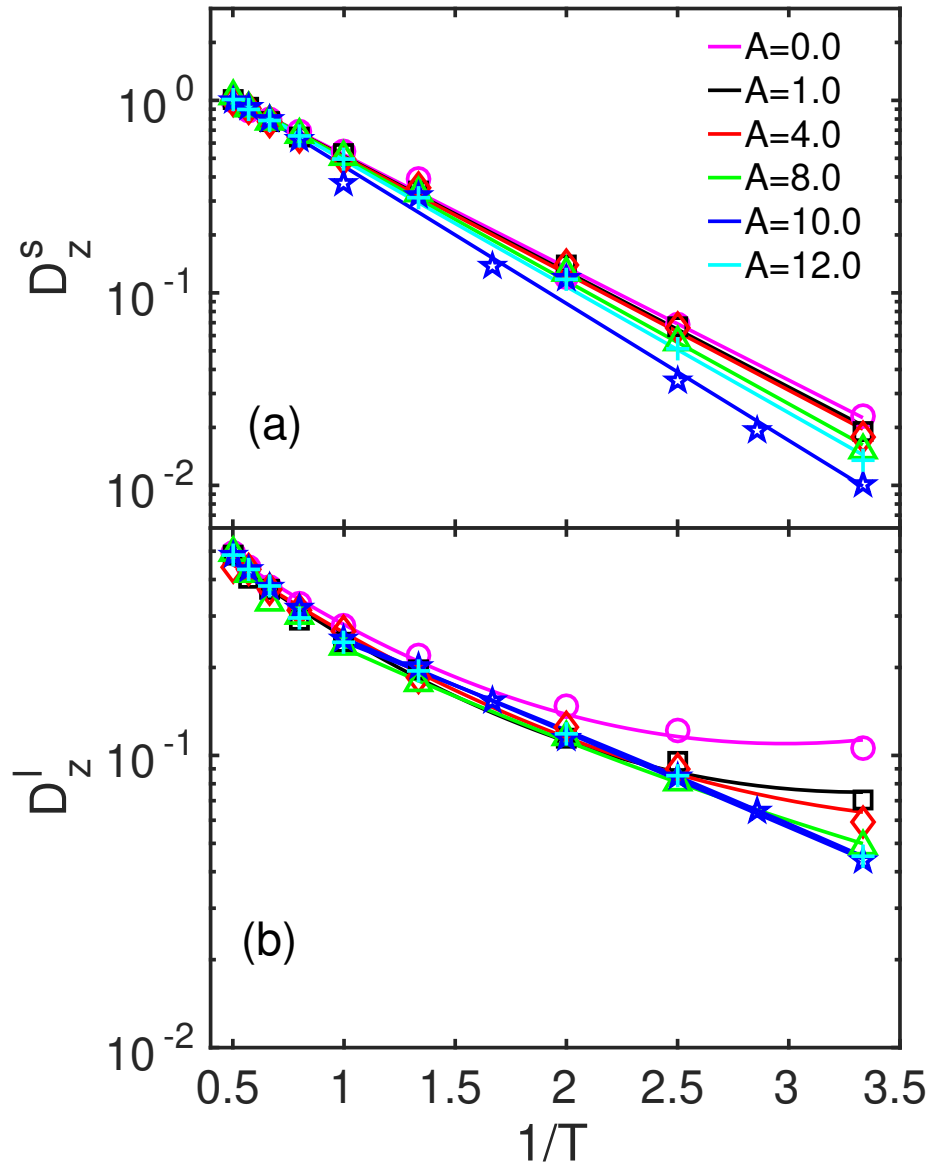
Figure 5.5:   Diffusion coefficient of the (a) smaller particles and the (b) larger particles at temperatures $T = 2.0$–$0.3$ along the $z-$direction. Solid lines are fit to the data points, whereas symbols correspond to the data at different asymmetry parameters. At $A = 8.0$ and above, the the diffusion data of the larger particles, is fitted in the temperature range $1.0$–$0.3$.
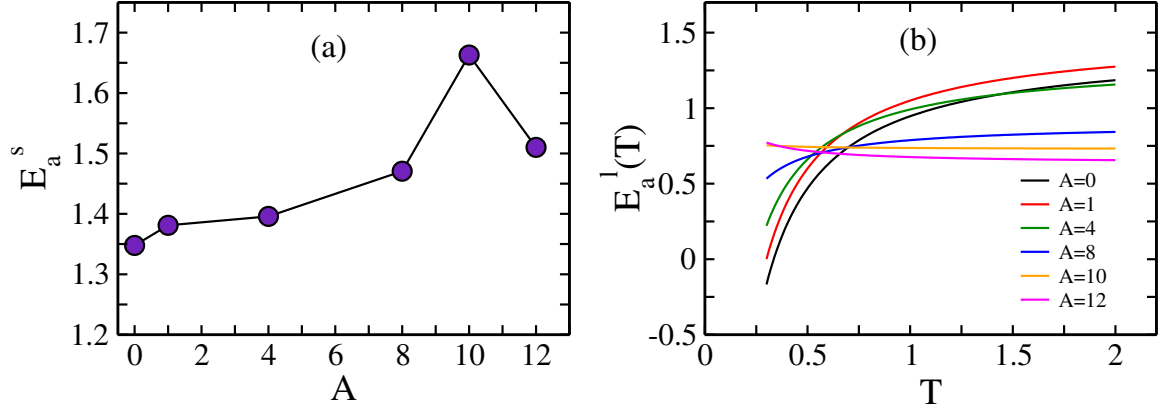
Figure 5.6: Activation energy of (a) small particles for different asymmetry values (b) larger particles as a function of temperature. The plot show activation energy for A=0,1,4,8,10,12.

cussed in chapter 2, temperature dependence of $D_z^l$ is found to be sub-Arrhenius in the case of symmetric potential barrier. From Fig. 5.5(b), it is clear that the dynamics of the larger particles is sub-Arrhenius at low values of asymmetry in the potential barrier. However, as the asymmetry increases the concave nature of the curve diminishes and become linear or convex. To find this, we have fitted the $d-$Arrhenius equation

$$D(T) = A\Big[1 - d\frac{E_0}{k_B T}\Big]^{1/d},\qquad(5.4)$$

where $E_0$ is the height of the barrier and $d$ is the deformation parameter [13] to the $\log(D_z^l)$ vs. $1/T$ curves. The values of the deformation parameter, $d$ obtained from this for different values of asymmetric parameter $A$ is shown in figure 5.7. As mentioned earlier, sign of $d$ decides the nature of the Arrhenius behavior : it's positive for super-Arrhenius and negative for sub-Arrhenius behavior and $d$=0 gives the original Arrhenius equation. With increase in asymmetry the dynamics of larger particles exhibit interesting behavior : a cross over from sub-Arrhenius to super-Arrhenius temperature dependence of diffusion coefficient. At $A$ = 10.0, the deformation parameter $d$ changes sign from negative to positive indicating this cross over. In general super-Arrhenius behaviour is found in high density systems where
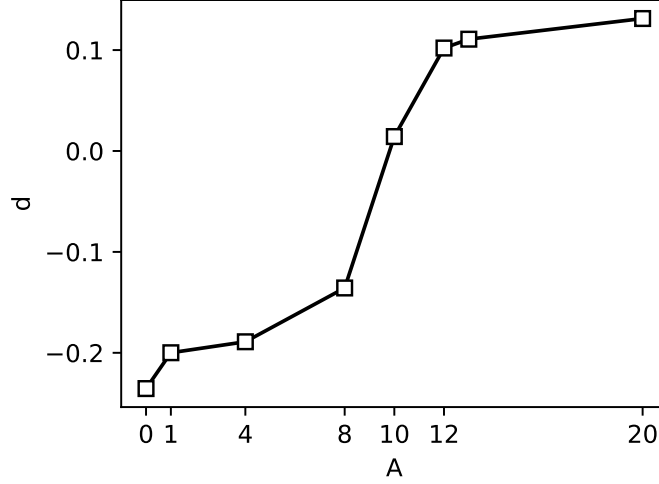
Figure 5.7: Deformation parameter $d$ is obtained from the fitting of the $d-$Arrhenius law (Eq. 5.4) to $\ln(D_z^l)$ *vs* $1/T$ curves, shown in Fig. 5.5(b), which is plotted against the asymmetry parameter $A$.

correlated dynamics is quite significant as in the case of super cooled liquid. Here our model system is comparatively at very low volume fractions, still the asymmetry in external potential causes the diffusion to be super-Arrhenius. On further increasing the asymmetry in the external potential, the $d$ value reached a plateau. This is because the shape of the external potential does not change significantly, at the higher $A$ (see Fig. 5.1), and the volume fraction of the system is very low. We expect that super-Arrhenius diffusion for the larger particles of the mixture, subjected to the asymmetric external potential barrier, may enhance at the higher system volume fractions, well below $\phi_g$. Deviation from the Arrhenius diffusion indicates that the activation energy for diffusion in the case of larger particles is temperature dependent in contrast to the case of smaller particles. We have calculated the activation energy for the large particles $E_a^l$ at different temperatures using the value of $d$ parameters obtained from fitting the $d$-Arrhenius equation. This is plotted in figure 5.6(b). $E_a^l$ decreases as the temperature decreases for smaller values of $A$ and at higher values of $A$ the activation energy starts increasing with decreasing temperature

which is the characteristics of super-Arrhenius behavior. However the values of $E_a^l$ at all temperatures is always lower than the values of $E_a^s$ confirming that the depletion interaction between the larger component and the barrier helps them diffuse faster than the smaller counter part even at lower temperature.

### 5.3.3 Density profile and effective volume fraction

The density profiles of both small and large particles as well as the the local volume fractions will give the further information about the effect of asymmetry in the external potential on the diffusivity in our model of binary colloidal system. The density profiles of larger particles $\rho_l(z)$ along the applied external potential are depicted in figure 5.8 for $T = 0.30, 0.50, 0.75, 1.00$ and asymmetry parameter $A = 0, 4, 8, 10, 12$. The larger particles, through depletion interaction, get attracted towards the barrier, diffuse faster than smaller particles for symmetric potential. For A=0 (symmetric potential barrier) the larger particles accumulate around the barrier symmetrically as expected, hence splitting of the curve to two peaks at the barrier. However the density profile becomes asymmetric as we introduce asymmetry in the external potential. As the asymmetry in potential increases, the asymmetry in the density profile also increases. More larger particles are there in the asymmetric side than the symmetric side of the potential, so the splitting of the curve is asymmetric about the barrier. As the asymmetry value increases, the peak height in the asymmetric also slightly increases. With decrease in temperature this peak increases, indicating that larger particles accumulate more near the barrier compared to smaller particles at low temperatures.

Figure 5.9 show the density profile of smaller particles for different asymmetry values and for $T$=0.30, 0.50, 0.75, 1.00. For the symmetric external potential (A=0) the density profile indicates very less number of smaller particles at the barrier. The density profile of smaller particles $\rho_s(z)$ along the $z$-direction clearly show how they get depleted from the
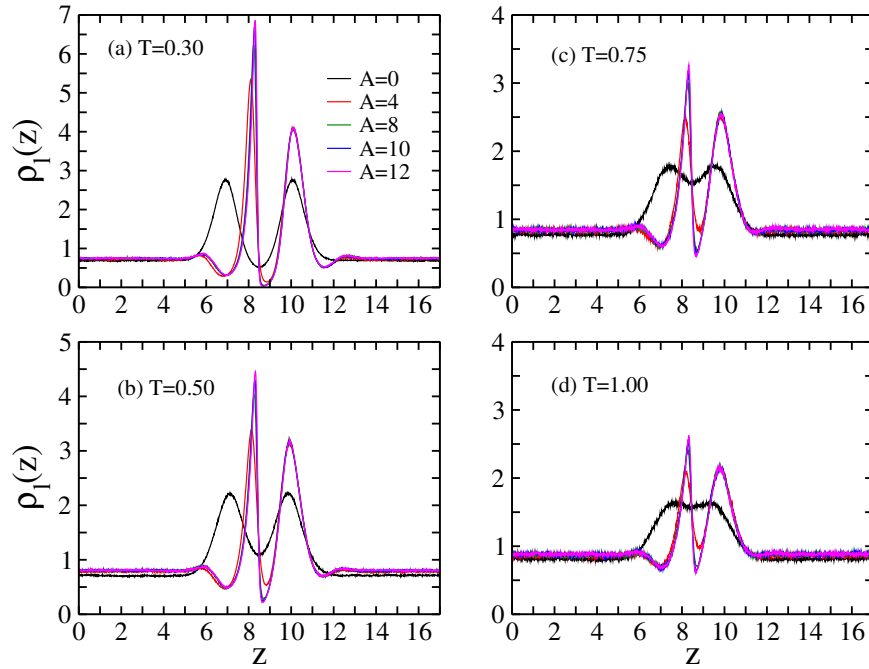
Figure 5.8: Density profile of larger particles along z-direction for asymmetry A=0,4,8,10,12. and temperatures T=0.30, 0.50, 0.75, 1.00
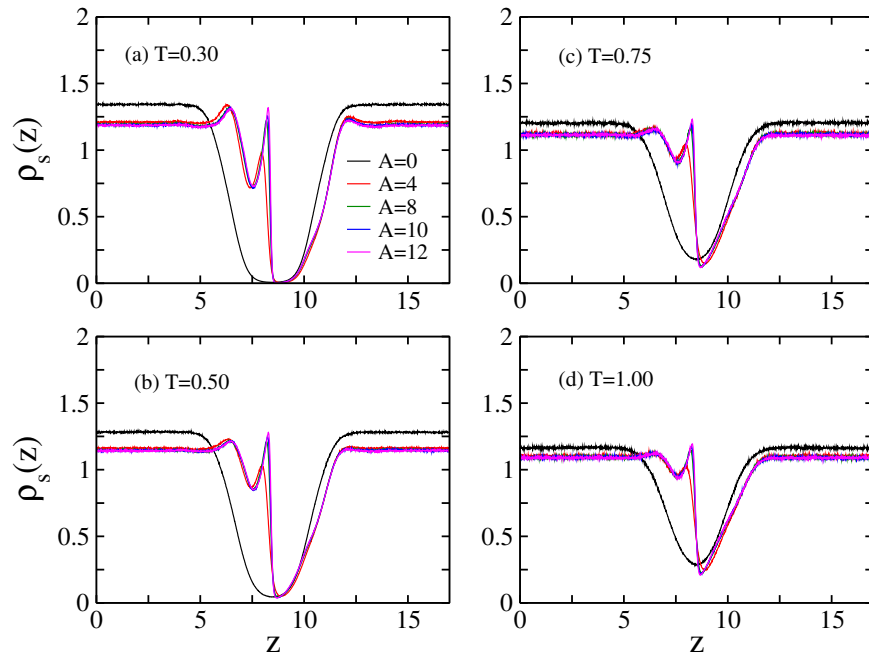


Figure 5.9: Density profile of smaller particles along z-direction for asymmetry A=0,4,8,10,12. and temperatures T=0.30, 0.50, 0.75, 1.00

barrier and have very low density around the barrier. For the symmetric external potential (A=0) the density profile indicates very less number of smaller particles at the barrier. The depth of the minima in the density profile of small particles increases and approaches to zero. This confirms the slow dynamics of smaller particles between the potential barriers and hence the localization at low temperatures [3]. However there is a small peak on the asymmetric side of the barrier which also increases slightly with the asymmetry. As the larger particles' density increases, they spend more time around the barrier before the jump. Hence some smaller particles get accumulated near the barrier accounting for the small peak in the density profile. Thus we see interesting signatures in the density profiles of both the species of particles due to the asymmetric potential barrier at the center. which explains the different dynamical behaviors exhibited by both the species in the mixture.

From the density profile of large particles, it can be seen that the change over from sub-Arrhenius to super-Arrhenius diffusion of large particles as the asymmetry parameter increases is correlated with the changes in the local densities (or volume fractions) of the system. To estimate the local density near the barrier, we calculate the effective volume fraction along z-direction by using the expression $\phi(z) = \frac{\pi}{6L^2 dz}[N_s(z)\sigma_{ss}^3 + N_l(z)\sigma_{ll}^3]$. Here $N_s(z)$, $N_l(z)$ are the number of small and large particles along $z$-direction respectively. The number of constituent particles are counted in a rectangular box of width $dz = 0.5$ along the $z$-direction, and by using the expression above we calculated the local volume fractions of the binary mixture. We have plotted the effective volume fraction against z for three temperatures $T$=0.30, 0.50, 1.00 for $A$=0,4,8,12 in figure 5.10. We can observe that the volume fraction away from the barrier is close to total volume fraction of the system, i.e, $\phi(z) \simeq \phi$ (= 0.2) for all $A$. But it increases near the barrier as seen in density profile also. Near the barrier the density of particles increases with decrease in temperature which is also evident in the density profile. For symmetric potential, effective volume fraction is also symmetric and increases equally on both sides of the barrier. The peaks on both
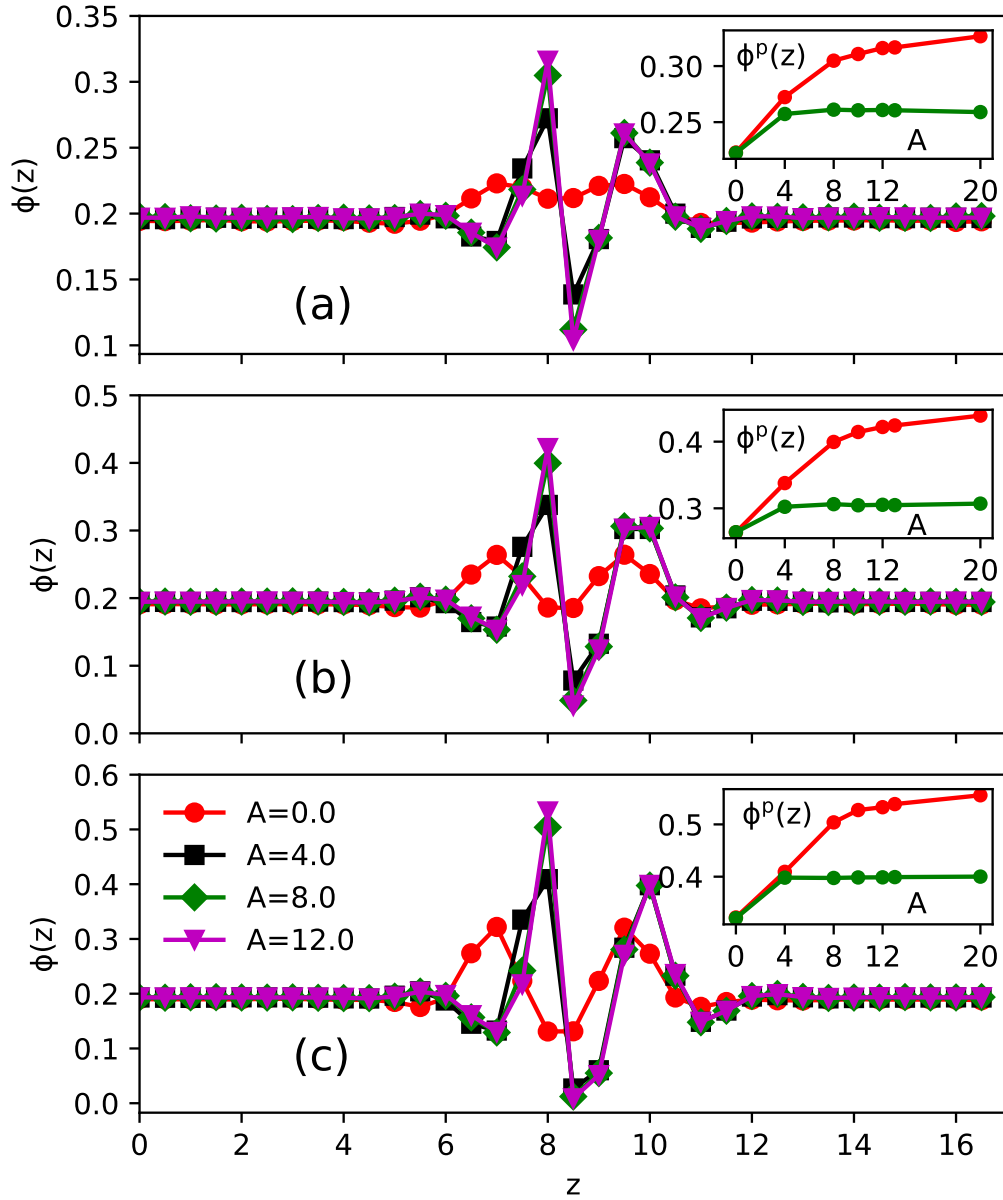
Figure 5.10: Effective volume fraction of the system (over all particles) along $z-$direction at asymmetry parameters $A = 0.0, 4.0, 8.0, 12.0.$ and for temperatures (a) $T = 1.0$, (b) $T = 0.5$, and (c) $T = 0.3$. Insets of plot show a variation in peak heights i.e., $\phi^p(z)$, on the asymmetric (*red*) and symmetric (*green*) side of the barrier, against the asymmetry parameter $A$.

sides of the barrier have heights greater than the bulk density of 0.2. For asymmetric potential the peaks around the barrier are also asymmetric; more in the asymmetric side of the barrier. The peak height ($\phi^p(z)$) versus asymmetry parameter $A$ are plotted in the insets of the figure 5.10. The peak height does not change in the symmetric side of the barrier from $A = 4$ onwards, while in the asymmetric side it increases with increase in $A$. This increase is rapid upto $A = 8.0$ and slows down upon further increase in $A$. It is interesting to note here is that at $T = 0.3$, $\phi(z) > 0.5$ or $\frac{\phi(z)}{\phi} > 2.5$ beyond $A = 8.0$. For $A = 20$, $\frac{\phi(z)}{\phi}$=0.56 which is nearly equal to the glass volume fraction for hard spheres, i.e., $\phi_g = 0.58$ [14]. This means asymmetry in the external potential can induce glass transition even for a low density system. The crossover from sub-Arrhenius to super-Arrhenius diffusion is observed beyond $A = 8$ (see Fig. 5.7). According to Angell's classifications of glass, super-Arrhenius temperature dependent of transport properties such as diffusion constant is a characteristics of fragile supercooled liquids [15]. It is believed that there are some regions in the glass forming materials where particles show cooperative motions which is called as "Cooperatively Rearranging Regions (CRR)". The relaxation process in intermediate scattering function can give more information about it, which we will discuss in the coming sections. Also, studies on the role of system density on the kinetic fragility and the configurational entropy show that the kinetic fragility increases whereas the configurational entropy decreases with density, showing a rapid slowing down at the higher densities, one of the key signatures of the supercooled liquids [16, 17]. An accumulation of the particles towards the asymmetric side of the barrier above $A = 8.0$ suggests a frequency of crossing over the barrier decreases with temperature, thus increases local density in the proximity of the barrier.
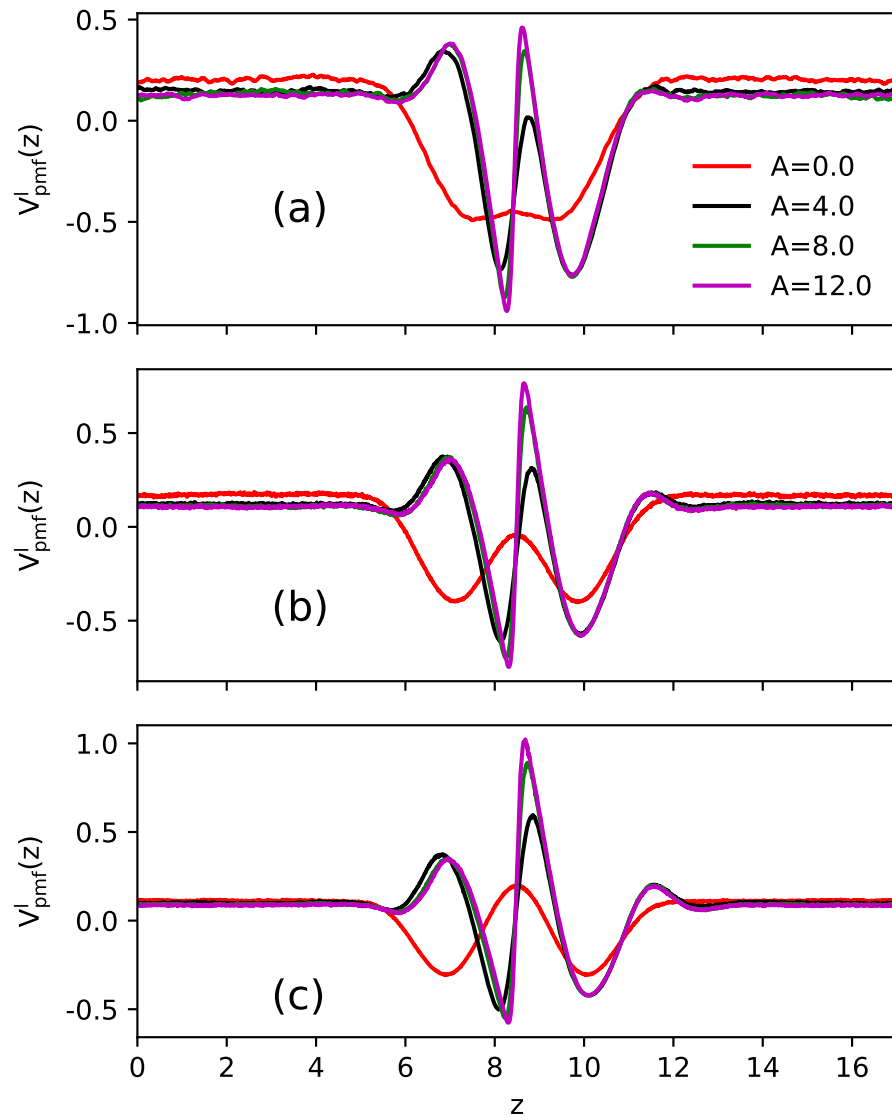
Figure 5.11: Potential of mean force of larger particles along z-direction for different asymmetry $A = 0, 4, 8, 12$ at (a) $T = 1.00$, (b) $T = 0.50$ and (c) $T = 0.30$
.

### 5.3.4 Potential of mean force

The potential of mean force(PMF) provides a measure of the effective difference in free energy between two states (in this case the difference in free energy between the minimum and the bulk) as a function of one or several interesting degrees of freedom. Here we have calculated the PMF of larger particles along z-direction where the external potential is applied (see figure 5.11).

$$V_{pmf}^l(z) = -k_B\,T\ln(\rho_l(z)) \tag{5.5}$$

Figures 5.11(a-c) compare $V_{pmf}(z)$ of the larger particles at the asymmetry parameters $A = 0.0, 4.0, 8.0, 12.0$ at temperatures $T = 1.0, 0.5, 0.3$. These figures indicates the changes in effective free energy barrier for diffusion of the larger particles due to the depletion interaction between the larger particles and the potential barrier. Again, for the symmetric potential (i. e. A=0) the PMF is symmetric around the barrier and the particles are crossing with equal probability from both the sides. Also, the barrier height decreases with decreasing temperature which can be seen as the reason for the sub-Arrhenius diffusion of larger particles in the symmetric potential case [4]. However when A increases the height as well as the asymmetry of the PMF increases. Since the crossing of the barrier becomes increasingly difficult for larger particles, they aggregate near the barrier, which leads to higher free energy barrier for diffusion at these temperatures.

### 5.3.5 2-d Structure factor

As shown in the density profile (figure 5.8), the larger particles show enhanced density profile and local volume fraction around the barrier, leading to super-Arrhenius diffusion at higher asymmetry and at low temperatures. We have suggested the possibility of larger particles undergoing correlated dynamics near the barrier like in supercooled liquids as the local volume fraction is similar to the glass volume fraction of hard sphere fluids at these

values of asymmetry parameter and temperature. Before going further with this suggestion, it will be worthwhile to rule out the possibility of crystallization of larger particles near the barrier. This is essential since the smaller particles stay away from the barrier and it is almost like one component system of larger particles near the barrier which can lead to crystallization. For this, we tried to characterize the structure through the two dimensional structure factor $S(k)$. Generally structure factor, $S(k)$ of crystal structures show sharp peaks which corresponds to well defined long range order of a specific crystalline lattice. In case of an ideal gas these peaks are absent because particles have no correlation between their positions and have uniform distribution in space. But for glass and liquid, $S(k)$ shows some short range order depending on the densities with some peaks which decays to $1$ (uniform distribution) as the value of k increases. The peaks correspond to the most probable distances at which one can find a pair of particles with the largest density-density correlation. So the highly correlated or ordered particles show sharp peaks at specific $k$. The height of the principal peak in the structure factor often informs whether a liquid is near to freezing or not. Therefore to enquire the local freezing of larger particles in our binary colloidal system we calculate the z-dependent 2D structure factor along the XY-plane (near and far from the barrier), which is defined as

$$S(k,z) = \frac{1}{N(z)} \sum_{i,j=1,\, j\neq i}^{N(z)} \exp[-i\{\mathbf{k}.(\boldsymbol{\xi}_i(z) - \boldsymbol{\xi}_j(z))\}], \qquad (5.6)$$

where $\boldsymbol{\xi}_i(z) = x_i\hat{x} + y_i\hat{y}$, and $N(z)$ is the total number of particles in a 2D layer (XY-plane) at $z$. The XY-plane is divided into thin strips of width 0.5 along $z$-direction and calculated $S(k,z)$ in teach of these strips. $S(k,z)$ at $z = 7, 7.5, 8.0, 8.5, 9.5, 10, 10.5$ (near the barrier) and $z = 4$ (far from the barrier) and at $T = 0.3, 0.5, 1.0$ for three asymmetry $A = 4.0, 8.0, 12.0$ as shown in the Figures 5.12(a-i). At $T = 1.0$ [Figs. 5.12(g-i)], $S(k,z)$ shows a single broad peak at $k \simeq 5$, away from the barrier, and this peak splits into two peaks around $k \simeq 3.0$ and $6.0$, near the barrier for all the asymmetry presented. Then it
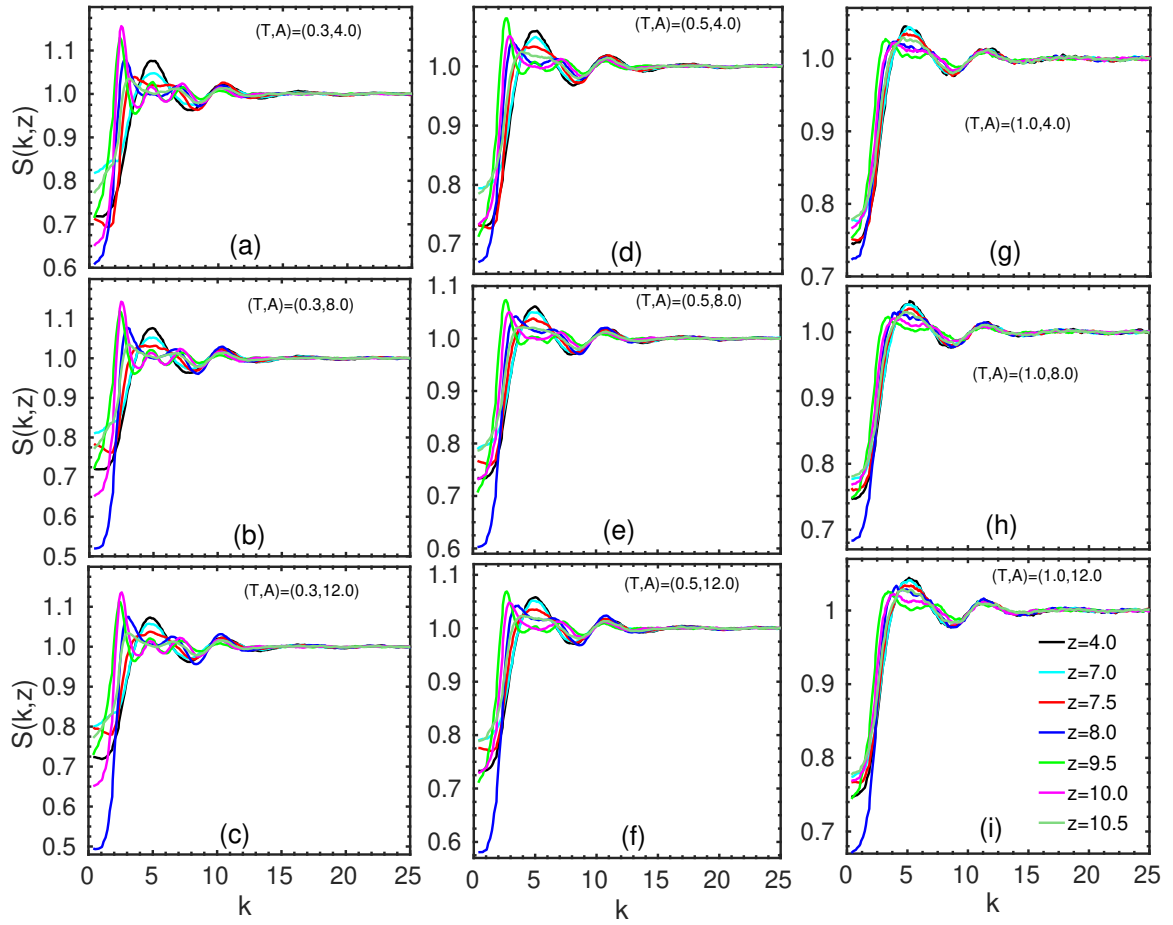
Figure 5.12: Two-dimensional structure factor near ($z = 7.0, 7.5, 8.0, 9.5, 10.0, 10.5$) and far ($z = 4.0$) from the external barrier at asymmetry parameter $A = 4.0, 8.0, 12.0$. (a–c) $T = 0.3$, (d–f) $T = 0.5$, and (g–i) $T = 1.0$. Legend of (i) is applied to (a–h).

decays to 1 at higher $k$ values. This means the binary mixture remains in liquid phase at higher temperature at both near and far from the potential barrier. The splitting of the principal peak into two near the barrier corresponds to the two length scales ($k = 2\pi/\sigma_{ss,ll}$) associated with the different sizes of the particles. At this temperature, there is slightly different in $S(k, z)$ near the barrier for different $A$ specifically near the barrier, which is expected because the density profile also differs slightly as discussed above. The non-zero values of $S(k, z)$ at low wavenumbers shows the demixing of the particles in the system. As we decrease the temperature the primary peak height increases and the splitting of peaks become more prominent. At $T = 0.5$ [see Figs. 5.12(d-f)], $S(k, z)$ shows some secondary peaks along with the primary peak near the barrier which corresponds to the local structures arising due to the crowding of larger particles near barrier. These can be verified from the density profile also. When the temperature further decreases the the local density of larger particles increases around the barrier. Hence, at $T = 0.3$ [see Figs. 5.12(a-c)], the first peak height of $S(k, z)$ further increases with more splitting in the secondary peak, near the barrier. These secondary peaks are due to multiple secondary structures near the barrier due to caging, which is pronounced at low temperatures. However there is no signature of freezing or crystallization near the barrier as at higher values of $k$, $S(k, z)$ goes to one indicating a liquid structure in the system. Even though there are some local density around the barrier, the particle density is not enough for crystallization to happen.

### 5.3.6 Non-Gaussian parameter

In earlier sections, we suggested that the crossover from sub-Arrhenius to super-Arrhenius diffusion as asymmetry parameter increases is due to the crowding of larger particles near the barrier and subsequent slow down of their dynamics. We have also ruled out the localised crystallization by calculating the 2-d structure factor. To examine further the local caging and slowing down of dynamics, we calculated the non-Gaussian parameter for the
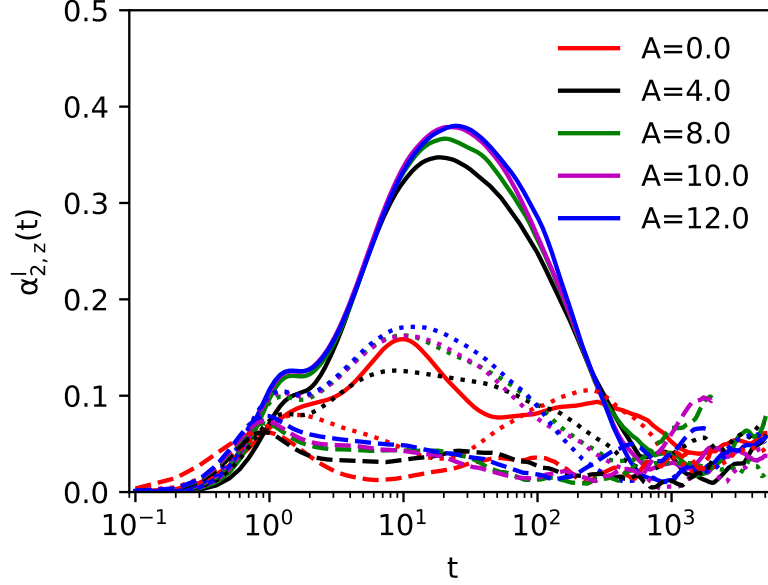
Figure 5.13: Non-Gaussian parameter of the larger particles along the applied external potential barrier at $A = 0.0$, 4.0, 8.0, 10.0, 12.0, and temperatures $T = 1.0$ (dashed lines), 0.5 (dotted lines), and 0.3 (solid lines).

dynamics of larger particles along the direction of applied external potential. In the case of the symmetric potential barrier, the NGP of the larger particles is (approximately) zero, which indicates that these particles are not localized between the barriers and their dynamics is diffusive even at low temperatures [3]. In contrast to this, the NGP of the smaller particles shows marked deviations from zero at intermediate times as we decrease the temperature. This corresponds to the localization of the smaller particles between the potential barriers resulting in a plateau in MSD at intermediate times[3]. From the MSD's of the smaller particles [see Fig. 5.4(a)], it is evident that their dynamics does not change qualitatively, though changes quantitatively, with $A$. Therefore, we show the NGP of the larger particles only (see Fig. 5.13) to examine the cagelike features due to their localization near the barrier, which is defined as,

$$\alpha_{2,z}^l(t) = \frac{1}{3} \frac{\langle (r_z(t) - r_z(0))^4 \rangle}{\langle (r_z(t) - r_z(0))^2 \rangle^2} - 1.0 \qquad (5.7)$$

The density of larger particles near the barrier is high, which leads to super-Arrhenius diffusion. This is also evident from the effective activation energy which increases with decreasing temperature. This kind of dynamics is generally observed in supercooled liquids where particles exhibit caged like motion in intermediate times, which leads to a non-Gaussian distribution of particles. It is often seen that non Gaussian parameter $\alpha_2(t)$ is evaluated to study the dynamic heterogeneity in the system. The non-Gaussian parameter (NGP) quantifies the deviations from the Gaussian distributions of the displacements of the particles. This distribution usually peaks at an intermediate time between the cage regime and the long time diffusive regime. This intermediate time where $\alpha_2(t)$ peaks also corresponds to the $\beta$-relaxation region of the self intermediate scattering function $F_s(k, t)$, and at long time this goes to zero corresponds to the $\alpha$- relaxation region (see section 3.8). Here in our binary colloidal system, the density profile of larger particles and the effective volume fraction of the system suggests that they show non homogeneous motion near the barrier, indicating a dynamic heterogeneity in the system. To further understand this, we have calculated the non-Gaussian parameter of larger particles along $z$- direction, which is given by equation 5.7.

In figure 5.13 for three temperatures $T = 0.3$ (solid lines), $T = 0.5$(dotted lines) and $T = 1.0$ (dashed lines), for different asymmetry $A$= 0, 4, 8, 10, 12. It is evident from the figure 5.13 NGP of the larger particles is below the value 0.1 at temperature $T = 1.0$, whereas it starts growing from $T = 0.5$ and $A = 4.0$ onwards. Interestingly, from $A = 4.0$ of $T = 0.5$, $\alpha_{2,z}^l(t)$ shows two peaks — first one at time $t \approx 1.0$, while second one at time $t \approx 10.0$ that is shifted towards the longer times at low temperatures and the larger $A$. At $T = 0.3$, both peaks of NGP grow, which is a clear signature of the onset of the cagelike motion found in supercooled liquids; the time scales of both peaks are akin to the $\beta$ and $\alpha$−relaxation time scales in the dynamics of supercooled liquids [18, 19]. Thus, these peaks show the cagelike motion of the larger particles near the barrier, which enhances with

the asymmetry parameter $A$, therefore, the larger particles exhibit super-Arrhenius diffusion at $A = 10.0$ onwards. On contrary, the large particles' NGP does not show any growth up to $A = 1.0$, where sub-Arrhenius diffusion is observed.

### 5.3.7 van Hove correlation function

To test our hypothesis further, we have calculated the self part of the van Hove correlation function. The van Hove correlation function, $G(r, t)$, is the real space dynamical correlation function for characterizing the spatial and temporal distribution of pairs of particles in a fluid . It basically shows the probability of finding a particle at position $\vec{r}$ at time $t$, given that at time $t = 0$, the particle was at the origin. In the case of isotropic systems, the van Hove function only depends on the magnitude of the displacements. $G(r, t)$ is also used in obtaining other dynamical properties such as intermediate scattering function, $F(k, t)$, which is the spatial Fourier transform of $G(r, t)$. Diffusion coefficients can be calculated from $G(r, t)$ and thermodynamic quantities such as internal energy and pressure can be related to spatial integrals involving the radial distribution function $g(r)$. The total van Hove correlation function has two parts in it : one is associated with finding the probability of the same particle at a time interval $t$ and at a distance $r$, known as the "self" part of the function and the other is the probability of finding a different particle at $r$ after time $t$, known as the "distinct" part of the function. The self part of van Hove correlation function $G_s(r, t)$ can provide a good understanding of our system where smaller particles show normal diffusion (liquid- like) while larger particles show cage-like motion near the barrier. The self part of van Hove correlation function along z-direction is defined as [20],

$$G_s(z, t) = \frac{1}{N} \left\langle \sum_{i=1}^{N} \delta[z - z_i(t) + z_i(0)] \right\rangle. \tag{5.8}$$

Generally $G_s(r, t)$ evolves in time in regular expected manner for a liquid; it shows one Gaussian peak that broadens in spatial direction with increasing time. If more than

Figure 5.14: Self part of van-Hove correlation function of the smaller particles at $A = 0.0$, 4.0, 8.0, 10.0, 12.0, and temperatures (a) $T = 1.0$ and (b) $T = 0.3$. The symbols $\bigcirc$, $\square$, $\triangleleft$, and $\triangledown$ ($T = 0.3$) correspond to times $t 1.0$, 10.0, 100.0, and 2000.0 (5000.0).
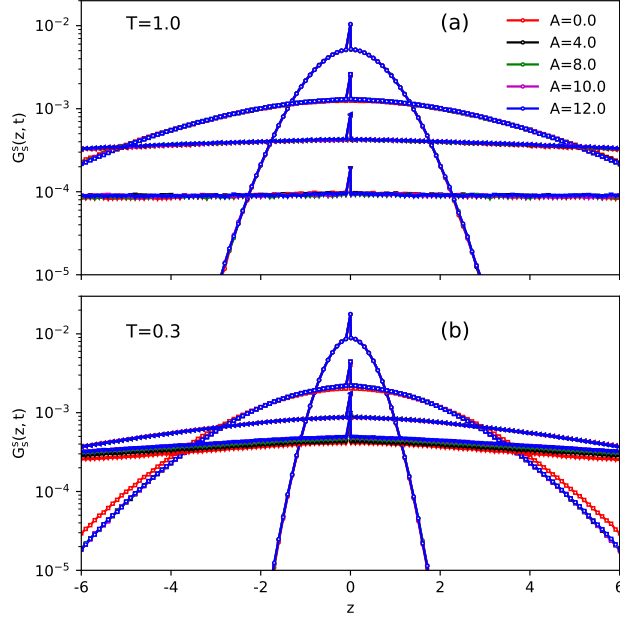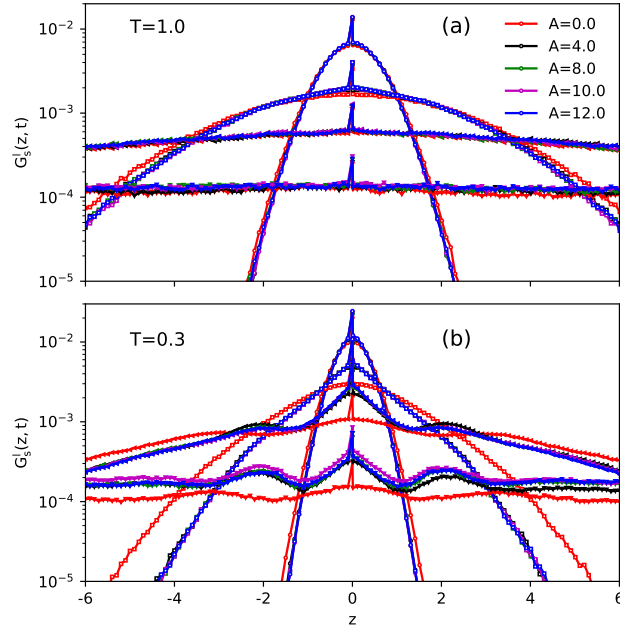


Figure 5.15: Self part of van-Hove correlation function of the larger particles at $A = 0.0$, 1.0, 4.0, 8.0, 10.0, and temperatures (a) $T = 1.0$ and (b) $T = 0.3$. The symbols $\bigcirc$, $\square$, $\triangleleft$, and $\triangledown$ ($T = 0.3$) correspond to times $t = 1.0$, 10.0, 100.0, and 2000.0 (5000.0).

one peaks are observed, then the system is transitioning from liquid to other phases. In figure 5.14(a–b) we have the self van Hove correlation function of smaller particles along one spatial direction, $G_s^s(z, t)$, at $T = 1.0$ and 0.3 for different times $t = 1, 10, 100, 2000$ (5000). For both low and high temperature $G_s^s(z, t)$ evolves with one peak and flattens out with increasing time in both the direction of $z$. As the distribution spread out the peak height also decreases with increase in time, indicating diffusive behavior of small particles at long times. This kind of distribution in $G_s(r, t)$ reveals that the smaller particles are in liquid phase at all temperatures and asymmetry parameters studied. There is no significant change due to increasing asymmetry in the barrier which is consistent with the MSD curve of small particles that they do not change with asymmetry parameter except at longer times at low temperatures ($T = 0.3$) (see figure 5.4 ) there is a marginal increase in the displacement. It is interesting to notice that the curve spreads faster (between $t$= 100 and 2000) at higher temperature $T = 1.00$ (figure 5.14(a)) than at lower temperature $T = 0.30$ (figure 5.14(b)) which explains the localization of smaller particles at intermediate times and at low temperatures. Moreover the self van Hove correlation function of smaller particles is invariant with respect to asymmetry parameter $A$.

On the other hand the self van Hove correlation function of larger particles along $z$-direction, $G_s^l(z, t)$, exhibits different phase behavior at low and high temperature (see figure 5.15). At high temperatures ($T = 1.0$), $G_s^l(r, t)$ evolves in regular manner like a liquid with one Gaussian peak with increase in time (with very insignificant change at t=2000). It does not change with asymmetry parameter similar to the case of smaller particles (figure 5.15(a)). The same behavior can be observed in the MSD and density profiles of larger particles where it does not change substantially with $A$ at higher temperature. However at low temperature ($T = 0.3$), $G_s^l(r, t)$ starts showing secondary peaks as the time increases (from $t \approx 100.0$ onwards). The peaks are found in both directions at a distance $z \simeq 2.0\sigma_{ll}$, which is twice the size of the larger particles. That means the larger particles can jump

long distances of the order of twice of their diameter which increases the probability of crossing the barrier even at low temperature. This is also evident from the potential of mean force (for $A = 0$) which shows very small effective barrier height ($\epsilon_{ext}^{eff} \simeq 0.2$) which helps the larger particles to jump over the barrier easily even at low temperatures. This increased probability of crossing the barrier is the reason for the larger particles to follow sub-Arrhenius diffusion in their dynamics in case of symmetric barrier[4]. At $T = 0.3$, when the asymmetry in the barrier increases ($A = 4$ onwards) these peaks start to shift towards the smaller distances in the intermediate times which is nearly of the order of the diameter of larger particles ($z \simeq \sigma_{ll}$). This indicates that the larger particles start to break the cages and hop large distances equal to the diameter of the particle. The cage formation near the barrier and the jumplike motion of the larger particles signifies that they behave like supercooled liquid and follow super-Arrhenius behavior of diffusion at low temperatures at intermediate times. To get a quantitative idea, the effective potential barrier height for $A = 10$ is $\epsilon_{ext}^{eff} \simeq 1.0$, five times that of at $A = 0$, at the lowest temperature $T = 0.3$. This is an indication for the localization of larger particles as the asymmetry in the barrier increases and hence a transition from sub-Arrhenius to super-Arrhenius diffusion in the dynamics of larger particles. The appearance of secondary peaks in the van Hove correlation function of larger particles with increase in asymmetry in the external potential and at low temperature confirms the super-Arrhenius behavior of larger particles, a characteristics of supercooled liquids.

### 5.3.8 Incoherent intermediate scattering function

The Fourier transform of the van Hove correlation function gives the intermediate scattering function $F(q, t)$ for wave vector $q$. Instead of the Fourier transform, it can also be computed directly from the particle trajectory obtained from the molecular dynamics simulations. Intermediate scattering function $F(q, t)$ basically shows how the fluctuations in local density
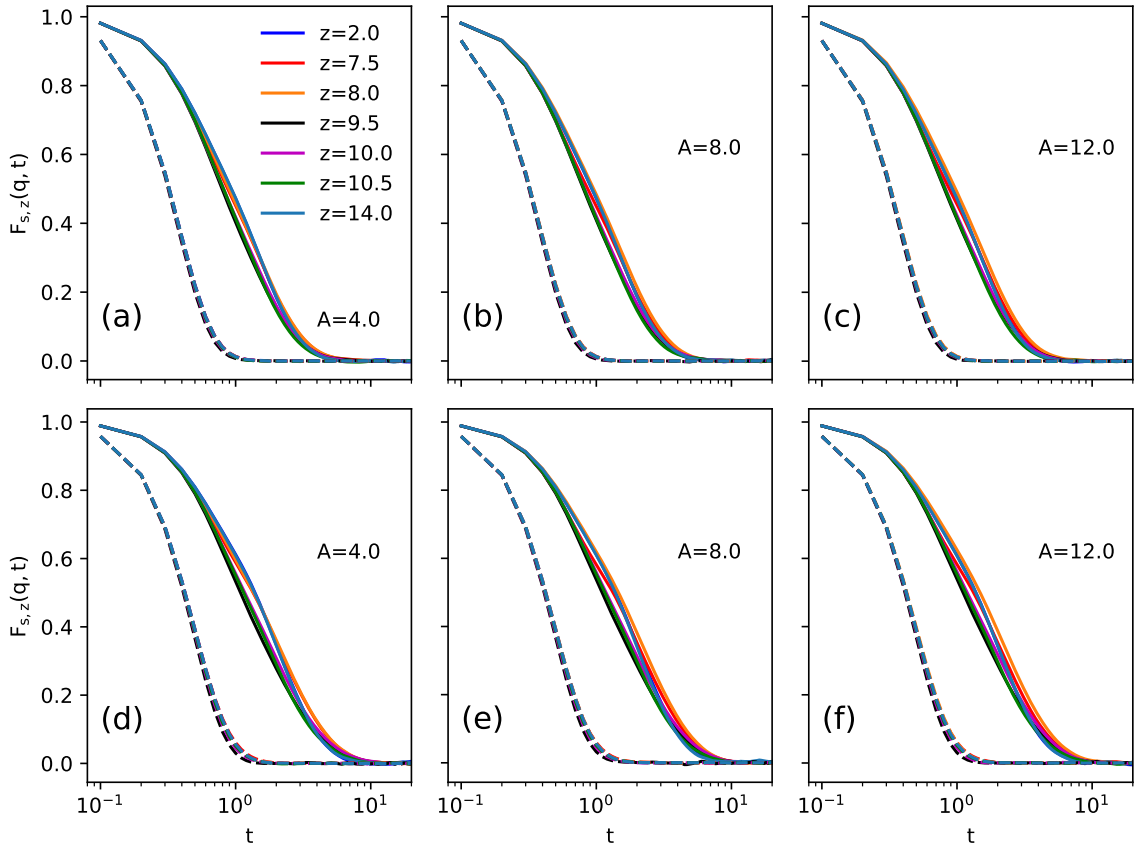
Figure 5.16:   Incoherent intermediate scattering function of the smaller (dashed lines) and the larger (solid lines) particles at low temperatures, $T = 0.5$ (a–c) and $T = 0.3$ (d–f), near and off the barrier, at varying asymmetry. This shows that dynamics of the larger particles is slower than the smaller particles near the barrier. Interestingly, a little hump appears in $F_{s,z}(q,t)$ near the asymmetric side of the barrier, showing their cage like motion.

distribution relax with time. It can be measured in incoherent inelastic neutron or X-ray scattering experiments. It characterizes the mean relaxation of the system; its fluctuation in space provides information about dynamical heterogeneities. Like the van Hove correlation function, $F(q,t)$ has also two parts : self part (Incoherent intermediate scattering function $F_s(q,t)$) and distinct part (Coherent intermediate scattering function $F_d(q,t)$). Generally in the case of a colloidal system in the low temperature, this correlation can be categorized into three regions depending on time: at short times it shows microscopic dynamics (ballistic regime), then at the intermediate times particles exhibit cage-like motion ($\beta$-relaxation) and at long times particles starts leaving the cages with long jumps which stretches the correlation curve ($\alpha$-relaxation). One can determine the state of the system by taking the long time limit of $F_s(q,t)$: for fluid, it is zero and for glass, it is non-zero. We are investigating a binary colloidal mixture in the presence of asymmetric external potential and it is revealed so far that the larger particles are localized near the asymmetric side of the barrier and their density increases with asymmetry parameter $A$ at low temperatures. There are many such examples of the system where particles concentrate near the barrier or confining wall, hence show slow relaxation dynamics in the system[21, 22, 23]. Hence to study the relaxation dynamics of caged particles, we calculated the self-intermediate scattering function in the vicinity of the barrier[21], where particles are gathering. The z-dependent incoherent intermediate scattering function is defined as

$$F_{s,z}(q,t) = \frac{1}{N} \left\langle \sum_{i=1}^{N} e^{-i\mathbf{q}.[\mathbf{r}_i(t)-\mathbf{r}_i(0)]} \delta[z - z_i(0)] \right\rangle. \tag{5.9}$$

Here $z_i$ is the position of $i^{th}$ particle in the $z$-direction. We have taken the wave numbers $q = 5.4$ and $2.8$, corresponding to peaks of the static structure factor for the smaller and the larger particles, respectively. $F_{s,z}(q,t)$ is calculated at different values of $z=$ 2.0, 7.5, 8.0, 9.5, 10.0, 10.5, 14.0, near and far from the barrier. In figure5.16 the dashed lines show the relaxation dynamics of smaller particles and solid lines for larger particles at T=0.5(a–c) and T=0.3(d–
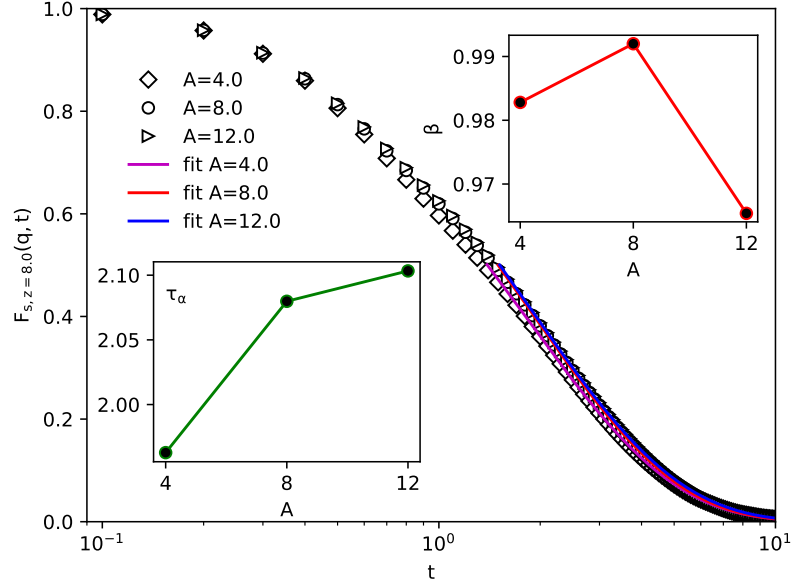
Figure 5.17: Self intermediate scattering function is plotted against time $t$ at $z = 8.0$ and $T = 0.3$, which is fitted with the empirical Kohlrausch-Williams-Watts (KWW) law. The exponent $\beta$ and the relaxation time $\tau_\alpha$, at $z = 8.0$, are plotted in the top-right and bottom-left insets, respectively.

f) for different $z$ with varying asymmetry, A=4,8,12. The $F_{s,z}(q,t)$ of smaller particles doesn't change for all values of asymmetry parameter at which calculations are done, even at the lowest temperature $T$=0.3. This is consistent with the results shown in mean-squared displacement, diffusion coefficient, van Hove correlation function, and the non-Gaussian parameter. On the other hand the relaxation dynamics of the larger particles varies with $A$ and also with the distance from the barrier. From the figure 5.16 it is evident that $F_{s,z}(q,t)$ of the larger particles is much slower than the smaller counterpart, hence show a slow decay of relaxation. At $T$=0.30, $F_{s,z}(q,t)$ of larger particles near the barrier, we can observe a little hump which grows with increasing asymmetry parameter $A$. A presence of the hump signifies the cage like motion of the larger particles near the barrier, which support the behavior of the non-Gaussian parameter and the self part of the van Hove correlation along the z-direction. The caged particles near the barrier at low temperatures start leaving their

cage which can be manifested by the stretched relaxation in $F_{s,z}(q,t)$. This can be fitted with Kohlrausch-Williams-Watts (KWW) law $[\propto exp[(-t/\tau)^{\beta}]]$, which gives the $\alpha-$relaxation time, $\tau_{\alpha}$ and the exponent $\beta$ [24, 25, 26]. Generally at higher temperature $\tau(T)$ follows Arrhenius law. At low temperatures it behaves as "fragile liquids" in the strong- fragile classification. At high temperatures the time dependence of $F_s(q,t)$ is exponential, whereas at lower temperatures, the KWW stretched exponential form provides a good fit for the long time behavior. The exponent $\beta(0 < \beta < 1)$ is a number that quantifies the deviation from strict exponential behavior. For example we fitted the $F_{s,z=8.0}(q,t)$ with the KWW function at the lowest temperature $T = 0.3$ and $z = 8.0$ for few values of asymmetric parameter, to calculate the $\alpha-$relaxation time, $\tau_{\alpha}$ and exponent $\beta$. Here the relaxation time $\tau_{\alpha}$ is the time when $F_{s,z}(q, t = \tau_{\alpha}) = e^{-1}$. Left bottom inset of Fig. 5.17 shows that $\tau_{\alpha}$ increases (though little) with the asymmetry parameter $A$. The KWW exponent $\beta$ is around 0.96 at $A = 12$, which implies the presence of non-exponential density relaxation near the barrier for the larger particles. Interestingly the relaxation of $F_{s,z}(q,t)$ for the smaller particles is significantly faster then the larger particles (almost 5 times) at both temperatures. This is because they move faster at the length scale of inter-particle separation which is the wave number corresponding to the first peak of static structure factor for smaller particles. As the volume fraction is low and smaller particles are mostly away from the barrier, this helps them move faster at the length scale of their diameter, hence the cause of faster relaxation dynamics.

## 5.4   Finite size effects

The structural and dynamical properties of the binary colloidal mixture outlined in this chapter are obtained from the MD simulations carried out for a simulation boxlength of $L = 17$. It will be interesting to check whether these dynamical properties has any finite
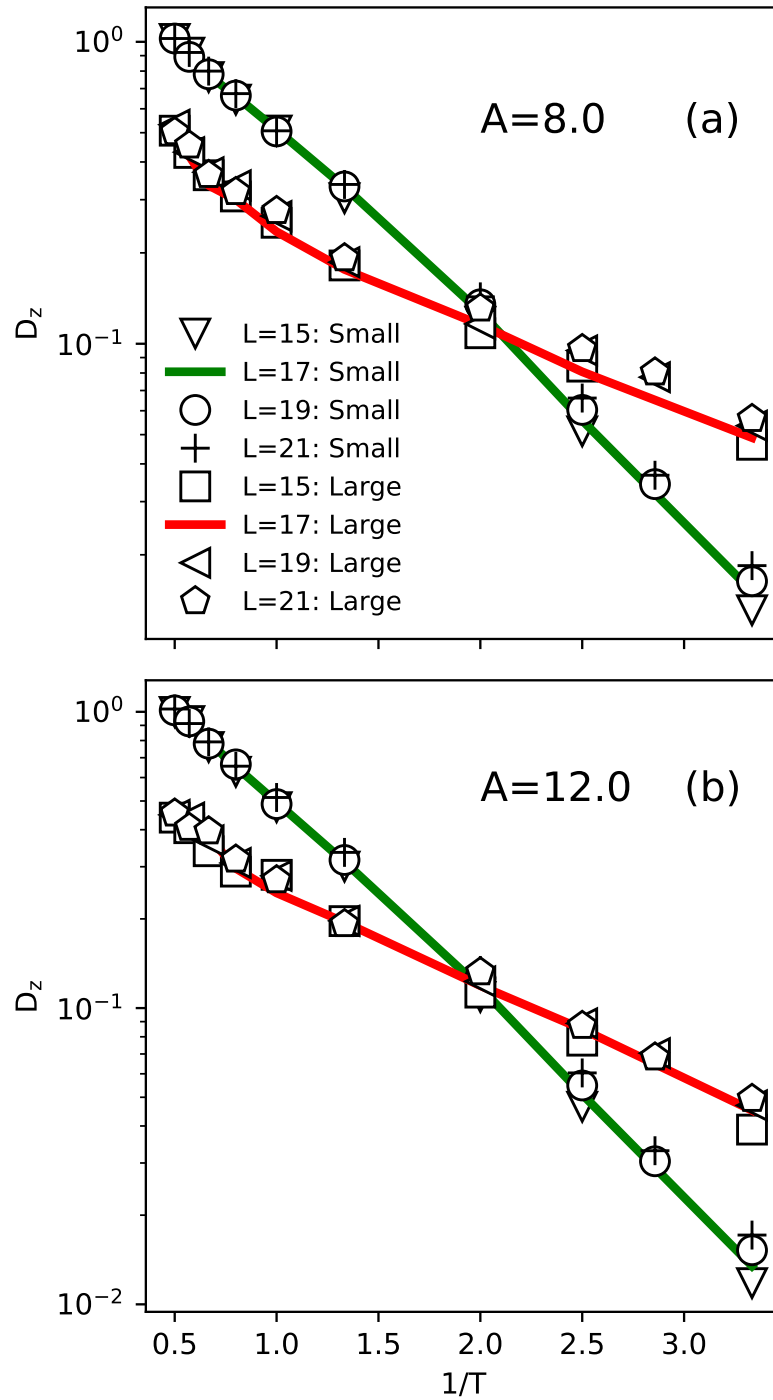
Figure 5.18: A comparison of diffusion constant at four different box lengths $L = 15, 17, 19, 21$ for (a) $A = 8.0$ and (b) $A = 12.0$

size effects. So we have we performed more simulations for different boxlengths $L$= 15, 19, 21 and compared it with results outlined earlier. As shown in chapter 2, when the barrier is symmetric ($A$=0) the dynamics is unaffected by changing different box lengths [4]. In the presence of asymmetric barrier we have observed that the transition in the dynamical properties are pronounced for $A = 8$ and onwards. So, we performed more simulations for two asymmetry values ($A = 8$, 12) at different box lengths to see whether the system has any finite size effects. In figure 5.18, we have plotted the diffusion constant for both small and large particles from a range of comparatively low system size ($L = 15$) to a large system size ($L = 21$) and for asymmetry values $A = 8.0$ and 12.0. There is no significant changes observed in the diffusivity of both the species of particles by changing the box lengths, their values matches quite well with each other. Because of the periodic boundary conditions and an external potential at the center of the simulation box along z-axis, the system is subjected to a periodic potential of wavelength equal to the box length. By changing the box length we are changing the periodicity of the external potential, hence there should not be any finite size effects on the dynamics of the system. We observed that the diffusivity of both small and large particles does not depend on the simulation box length. Thus, at the given simulation parameters the finite size effects are negligible on the system due to asymmetric external potential.

## 5.5   Conclusion and summary

We study the effect of asymmetry in the external potential on the structure and dynamics of the binary colloidal system of soft spheres through molecular dynamics simulations. Due to the depletion interaction between the larger particles and barrier, the diffusivity of larger components of the mixture show sub-Arrhenius behavior for symmetric potential barrier. However by introducing asymmetry in the potential, the structure and dynamics of

the system changes significantly. Due to the depletion interaction between the asymmetric potential barrier and the larger particles, density of larger particles increases near the barrier. However, as the asymmetry in the potential barrier increases, barrier crossing becomes less probable, leading to even higher densities near the barrier especially on the asymmetric side. This leads to transient caging of larger particles near the barrier. Due to this, the larger particles' diffusivity show a cross over from sub-Arrhenius to super-Arrhenius behavior as the asymmetry increases. The activation energy show temperature dependency for larger particles : it decreases with decreasing temperature for low values of asymmetry (sub-Arrhenius) and increases for decreasing temperature for high values of asymmetry parameter(super-Arrhenius diffusion). The non-Gaussian parameter (NGP), potential mean force(PMF), self intermediate scattering function, all confirm the slowing down of dynamics of larger particles as asymmetry increases in the potential. However the smaller particles show normal Arrhenius behavior for all asymmetry and temperature. The behavior of larger particles at higher asymmetry is very similar to the dynamics of supercooled liquids [27, 28, 29]. We expect that at the larger asymmetric potential barrier heights, the super-Arrhenius diffusion will enhance and subsequently the deformation parameter will further increase. This will be interesting since the volume fraction we have used in this study is very low compared to that of supercooled liquids. Moreover, asymmetric potentials are used in the transport of molecules in biological channels [7, 30, 31], targeted delivery of colloids by bacteria [32], and Brownian motors [33, 34]. Most of these studies are carried out for single-component systems in an asymmetric potential subjected to various conditions of driving. It will be interesting to investigate the dynamics of binary mixtures in these scenarios and the system we simulated provides a model for these investigations. Finally, we expect that the experimental realization of our model is straight forward. Spatially asymmetric periodic potentials have been realized in experiments via dielectrophoretically induced forces [35, 36] as well as using optical tweezers [37]. Dynamics of single-component colloidal

systems subjected to an external sinusoidal potential has been studied experimentally by Dalle-Ferrier et al. [38]. They have carried out these investigations on two different colloidal systems whose size ratio is close to 1:2, which has been used in our simulations.

# References

[1] A. V. Anil Kumar, *J. Chem. Phys.* **138**, 154903 (2013).

[2] M. Mustakim, A. V. Anil Kumar, *J. Phys. Chem. B* **126**, 1, 327–335 (2022).

[3] A. V. Anil Kumar, *J. Chem. Phys.* **141**, 034904 (2014).

[4] M. Mustakim, A. V. Anil Kumar, *Physica A* **563** 125462 (2021).

[5] I. Kosztin, K. Schulten, *Phys. Rev. Lett.* **93** 238102 (2004).

[6] A. B. Kolomeisky, *Phys. Rev. Lett.* **98** 048105 (2007).

[7] R. S. Shaw, N. Packard, M. Schröter, H. L. Swinney, *Proc. Natl. Acad. Sci.* **104** 9580 (2007).

[8] R. Di Leonardo, *et. al.*, *Proc. Natl. Acad. Sci.USA* **107**, 9541 (2010)

[9] A. Sokolov, M. M. Apodaca, B. A. Grzybowski, I. S. Aranson, *Proc. Natl. Acad. Sci. U.S.A.* **107**, 969 (2010).

[10] M. B. Wan, C. J. Olson Reichhardt, Z. Nussinov, C. Reichhardt, *Phys. Rev. Lett.* **101**, 018102 (2008).

[11] J. Singh, M. Mustakim, A. V. Anil Kumar, *J. Phys.:Condens. Matter* **33** 125101 (2021).

[12] G. Pawin, *et. al.*, *J. Am. Chem. Soc* **130**, 15244 (2008).

[13] V. Aquilanti, K. C. Mundim, M. Elango, S. Kleijn, T. Kasai, *Chem. Phys.Lett.* **498** 209 (2010).

[14] W. van Megen, T. C. Mortensen, S. R. Williams, J. Müller, *Phys. Rev.E* **58** 6073 (1998).

[15] C. A. Angell, *J. Non-cryst. Solids* **13** 131-133 (1991).

[16] S. Sastry, *Nature* **409** 164 (2001).

[17] S. Sengupta, T. B. Schrøder, S. Sastry, *The Eur. Phys. Journal E* **36** 141 (2013).

[18] L. Berthier, G. Biroli, J. Bouchaud, L. Cipelletti, W. Saarloos, Eds. Dynamical Heterogeneities in Glasses, Colloids and Granular Media, (Oxford Univ. Press, New York, 2011)

[19] S. Karmakar, C. Dasgupta, S. Sastry, *Phys. Rev. Lett.* **116** 085701 (2016).

[20] J. P. Hansen, I. R. McDonald, Theory of Simple Liquids (Academic Press, London, 2006)

[21] Y. C. Hu, *et. al.*, *Proc. Natl. Acad. Sci.* **115** 6375 (2018).

[22] K. Watanabe, T. Kawasaki, H. Tanaka, *Nature Mater.* **10** 512 (2011).

[23] G. M. Hocky, L. Berthier, W. Kob, D. R. Reichman, *Phys. Rev. E* **89** 052311 (2014).

[24] R. Böhmer, K. L. Ngai, C. A. Angell, D. J. Plazek, *J. Chem. Phys.* **99** 4201 (1993).

[25] L. Berthier, G. Biroli, *Rev. Mod. Phys.* **83** 587 (2011).

[26] J. Singh, P. P. Jose, *J. Phys.: Condens. Matter* **33** 055401 (2021).

[27] V. K. de Souza, D. J. Wales, *Phys. Rev. B* **74** 134202 (2006).

[28] V. K. de Souza, D. J. Wales, *Phys. Rev. Lett.* **96** 057802 (2006).

[29] A. Singh, Y. Singh, *Phys. Rev. E* **99** 030101 (2019).

[30] M. Chinappi, *et. al.*, *Phys. Rev. Lett.* **97** 144509 (2006).

[31] J. Comelles, *et. al.*, *Biophys. J.*, **107** 1513 (2014).

[32] N. Koumakis, A. Lepre, C. Maggi, R. D. Leonardo, *Nat. Comm.* **4**, 2558 (2013).

[33] V. M. Rosenbaum, T. Y. Korochkova, A. A. Chernova, M. L. Dekhtyar, *Phys. Rev. E* **83**, 051120 (2011).

[34] B. Q. Ai, L. G. Liu, *Phys. Rev. E* **76**, 042103 (2007).

[35] J. Rouselet, L. Salome, A. Ajdari, J. Prost, *Nature* **370**, 446 (1994).

[36] L. Gorre-Talini, S. Jeanjean, P. Silberzan, *Phys. Rev. E* **56** 2025 (1997).

[37] J. J. Thorn, E. A. Schoene, T. Li, D. A. Steck, *Phys. Rev. Lett.* **100**, 240407 (2008).

[38] C. Dalle-Ferrier, *et. al.*, *Soft Matter* **7** 2064 (2011).

# Chapter 6

# Summary and Future directions

## 6.1   Summary of the Thesis

In this thesis, we have investigated the effect of depletion interactions on the structure and dynamics of a binary colloidal mixture of large and small colloidal interacting particles in the presence of external repulsive potential barrier. We carried out the classical molecular dynamics simulations in canonical ensemble to study the structural and dynamical properties of the system at different state points. The interparticle interaction between the colloidal particles is taken to be purely soft sphere repulsion. The external potential barrier is applied along the $z$-direction only so that the dynamical properties along different directions can be compared and contrasted. It is shown that the depletion interaction between the larger particles in the mixture and the external barrier particularly affects the dynamics and structure along the $z$-axis and does not effect the system along the directions perpendicular to the potential barrier. This thesis constitutes the results, obtained from the molecular dynamics simulations of the binary colloidal system, on the effect of this depletion interaction in the structure as well as the dynamics of the components in the mixture at different temperatures, volume fractions and system size. We has applied two different external potentials in our system : (a) a symmetric potential barrier of Gaussian form at the center along z-direction and (b) an asymmetric potential barrier at the center along z-direction. Chapter-2,3,4 contains the results obtained from the simulations in the presence of a symmetric potential

and chapter-5 contains the results from the simulations in the presence of an asymmetric potential barrier.

In the presence of external repulsive potential of Gaussian form, It is observed that the binary colloidal mixture at low volume fraction ($\phi = 0.20$) undergoes significant dynamical changes. The depletion interaction between the barrier and larger particles significantly alters the dynamical behavior of both constituent species in the binary mixture, especially at lower temperatures. While the dynamics of the larger particles are diffusive even at lower temperatures, the smaller particles form a plateau in their mean squared displacement(MSD) at the intermediate times, indicating the slowing down of dynamics similar to supercooled liquids. These are also evident in the self diffusion coefficient of both the species. We further investigated the barrier crossing problem by studying the temperature dependence of diffusivities. The temperature dependence of diffusivity reveals that the diffusion of smaller particles follows Arrhenius law, but that of larger particles follows sub-Arrhenius diffusion. The activation energy of larger particles is found to be temperature dependent and hence changes the effective barrier height accordingly. We have shown that, contrary to the agreement in the literature that sub-Arrhenius diffusion is related to quantum phenomena, a classical system exhibits sub-Arrhenius temperature dependence of diffusivity. Our results show that the increase in the probability of barrier crossing can lead to sub-Arrhenius behavior irrespective of the nature of the process involved. In this sense, the depletion interactions in the present investigation or quantum tunneling in the earlier reported investigations have similar effects on the barrier crossing.

Next, we have investigated the effect of depletion interactions at higher volume fractions. For this, we have extended our simulations by systematically increasing the total volume fraction of the binary colloidal mixture from $0.20$ to $0.50$, still keeping the mixture to be equi-volume. The attractive depletion interaction between the potential barrier and larger particles in the binary mixture causes it to phase separate into two regions: one a pure

165

phase comprised of only larger particles in the region of the potential barrier and another a mixed phase elsewhere. The layering observed in the density profile of larger particles also indicates that this phase separation becomes stronger as we decrease the temperature and increase the volume fraction. From the radial distribution function $g(r)$ it is revealed that the smaller particles are in the liquid state at all volume fractions and temperatures and at low volume fractions, larger particles are in a liquid state at all temperatures. But with the increase in volume fractions above $0.40$, the $g(r)$ of larger particles show multiple peaks at low temperatures. The larger particles form fcc crystal structures in the domain of the external potential barrier. The phase separation allows one to manipulate the local volume fraction of large particles high enough that they undergo crystallization into an fcc structure. The volume fraction of larger particles is still much lower than the volume fractions of particles in a single component system to undergo crystallization. In general, such manipulations of local density are done by nonequilibrium processes like dielectrophoresis and diffusiophoresis. However, the binary colloidal mixture we have investigated is in equilibrium and, the changes in the local density of colloidal particles are done through the depletion interaction. The crystal domain, formed in the region of the external potential barrier, moves perpendicular to the external potential. The temperature dependence of diffusivity reveals that the smaller particles follow Arrhenius behavior for all volume fractions studied, while the larger particles experience a cross over from sub-Arrhenius diffusion at low volume fractions to a super-Arrhenius diffusion at higher volume fraction (above $\phi = 0.425$). This crossover from sub-Arrhenius to super-Arrhenius diffusion coincides with the structural changes in the mixture; i.e., the cross over happens at the volume fraction where the larger particles form crystalline domain near the barrier.

We have further investigated how our results depend on the system size and whether any scaling exist in the dynamics of the system. For this, we have carried out molecular dynamics simulations of the binary mixture of various sizes (L=9,10,11,13,15,17), keeping

the volume fraction constant($\phi = 0.20$). It has been shown that, at larger box-lengths, by choosing the appropriate lengthscale and timescale, the mean squared displacements can be scaled so that the curves lie on top of each other for different system sizes. The lengthscale is basically set by the periodicity of the external potential barrier, which is the same as the simulation boxlength along the $z$-direction. The time scale is set by the time taken by a particle to diffuse the distance between the successive barriers. This reveals that there are no finite size effects on the dynamics of both species for particles for relatively large simulation boxlengths. However, the scaling breaks down below a certain system size (for L=9,10) at low temperatures. The small box lengths affect the dynamics of larger particles in such a way that some of them undergo jump diffusion with displacement more than the magnitude of their diameter. The deviations from the scaling law for the mean squared displacement of larger particles at lower boxlengths and low temperatures can be attributed to the increased effective density of smaller particles in between the successive potential barriers. We have also observed that while the displacement distribution of smaller particles is Gaussian for all the boxlengths and temperatures studied, that of larger particles, the displacement distributions deviate from the Gaussian behavior at low temperatures, at all system sizes and exhibit secondary peaks on both sides, indicating that particles undergo jump diffusion. The secondary peaks correspond to the jump over the barrier and are in agreement with the observation that the waiting time distribution of particles has two length scales associated with it.

In the next part of our work, we carried out simulations of the same model system in the presence of an asymmetric external potential along the $z$-direction. The asymmetry in the external potential is achieved by introducing an error function in the Gaussian potential. When acted upon by an asymmetric external potential instead of symmetric potential, the colloidal particles show interesting changes in the dynamical behavior for a system of low volume fraction ($\phi = 0.20$). The temperature dependence of diffusivity shows that the

diffusivity versus inverse temperature curve changes from concave to convex as the asymmetry value increases. That means, as the asymmetry in the external potential increases, the diffusion of the larger particles changes from sub-Arrhenius to super-Arrhenius behavior, as indicated by the deformation parameter which changes its sign from negative to positive as the asymmetry increases. Since the activation energy is temperature dependent, the effective barrier height decreases for the larger particles for sub-Arrhenius diffusion whereas it starts increasing at low temperatures for the systems which shows super-Arrhenius diffusion. Generally, super-Arrhenius behavior is seen in the higher density system where particles show collective motions. However, due to the presence of asymmetric potential, the local density of larger particles increases and this leads to super-Arrhenius diffusion even for such a low density system. The density profile shows that, near the asymmetric side of the barrier, larger particles show higher local density forming a transient caging. The effective volume fractions calculated confirm the accumulation of larger particles at the asymmetric side more than the symmetric side. The non-Gaussian parameter, potential mean force, self intermediate scattering function, all confirm the interesting dynamics of larger particles as asymmetry increases in the potential. The larger particles show caged like motion near the barrier at the asymmetric side. However, the smaller particles remain away from the barrier and follow Arrhenius law in diffusivity for both symmetric and asymmetric potential barriers. Interestingly, by calculating the self part of the van-Hove correlation function of small and large particles, along with the applied external potential, we reveal that the transport of the particles is bidirectional. Our model can be realized in such experiments where the external potential remains asymmetric while maintaining bidirectional transport. The behavior of larger particles at higher asymmetry is equivalent to the behavior of some supercooled liquids.

In conclusion, we have studied the structure and dynamics of a binary colloidal mixture subjected to the external potential of both symmetric and asymmetric forms. The depletion

interaction plays a significant role in describing many interesting structural and dynamical changes in the constituent particles. Even though the results we obtained are for a binary mixture of colloids, we believe our findings are applicable to many other systems which involve barrier crossing. Many of the biological transport process which involve more than one components, differing in their dimensions, shows faster diffusivity for bigger components. Therefore, our results contribute to the understanding of such processes.

## 6.2   Future Directions

We see several future directions for the work outlined in this thesis. Some of the important directions are listed below.

- The dynamics of a binary colloidal system in the influence of an external repulsive potential reveals the sub-Arrhenius temperature dependence of diffusivity of the larger components of the mixture. Depletion interaction, induced by the mere presence of smaller particles, and completely entropic origin, causes sub-Arrhenius diffusion in the larger colloidal particles in the mixture. This happens because the activation energy is temperature dependent and decreases with decreasing temperature. The temperature dependence of activation energy can be studied more rigorously to include the inverse activation energy or the transitivity vs inverse temperature to find any universal behavior in the process.

- Our model includes only the repulsive interaction among the particles and there was no attractive part in the interatomic interactions. However, the depletion interaction causes attraction among larger particles and with the barrier which leads to sub Arrhenius diffusion. We can include the attractive part in the interparticle interactions to see its combined effect on the dynamics and structure of binary colloids along with the attractions caused by depletion effect.

- The size ratio of our model is 1:2 mixture of small and large soft spheres. To make it more broad we wish to include other size ratio and can investigate the effect of particles size in the dynamics of the system. It will be interesting to study the dynamics in extreme size asymmetry.

- We have kept the mass ratio to be 1:1 for the components in the mixture, even though the sizes are different, to primarily focus on the effect of depletion interaction on the dynamics of the system. However, in real systems, masses also vary with respect to size. So it will be interesting to look at the dynamics of particles where the components differ both in size and mass. We do expect that the larger particles will undergo sub-diffusive behaviour because of the depletion interaction, but the quantitative values of diffusivity, deformation parameter etc. will be different.

- In real systems, it will be difficult to have monodisperse particles. So we would like to investigate the effect of polydispersity in both components of the mixture in the temperature dependence of diffusion.

- At higher volume fraction the larger particles form fcc crystal at the barrier region along the z-axis, but move perpendicular to the direction of potential barrier. It acts as a moving crystal though being an equilibrium system. Generally this kind of moving crystal is seen in non-equilibrium systems. But it is interesting to find this in an equilibrium system like the one we studied. We wish to further investigate to have insight in this phenomena in an equilibrium system.

- The asymmetry in the potential lead to caging which causes super Arrhenius diffusion. So the potential can be manipulated to have this behavior even in low volume fractions. We can investigate the effect of depletion interaction in the presence of asymmetric potential at higher volume fractions.

170